Targeted Sensors for Investigating Mobile Zinc in Biology

by

Wen Chyan

Submitted to the Department of Chemistry in Supplement to
Requirements for the Degree of

BACHELOR OF SCIENCE IN CHEMISTRY

at the

MASSACHUSETTS INSTITUTE OF TECHNOLOGY

JUNE 2013

Author: _____
Department of Chemistry
May 10, 2013

Certified by: _____
Stephen J. Lippard
Arthur Amos Noyes Professor of Chemistry
Thesis Supervisor

Approved by: _____
Rick L. Danheiser
Arthur C. Cope Professor of Chemistry
Undergraduate Officer, Department of Chemistry

Targeted Sensors for Investigating Mobile Zinc in Biology

by

Wen Chyan

Submitted to the Department of Chemistry on May 10, 2013

ABSTRACT

CHAPTER 1. Sensing Strategies for Detection of Mobile Zinc

Mobile zinc plays important physiological roles in areas such as the hippocampus, prostate, and pancreas. A better understanding of the distribution of intracellular mobile zinc could provide insight into the pathology of diseases including prostate cancer and Alzheimer's disease, both of which have been linked to abnormal mobile zinc levels. Accordingly, a palette of spatially-specific mobile zinc sensors is needed to investigate mobile zinc in important areas such as the mitochondria or zinc vesicles in neurons. Instead of repeating the *de novo* sensor design process for each target, a modular approach was developed to take advantage of the existing library of sensors and enable rapid creation of targeted probes.

CHAPTER 2. Targeting Fluorescent Zinc Sensors to the Mitochondria Using Triphenylphosphonium Ions

Mitochondrial mobile zinc plays an important, although poorly understood, role in prostate cancer. To investigate the biology of zinc in the mitochondria, constructs incorporating fluorophores and the mitochondria-targeting triphenylphosphonium (TPP) moiety were tested and used to study sensor uptake and localization to the mitochondria.

CHAPTER 3. Peptide-based Targeting of Fluorescent Zinc Sensors to the Plasma Membrane and Intracellular Targets in Live Cells

Peptide-sensor constructs were explored as a modular method of targeting sensors to specific locations. Taking advantage of the synthetic flexibility and targeting advantages of peptide-sensor constructs, mobile zinc sensors were directed to the exterior of the plasma membrane and to intracellular targets. A series of peptide-sensor constructs were created to further investigate fluorophore effects on sensor uptake and localization.

CHAPTER 4. Improvement of Sensor Uptake, Localization, and Photophysics Through Acetylation of Fluorescein-based Sensors

A generalizable strategy for improving the uptake and photophysics of mobile zinc probes was explored. The ZP1-TPP sensor construct was modified by one-step acetylation of phenolic oxygen atoms. This modification dramatically improved photophysics and eliminated problems with membrane impermeability that would otherwise result in endosomal sequestration. The resulting DA-ZP1-TPP sensor was highly selective for zinc, resilient against cellular esterases, and, most importantly, was specifically targeted to the mitochondria.

Thesis Supervisor: Professor Stephen J. Lippard
Title: Arthur Amos Noyes Professor of Chemistry

Dedicated to Joyce Wang and my family

ACKNOWLEDGEMENTS

Research in the Lippard laboratory has been one of the most educational and rewarding experiences during my time at MIT, and I would like to express my sincere gratitude to Professor Stephen J. Lippard for providing the opportunity to work in his laboratory. Professor Lippard is a true inspiration because of his passion for science, care for undergraduate students, and ability to inspire others to their best. Working in the Lippard lab and learning from Professor Lippard has been an invaluable experience.

As my UROP mentor, Robert Radford is an excellent scientist and role model who is fully invested in nurturing a passion for science and in the development of his students. I greatly appreciate his trust (and verification) of my ability to do science, and the freedom to plan and execute research. Robert was always available to lend a listening ear or provide advice whenever needed, and was always happy to help whenever the need arose. I am proud to have had the opportunity to help expand Robert's original peptide idea into the multifaceted project it is today.

I would also like to thank the Lippard group members; due to the variety of backgrounds represented in the group, I had the opportunity to learn a wide spectrum of skills and knowledge from group members including Ulf-Peter Apfel, Zhen Huang, Pablo Rivera, Wei Lin, and Patricia Gallego. It was my pleasure to work with Dan Zhang, whose assistance with cell culture whenever I was travelling or writing was much appreciated.

I thank my parents, Oliver and Jin-Jian Chyan, for their effort and sacrifice on my behalf. My parents' passion for chemistry inspired my initial interests and I also appreciate the time they spent teaching my brother and me. My parents have always encouraged me to pursue my dreams and have taught me the value of diligence and perseverance. I am also fortunate to have grown up with the wonderful camaraderie of my brother, Yieu.

Finally, I would like to express my utmost gratitude to my fiancée, Joyce Wang, without whom none of my work would have been possible. Joyce has been the perfect counterpart to keep me grounded and in touch with reality. As a fellow MIT student, Joyce believed in me and often helped to refine my ideas; her input and advice vastly improved my writing, including this thesis. I am eternally grateful for her sacrifices and her willingness to delay her education and professional career to support my research and final year at MIT. Joyce believed in me and provided unconditional support; her unwavering encouragement has been my source of motivation these past few years and this short acknowledgement does not begin to do justice to her dedication and support.

TABLE OF CONTENTS

LIST OF FIGURES AND TABLES

CHAPTER 1

CHAPTER 2

CHAPTER 3

CHAPTER 4

CHAPTER 1. Sensing Strategies for Detection of Mobile Zinc

1.1. Introduction

Zinc, one of the most abundant d-block elements in biology, serves important structural and catalytic roles in proteins such as carbonic anhydrase or alcohol dehydrogenase.[1] Although the majority of biological zinc is tightly bound to protein frameworks, a pool of mobile zinc ions (Zn^{2+}) also exists in a mobile, or chelatable form.[2] Intracellular pools of mobile zinc are highly regulated due to their important biological roles and cytotoxicity at concentrations in excess of normal physiological conditions.[3] Abnormalities in mobile zinc homeostasis and distribution have been linked to Alzheimer's disease,[4] prostate cancer,[5-6] and diabetes.[7] Homeostasis of mobile zinc is maintained by a variety of metallothioneins and zinc transporter proteins including the Zip and ZnT families.[8-9] Mobile zinc is also stored in cytosolic vesicles in many mammalian cell types, possibly serving as an additional mechanism to maintain cytosolic zinc homeostasis.[8,10-12]

One example of the multifaceted roles of mobile zinc in biology is the regulatory role of mobile zinc in the brain. In the brain, mobile zinc is primarily located in presynaptic zinc vesicles in axons of the hippocampus, cortex, and amygdala.[13] Presynaptic zinc vesicles in these tissues are loaded with zinc by the ZnT3 transporter in areas of the brain typically associated

---

[1] Bertini, I.; *Biological Inorganic Chemistry*. Sausalito, CA: University Science Books, **2007**.
[2] Pluth, M.D.; Tomat, E.; Lippard, S.J. *Annu. Rev. Biochem.* **2011**, 80, 333-355.
[3] Colvin, R.A.; Holmes, W.R.; Fontaine, C.P.; Maret, W. *Metallomics.* **2010**, 2, 306-317.
[4] Pan, E.; Zhang, X. A.; Huang, Z.; Krezel, A.; Zhao, M.; Tinberg, C. E.; Lippard, S. J.; McNamara, J. O. *Neuron* **2011**, *71*, 1116.
[5] Costello, L. C.; Franklin, R. B.; Feng, P. *Mitochondrion* **2005**, *5*, 143
[6] Costello, L. C.; Franklin, R. B. *J. Biol. Inorg. Chem.* **2011**, *16*, 3.
[7] Taylor, C. G. *Biometals* **2005**, *18*, 305.
[8] Eide, D.J. *Biochim. Biophys. Acta.* **2006**, 1763, 711-722.
[9] Litchten, L.A.; Cousin, R.J. *Annu. Rev. Nutr.* **2009**, 29, 153-76.
[10] Palmiter, R.D.; Cole, T.B.; Findley, S.D. *EMBO J.* **1996**, 15, 1784-1791.
[11] Haase, H.; Beyersmann, D.; *Biochem. Biophys. Res. Commun.* **2002**, 296, 923-928.
[12] St Croix, C.M.; Wasserloos, K.J.; Dinely, K.E.; Reynolds, I.J.; Levitan, E.S.; Pitt, B.R. *Am. J. Physiol.* **2002**, 282, L185-L192.
[13] Toth, K. *Annu. Rev. Nutr.* **2011**, 31, 139-153.

with memory and learning.[14-15] Because of the location and abundance of these zinc vesicles, mobile zinc in the brain acts as a neurotransmitter or neuromodulator regulating long-term potentiation.[4,16] The release of zinc from presynaptic vesicles affects signaling pathways related to neuronal death processes, long-term potentiation, and synaptic plasticity, among other neural functions.[16-18] A better understanding of the physiology and pathology of mobile zinc in the brain would be valuable for deciphering neurological diseases such as Alzheimer's disease.[19]

Another example of the important physiological role of labile zinc is the human prostate, which contains the highest mobile zinc levels of any tissue in the body.[20] In the healthy non-cancerous prostate, zinc inhibits mitochondrial aconitase, resulting in the buildup of citrate.[21] Citrate is excreted from the prostate cell as an essential component of seminal fluid due to its buffering properties.[22] In contrast, cancerous prostate cells are characterized by significantly lower zinc levels than non-cancerous prostate cells.[23] Evidence suggests that the lower mobile zinc levels in cancerous prostate cells suppress mitochondrial apoptosis caused by cancerous prostate cell sensitivity to zinc-induced apoptosis.[24] Lower mobile zinc concentrations could also attenuate the inhibition of mitochondrial aconitase, resulting in unrestricted energy production through the TCA cycle to fuel tumor growth. Characterization of mobile zinc distributions in

---

[14] Perez-Claussell, J.; Danscher, G. *Brain Res.* **1985**, 337, 91-98.
[15] Malenka, R.C.; Nicoll, R.A. *Science.* **1999**, 285, 1870-1874.
[16] Kay, A.R.; Toth, K. *Sci. Signal.* **2008**, 1:re3.
[17] Sensi, S.L.; Paoletti, P.; Bush, A.I.; Sekler, I. *Nat. Rev. Neurosci.* **2009**, 10, 780-791.
[18] Takeda, A.; Tamano, H. *Nat. Brain Res. Rev.* **2009**, 62, 33-44.
[19] Cuajungco, M.P.; Lees, G.J. *Brain Res Brain Res Rev.* **1991**, 23, 219.
[20] Costello, L.C.; Franklin, R.b. *Mol. Cancer.* **2006**, 5, 17.
[21] Costello, L.C.; Liu, Y.; Franklin, R.B.; Kennedy, M.C. *J. Biol. Chem.* **1997**, 272, 28875-28881.
[22] Kavanagh, J.P. *J. Reprod. Fer.* **1985**, 75, 35-41.
[23] Feng, P.; Li, T.; Guan, Z.; Franklin, R.B.; Costello, L.C. *Mol. Cancer.* **2008**, 7, 25.
[24] (a) Sharpley, M.S.; and Hirst, J. *J. Biol. Chem.* **2006**, 281, 34803-34809. (b) Feng, P.; Li, T.; Guan, Z.; Franklin, R.B.; Costello, L.C. *The Prostate.* **2002**, 52, 311-318.

malignant prostate cells could facilitate the use of prostate zinc levels as a biomarker for early prostate cancer detection.

The widespread biological importance of mobile zinc in areas including prostate cancer and neurological disease underscore the benefits of understanding the pathology and physiology of mobile zinc. Although abnormal distributions of mobile zinc in tissues such as the brain and prostate have deleterious effects, the spatial distribution and cellular physiology of mobile zinc are incompletely understood for both healthy and diseased cell function. Therefore, development and improvement of spatially informative zinc-sensing capabilities are essential for investigation of mobile zinc biology.

1.2. Small-Molecule Fluorescent Zinc Sensors

Fluorescent small-molecule sensors have been the most commonly-used and well-characterized zinc sensors. Because zinc is a "spectroscopically silent" metal with a closed-shell d^{10} configuration, fluorescent sensors provide a convenient method of monitoring zinc.[25] Small-molecule zinc sensors represent an attractive option for imaging biological zinc due to their brightness and ability to precisely tune metal binding and photophysical properties through chemical synthesis.[27] In addition, many small-molecule zinc probes are fairly selective for zinc over other biologically-abundant cations including calcium (Ca^{2+}) and magnesium (Mg^{2+}).[26] Most small-molecule sensors offer the additional benefit of being able to diffuse across the cell membrane, obviating the need for complex transfection or protein engineering procedures normally required for protein-based probes.[27] In contrast to protein-based probes, however,

---

[25] Dean, K.M.; Qin, Y.; Palmer, A.E. *Biochim. Biophys. Acta.* **2012**, 1823, 1406-1415.

[26] (a) Pluth, M.D.; Tomat, E.; Lippard, S.J. *Annu. Rev. Biochem.* **2011**, 80, 333-355. (b) Woodroofe, C.C.; Masalha, R; Barnes, K.R.; Frederickson, C.J.; Lippard, S.J. *Chem. Biol.* **2004**, 11, 1659-1666.

[27] (a) Nolan, E.M.; Lippard, S.J. *Acc. Chem. Res.* **2009**, 42, 193-203. (b) Domaille, D.W.; Que, E.L.; Chang, C.J. *Nat. Chem. Biol.* **2008**, 4, 168-175.

predicting the localization of a small-molecule fluorescent sensor *a priori* is difficult due to an incomplete understanding of how small-molecules are distributed within the cellular environment.

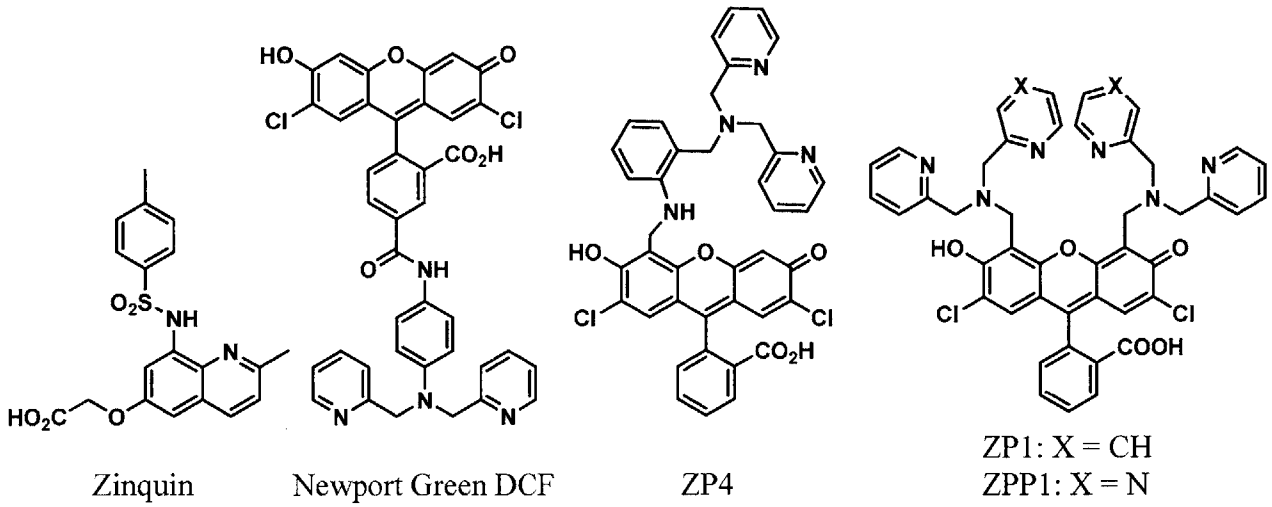

Figure 1.1. Selected small-molecule fluorescent zinc sensors. The carboxylic acid form of Zinquin is depicted along with line structures of fluorescein-based sensors Newport Green DCF, ZP4, ZP1, and ZPP1.

Most small-molecule zinc sensors have zinc-induced fluorescence turn-on or turn-off, which can be easily imaged by fluorescence microscopy. Zinquin and 6-methoxy-8-*p*-toluenesulfonamidequinoline (TSQ), both based on 8-substituted quinoline platforms, are some of the earliest fluorescent small-molecule zinc sensors.[28] Both of these sensors are turn-on sensors with large responses upon binding zinc. TSQ and Zinquin, however, form a mixture of single-sensor complexes (1:1 sensor:Zn) and bis complexes (2:1 sensor:Zn) with Zinc, require cell-damaging UV excitation, and are less bright than other fluorophores.[29] In contrast, mobile zinc probes using fluorescein scaffolds are significantly brighter than quinoline-based sensors and have visible-region excitation wavelengths.[30] Structurally, many of the fluorescein-based

---

[28] Fahrni, C. J.; O'Halloran, T. V. *J. Am. Chem. Soc.* ***1999,*** *121,* 11448-11458.
[29] Hendrickson, K.M.; Geue, J.P.; Wyness, O.; Lincoln, S.F.; Ward, A.D. *J. Am. Chem. Soc.* **2003**, 125, 3889-3895.
[30] Nolan, E.M.; Lippard, S.J. *Acc. Chem. Res.* **2009**, 42, 193-203.

mobile zinc reporters share similarities such as the use of secondary or tertiary amines to quench fluorescence in the absence of zinc (Figure 1.1).[31] For example, Newport Green DCF has one di(2-picolyl)amine (DPA) that binds zinc via three nitrogen atoms (Figure 1.1).

The Zinpyr family, an example of fluorescein-based sensors, is characterized by facile synthesis and use of the DPA ligand.[32] Electron-rich tertiary nitrogen atoms in each DPA arm quenches the fluorescein core by photoinduced electron transfer (PeT). Upon binding zinc, the PeT effect of the DPA arm is attenuated, resulting in restoration of fluorescence. The first member of the Zinpyr family, ZP1, affords good optical brightness, cell permeability, and localization to the Golgi apparatus.[33] ZP1 provides a fivefold increase in florescence brightness upon binding zinc at physiological pH. Other variants in the Zinpyr family include an asymmetric extracellular sensor (ZP4),[33] an esterase-trappable version,[34] and an improved zinc probe (ZPP1).[35]

1.3. Improving and Targeting Sensors to Discrete Cellular Locales

Instead of repeating *de novo* sensor design and synthesis for each desired target or application, a modular approach towards sensor targeting takes advantage of the extensive existing zinc sensor library. The ability to direct sensors to different targets by simple conjugation to a targeting moiety would allow rapid generation of sensors tailored for specific applications, without having to repeat the sensor development process. In a modular approach to sensor targeting, the sensor has an attachment site for the targeting moiety, preferentially through

---

[31] Pluth, M.D.; Tomat, E.; Lippard, S.J. *Annu. Rev. Biochem.* **2011**, 80, 333-355.
[32] Walkup, E.; Burdette, S.; Lippard, S.; Tsien, R. *J. Am. Chem. Soc* 2000, 12, 5644-5645
[33] Woodroofe, C.C.; Masalha, R; Barnes, K.R.; Frederickson, C.J.; Lippard, S.J. *Chem. Biol.* **2004**, 11, 1659-1666.
[34] Woodroofe, C.C.; Won, A.C.; Lippard, S.J.; *Inorg. Chem.* **2005**, 44, 3112.
[35] Zhang, X.; Hayes, D.; Smith, S.J.; Friedle, S.; Lippard, S.J. *J. Am. Chem. Soc.* **2008**, 130, 15788-15789.

a reliable high-yield reaction. The targeting moiety plays two major roles—augmentation of sensor uptake through diffusion or endocytic transport through the cell wall and subsequent direction of the sensor to its appropriate intracellular target. To accomplish the first goal, the targeting moiety is preferentially positively charged or overall neutral, because nonpolar, cationic molecules are better suited to translocate across the cytoplasmic membrane.[36] In contrast, negatively charged species are typically membrane-impermeable, partially due to repulsion between the membrane surface and anionic species and also due to the negative potential across most plasma membranes. If the sensor enters the cell through the endocytic pathway instead of diffusion, positively-charged sensor constructs are favorable owing to interactions with the negatively-charged cell surface, leading to enhanced uptake.[37]

Cell-penetrating peptides (CPP) and the triphenylphosphonium ion (TPP) are two commonly used targeting moieties that employ these transport strategies to assist uptake and targeting. CPPs are typically short peptides with positively-charged residues and may include hydrophobic residues.[37] One of the earliest CPPs was derived from the trans-activating transcriptional factor (Tat) isolated from human immunodeficiency virus 1.[38] Cargos conjugated to the Tat peptide were able to penetrate the outer membrane and stain the cytosol of various cell types. Subsequently, synthetic polycationic and amphipathic CPPs were developed to improve the uptake and localization benefits of Tat (Table 1.1.).[39] Although uptake mechanisms of CPPs are not conclusively understood, evidence suggests that CPPs enter the cell through endocytic

---

[36] Lodish H, Berk A, Zipursky SL, et al. Molecular Cell Biology. 4th edition. New York: W. H. Freeman; 2000. Section 15.1.

[37] (a) Stewart, K.M.; Horton, K.L.; Kelley, S.O. *Org. Biomol. Chem.* **2008**, 6, 2242-2255. (b) Davies, P.f.; Rennke, H.G.; Cotran, R.S. *J. Cell Sci.* **1981**, 49, 69-86.

[38] Brooks, H.; Lebleu, B.; Vives, E. *Adv. Drug Deliv. Rev.* **2005**, 57, 559-577.

[39] (a) Horton, K.L.; Stewart, K.M.; Fonseca, S.B.; Guo, Q.; Kelley, S.O. *Chem Biol.* **2008**, 15, 375. (b) Horton, K.L.; Pereira, M.P.; Stewart, K.M.; Fonseca, S.B.; Kelley, S.O. *Chem Bio Chm.* **2012**, *13*, 476. (c) Huang, C.; Li, Z.; Cai, H.; Shahinian, T.; Conti, P.S. *Mol. Imaging.* **2011**, 10, 284-294.

pathways. CPPs offer the advantages of improved biocompatibility, easy sensor incorporation (attachment to *N*-terminus, attachment to ε-amines, incorporation as an artificial amino acid), and straightforward synthesis and purification using solid phase peptide synthesis (SPPS).

In contrast to the biological origin of CPPs, the triphenylphosphonium (TPP) targeting moiety is a hydrophobic small ion that can be conjugated to payloads via an ethylamine linker. TPP is positively charged and moderately hydrophobic, promoting diffusion of the TPP-conjugated cargo across the phospholipid bilayer. Although TPP ions do not offer the same flexibility in structure and connectivity as peptides, they are much smaller in size than CPPs and thus more likely to diffuse across the membrane. TPP also has an extensive record of successfully localizing payloads to the mitochondria, and it has been used in a few cases for sensing mitochondrial zinc, although these applications typically require lengthy syntheses and have unfavorable brightness, selectivity, or zinc-binding properties relative to Zinpyr sensors.[40] Selection and design of CPP and TPP targeting moieties requires an appropriate balance of charge, size, and hydrophobicity to maximize uptake without encountering toxicity or solubility issues.

Name	Sequence
Polyarginine (R_9)	RRRRRRRRR
Tat	GRGRKKRRQRRPPQ
Penetratin	RQIKIWFQNRRMKWKK
NLS[a]	SKKKKIKV
Integrin	RGD, DGEA
MPP[b]	$F_xrF_xrF_xr$, F_xrF_xK

Table 1.1 List of selected cell-penetrating peptides commonly used to improve uptake or specificity of localization.[40] [a]NLS stands for nuclear localization signal. [b]MPP is a synthetic sequence primarily consisting of D-arginine (r) and cyclohexylalannine (F_x).

Conjugation of peptides and TPP represent two methods to improve the uptake and localization of mobile zinc probes. Peptide-sensor constructs offer the advantage of better

[40] (a) Baek, N.Y.; Heo, C.H.; Lim, C.S.; Masanta, G.; Cho, B.R.; Kim, H.M. *Chem. Commun.* **2012**, 48, 4546-4548. (b) Xue, L.; Li, G.; Yu, C.; Jiang, H. *Chem. Eur. J.* **2012**, 18, 1050-1054.

synthetic flexibility, biocompatibility, and modularity than TPP-sensor constructs, but also take somewhat more time to synthesize and purify. Although TPP ions have an extensive record of mitochondrial delivery of payloads, TPP-sensor constructs are also restricted to mitochondrial targeting, whereas peptide-sensor constructs can be targeted in a programmable manner to different intracellular and extracellular locations. Each targeting method offers advantages and disadvantages; efforts towards targeting with TPP ions are outlined in Chapter 2 and research investigating peptide-based zinc sensor targeting is described in Chapter 3. In addition to targeting mobile zinc probes to specific locations, methods enhancing sensor uptake and photophysics were explored. Chapter 4 details research on zinc sensor acetylation, a facile one-step chemical modification that can be generalized to multiple sensing applications.

CHAPTER 2. Targeting Fluorescent Zinc Sensors to the Mitochondria Using Triphenylphosphonium Ions

2.1 Introduction

In the prostate, mobile zinc plays several important roles. It affects mitochondrial electron transport and can induce apoptosis via Bax-associated pores that permeabilize the mitochondria.[1] Many malignant prostate cancer cell lines are characterized by significantly lower levels of zinc than non-cancerous prostate cells, which reduces mitochondria-induced apoptosis, allowing continued proliferation.[2] Another role of zinc in prostate cells is the inhibition of mitochondrial aconitase, an enzyme that is part of the citric acid cycle.[3] Aconitase catalyzes the isomerization of citrate to isocitrate through a cis-aconitate intermediate.[4] In non-cancerous cells, high levels of intracellular mobile zinc suppress aconitase activity, resulting in the build-up of citrate and secretion of citrate and zinc out of the cell.[3] Citrate is an important component of seminal fluid due to its pH- and zinc-buffering properties.[5] In cancerous prostate cells, mobile zinc levels are significantly lower, resulting in a reduction of citrate secretion due to continuous consumption of citrate in the TCA cycle, which could also function to supply additional energy for unrestricted tumor growth.[6] Since the role of mobile zinc in both cancerous and non-cancerous cells is not well understood, mitochondria-localized zinc probes are valuable tools for elucidation of the physiological role of mobile zinc, which can potentially serve as a diagnostic biomarker for prostate cancer.

To target the mitochondria, fluorophores were conjugated to the lipophilic triphenylphosphonium (TPP) cation. Historically, TPP ions were first employed to demonstrate

---

1 Feng, P.; Li, T.; Guan, Z.; Franklin, R.B.; Costello, L.C. *Mol. Cancer.* **2008**, 7, 25.
2 Feng, P.; Li, T.; Guan, Z.; Franklin, R.B.; Costello, L.C. *The Prostate.* **2002**, 52, 311-318
3 Costello, L.C.; Liu, Y.; Franklin, R.B.; Kennedy, M.C. *J. Biol. Chem.* **1997**, 272, 28875-28881.
4 Beinert, H.; Kennedy M.C. *FASEB J.* **1993**, 7, 1442-1449.
5 Kavanagh, J.P. *J. Reprod. Fer.* **1985**, 75, 35-41.
6 Gomez, Y.; Arocha, F.; Espinoza, F.; Fernandez, D.; Vasquez, A.; Granadillo, V. *Invest Clin.* **2007**, 48, 287-294.

the existence of a potential across the mitochondrial membrane,[7] and were subsequently used for various targeting purposes. Recent applications have included targeted mitochondrial delivery of lipids,[8] NO-releasing prodrugs,[9] and sensors,[10] although some constructs showed improper localization and endosomal trapping.[10] The cationic, lipophilic nature of TPP improves uptake into the cell and subsequent mitochondrial localization due to the large potential across the inner membrane of the mitochondria. A functionalized version of ZP1, a zinc sensor from the Zinpyr family, was conjugated to TPP in an attempt to direct the sensor to mitochondria. The Zinpyr family was a logical choice because of its record of in-cell functionality, wide span of zinc binding affinities, and brightness. Two other fluorophores of differing size, charge, and hydrophobicity were also conjugated to TPP to further investigate the cellular trafficking process (Figure 2.1). Each of these fluorophores has carboxyl groups that serve as sites for facile conjugation to the (2-aminoethyl)triphenylphosphonium bromide targeting moiety.

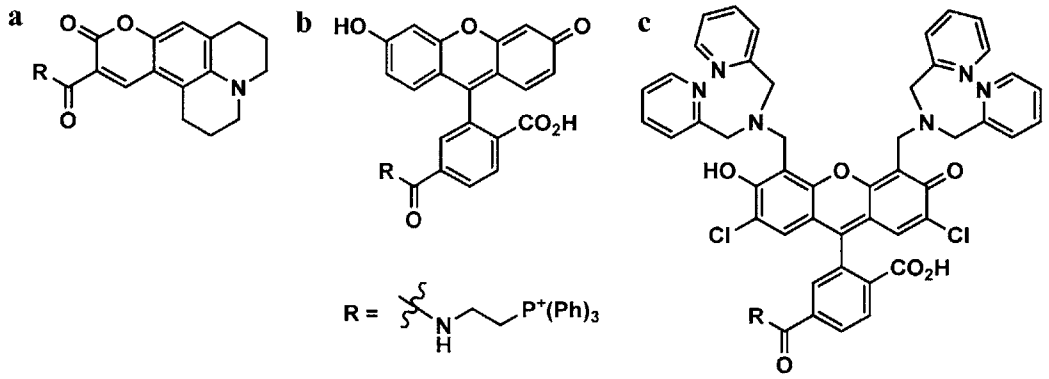

Figure 2.1. Mitochondria-targeted fluorophore constructs incorporating (a) coumarin 343 (C343), (b) 6-carboxyfluorescein (Fl), and (c) 6-CO_2H Zinpyr1 (ZP1) and the targeting moiety (2-aminoethyl) triphenylphosphonium (TPP).

---

7 Ross, M.F.; et al. *Biochemistry (Moscow)*, **2005**, *70*, 222-230.

8 Tyurina, Y.Y.; et al. *FEBS Letters*, **2012**, *586*, 235-241.

9 Belikova, N.A.; Jiang, J.; Stoyanovsky, D.A.; Glumac, A.; Bayir, H; Greenberger, J.S.; Kagan, V.E. *FEBS Letters*, **2009**, *583*, 1945-1950.

10 Sreenath, K.; Allen, J.R.; Davidson, M.W.; Zhu, L. *Chem. Commun.*, **2011**, *47*, 11730-11732.

2.2. Materials and Methods

General Considerations. HPLC grade acetonitrile, anhydrous *N,N*-diisopropylethylamine (DIPEA), *N,N*-dimethylformamide (DMF), dichloromethane, 4-methylpiperidine, 1-(4,5-Dimethylthiazol-2-yl)-3,5-diphenylformazan, ammonia hydroxide, coumarin 343, and 5(6)-carboxyfluorescein were purchased from Sigma-Aldrich. 2-(7-Aza-1H-benzotriazole-1-yl)-1,1,3,3-tetramethyluronium hexafluorophosphate (HATU, Oakwood Chemicals). MitoTracker Red FM, Hoechst 34580 stain, and Lysotracker Red DND-99 were purchased from Life Technologies. All solvents were reagent grade unless otherwise specified and commercially available reagents were used as received. 6-CO_2H Zinpyr1[11] and (2-aminoethyl) triphenylphosphonium bromide[12] were prepared according to literature procedures. The purity of each construct was assayed by reverse-phase HPLC carried out on an Agilent Technologies 1200 Series HPLC system. Mass spectra were collected on an 1100-series Agilent LC/MSD ion trap. ^1H and ^{31}P NMR samples spectra were acquired on a Varian Mercury 300 NMR spectrometer. ^{31}P NMR samples were referenced to phosphoric acid in D_2O (δ - 0.00 ppm). Aqueous solutions were prepared using Millipore water. Molecular biology grade piperazine-*N,N'*-bis(2-ethanesulfonic acid) (PIPES) and 99.999% KCl were purchased from Aldrich. In order to remove adventitious metal ions, buffered solutions were treated with Chelex resin (Bio-Rad) according to manufacturer specifications. A 50 mM zinc(II) stock solution was prepared using 99.999% $ZnCl_2$ (Aldrich). UV-vis spectra were recorded on a Varian Cary 50 Bio UV-visible spectrophotometer. Fluorescence spectra were recorded in quartz cuvettes (Starna) with 1 cm path lengths on a Quanta Master 4 L-format scanning spectrofluorimeter (Photon Technology

---

[11] (a) Woodroofe, C. C.; Masalha, R.; Barnes, K. R.; Frederickson, C. J.; Lippard, S. J. *Chem. Biol.* **2004**, *11*, 1659; (b) Nolan, E. M.; Lippard, S. J. *Acc. Chem. Res.* **2009**, *42*, 193.

[12] Maryanoff, B.E.; Reitz, A.B.; Duhl-Emswiler, A.D. *J. Am. Chem. Soc* **1985**, *107*, 218.

International). The acquisition temperature was kept at 25 ± 0.1 °C by circulating water bath. Stock solutions of C343-TPP, Fl-TPP, and ZP1-TPP were prepared in DMSO, partitioned in 50 μL aliquots and stored in the dark at – 40° C.

Synthesis and Purification of C343-TPP. (2-Aminoethyl)triphenylphosphonium bromide (31 mg, 0.081 mmol, 1 equiv) was dissolved in 1 mL DMF and purged with N_2 for 5 min. Separately, coumarin 343 (23 mg, 0.081 mmol, 1 equiv) and HATU (31 mg, 0.081 mmol, 1 equiv) were dissolved in 1mL of a 10% solution of DIPEA in anhydrous DMF. The C343-HATU solution was added and the mixture stirred at room temperature for one hour under N_2, then precipitated in 10 mL of H_2O and lyophilized. Purification by column chromatography (Silicycle 60 Å ultrapure silica gel, 1-3% MeOH gradient in DCM) yielded 25.7 mg of C343-TPP (55% yield). Purity was assessed by analytical HPLC (Vydac C18, 5 μm, 4.6 mm i.d. x 250 mm). After a 5 min isocratic wash, a 30-minute linear gradient of 5-60% B was run at 1 mL min^{-1}. C343-TPP (retention time = 30.4 min) was judged to be ≥ 95% pure based on the integrated chromatogram (Figure 2.2). ^1H NMR (DMSO-d_6, 300 MHz): δ 8.95 (1H, t), 8.44 (1H, s), 7.87 (9H, M), 7.75 (6H, m), 7.24 (1H, s), 3.86 (2H, m), 3.67 (2H, q), 3.35 (3H, m), 2.73 (4H, q), 1.88 (4H, m). ^{31}P NMR (DMSO-d_6, 300 MHz): δ 22.16 ppm. ESI-MS: observed (expected) M/Z for $[M+H]^+$ = 574.3 (574.65).

Synthesis and Purification of Fl-TPP. (2-Aminoethyl)triphenylphosphonium bromide (31 mg, 0.081 mmol), 5(6)-carboxyfluorescein (30.5 mg, 0.081 mmol), and HATU (31 mg, 0.081 mmol) were used to prepare Fl-TPP using procedures analogous to C343-TPP. The resulting solid was purified by HPLC on the semi-preparative scale using a C18 reverse-phase column (VYDAC,

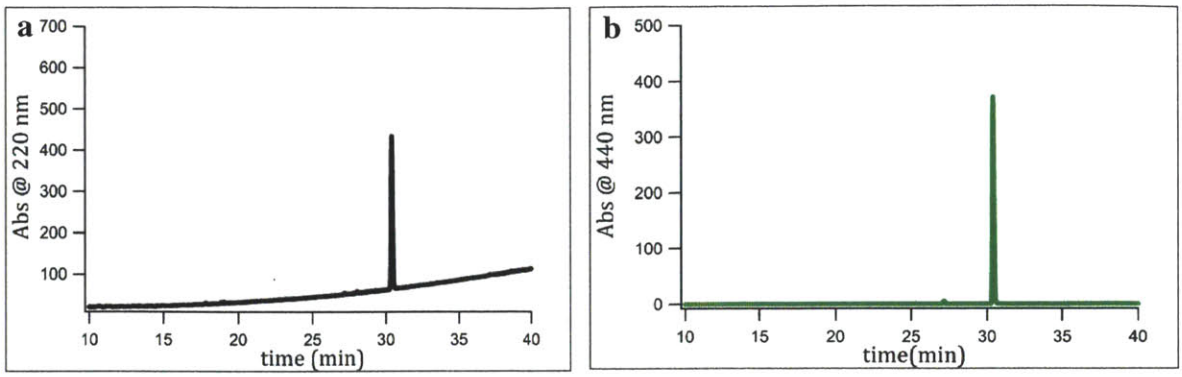

Figure 2.2. Analytical HPLC chromatogram of C343-TPP, monitoring at 220 nm (a) and 440 nm (b). C343-TPP was judged to be ≥ 95% pure based on the integrated absorbance signal.

9.5 mm × 250 mm). A two-solvent system (A = 0.1% (v/v) TFA in H_2O; B = 0.1% TFA in acetonitrile (v/v)) was employed as follows: isocratic flow, 5% B, 0-5 min; gradient, 5-70% B, 5-35 min. The flow-rate was 3 mL min^{-1} throughout the purification. The 5-carboxyfluorescein and 6-carboxyfluorescein product isomers were well resolved, allowing them to be collected and pooled separately. The isomeric identify of each fraction was confirmed by characteristic ^1H NMR peaks for each isomer,[13] and the 6-carboxy isomer was selected for further studies (3.5 mg, 8.6% yield). Purity of the 6-carboxyfluorescein product was assessed by analytical HPLC (Vydac, C18, 5 μm, 4.6 mm i.d. x 250 mm). After a 5 min isocratic wash, a 30-minute linear gradient of 5-60% B was run at a flow rate of 1 mL min^{-1}. Fl-TPP (retention time = 30.7 min) was judged to be ≥ 95% pure based on the integrated chromatogram (Figure 2.3.). ^1H NMR (DMSO-d_6, 300 MHz): δ 10.22 (2H, s), 9.00 (1H, t), 8.09 (1H, d), 8.04 (1H, d), 7.82 (9H, m), 7.76 (6H, m), 7.48 (1H, s), 6.72 (2H, d), 6.60 (4H, s), 3.81 (2H, M), 3.55 (2H, M). ^{31}P NMR (DMSO-d_6, 300 MHz): δ 22.35 ppm. ESI-MS: observed (expected) M/Z for $[M+H]^+$ = 664.3 (664.68), $[M+2H]^{2+}$ = 332.6 (332.84).

---

[13] Ueno, Y.; Jiao, G.S.; Burgess, K. *Synthesis.* **2004**, 15, 2591-2593.

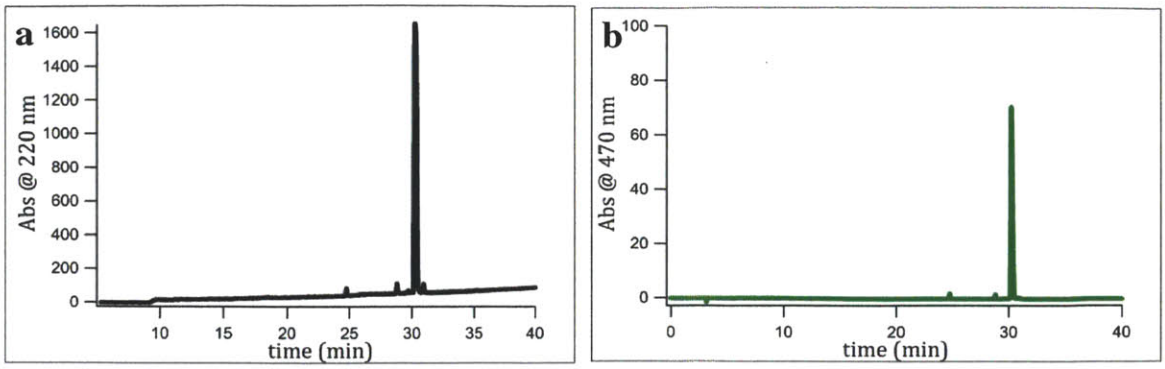

Figure 2.3. Analytical HPLC chromatogram of Fl-TPP, monitoring at 220 nm (a) and 470 nm (b). Fl-TPP was judged to be ≥ 95% pure based on the integrated absorbance signal.

Synthesis and Purification of ZP1-TPP. (2-Aminoethyl)triphenylphosphonium bromide (3.5 mg, 11.5 μmol, 1 equiv) was dissolved in 1 mL DMF and purged with N_2 for 5 min. Separately, 6-CO_2H Zinpyr1 (10 mg, 11.5 μmol, 1 equiv) and HATU (4.38 mg, 11.5 μmol, 1 equiv) were dissolved in 1mL of a 10% solution of DIPEA in anhydrous DMF. The 6-CO_2H ZP1-HATU solution was added and the resulting mixture stirred at room temperature for 1 hour, then was precipitated in 10 mL of cold (-40°C) diethyl ether and the resulting solid purified by HPLC on the semi-preparative scale using a C18 reverse-phase column (VYDAC, 9.5 mm × 250 mm). A two-solvent system (A = 0.1% (v/v) TFA in H_2O; B = 0.1% TFA in acetonitrile (v/v)) was employed as follows: isocratic flow, 10% B, 0-10 min; gradient, 10-50% B, 10-40 min. The flow-rate was kept at 3 mL min^{-1} throughout. Similar fractions were pooled and lyophilized, yielding ZP1-TPP as an orange solid (7.4 mg, 56% yield). Purity was assessed by analytical HPLC (Vydac, C18, 5 μm, 4.6 mm i.d. x 250 mm). After a 5 min isocratic wash, a 30-minute linear gradient of 5-60% B was run at 1 mL min^{-1}. ZP1-TPP (retention time = 24.2 min) was judged to be ≥ 95% pure based on the integrated chromatogram (Figure 2.4). ^{1}H NMR (DMSO-d_6, 300 MHz): δ 9.10 (1H, t), 8.58 (4H, d), 8.12 (1H, d), 8.03 (1H,d) 7.84 (15H, m), 7.65 (4H, m)

7.55 (1H, s), 7.45 (4H, d), 7.38 (4H, ψt), 6.66 (2H, s), 4.33 (8H, s), 4.25 (4H, s), 3.82 (2H, m), 3.58 (2H, m). ^{31}P NMR (DMSO-d_6, 300 MHz): δ 22.29 ppm. ESI-MS: observed (expected) M/Z for $[M+2H]^{2+}$ = 578.5 (578.1).

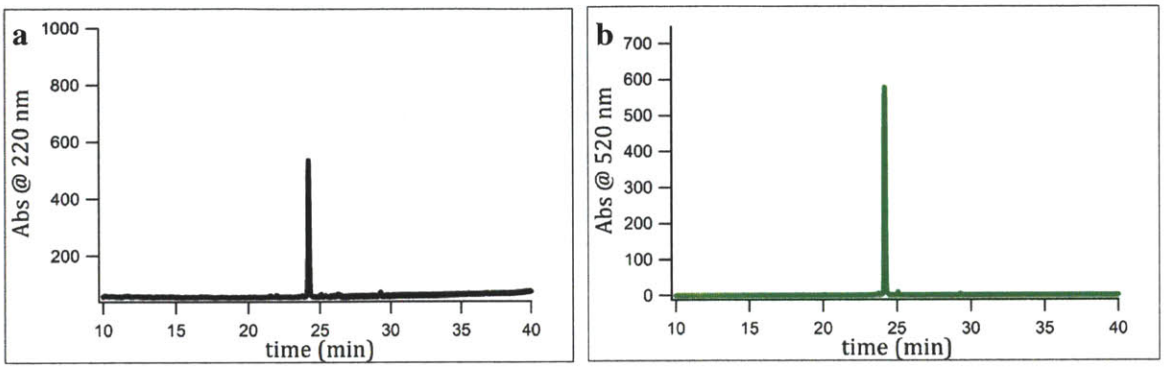

Figure 2.4. Analytical HPLC chromatogram of ZP1-TPP, monitoring at 220 nm (a) and 520 nm (b). ZP1-TPP was judged to be ≥ 95% pure based on the integrated absorbance signal.

Photophysical and Zinc-Binding Properties of ZP1-TPP. Spectroscopic measurements for ZP1-TPP were carried out in 50 mM PIPES buffer (pH 7) with 100 mM KCl. Except where noted, all fluorescence data were obtained by exciting at 495 nm and observing from 500-650 nm, with 0.1 sec integration time and slit widths of 0.4 mm (1.6 nm). Emission spectra represent the average of three scans. The extinction coefficient of ZP1-TPP was measured by serial dilution of an analytically prepared stock. The quantum yield of ZP1-TPP was referenced to fluorescein in 0.1 M $NaOH_{(aq)}$, which has a known quantum yield of $\Phi = 0.95$.[14]

Apparent $K_{d\text{-}Zn}$ for ZP1-TPP. Apparent zinc-binding affinities ($K_{d\text{-}Zn}$) were determined by a modified literature procedure.[15] For each zinc-binding titration, 1 mM EDTA and 2 mM $CaCl_2$ were added to the PIPES-buffered solution. ZP1-TPP was added, and the system was allowed to reach equilibrium (30 min). Aliquots of $ZnCl_2$ were successively added with care to maintain

---

[14] Lakowicz, J. R. *Principles of fluorescence spectroscopy*; 2nd ed.; Kluwer Academic/Plenum: New York, 1999.
[15] Walkup, G. K.; Burdette, S. C.; Lippard, S. J.; Tsien, R. Y. *J. Am. Chem. Soc.* **2000**, *122*, 5644.

overall dilution of less than 5%, and the emission spectra recorded once the sample stabilized (~30 min). For each data point, the amount of free zinc for that given concentration of total zinc was calculated using the maxchelator program (http://maxchelator.stanford.edu/webmaxc/webmaxcS.htm) based on initial values of 1 mM EDTA, 2mM $CaCl_2$, an ionic strength of I = 0.100 mol dm^{-3} , and a pH of 7.0. Collected data was then fit and the apparent $K_{d\text{-}Zn}$ of ZP1-TPP and ZP1 were compared.

pH-Dependence of ZP1-TPP Zinc-response. A series of sodium citrate/citric acid buffers were prepared to pH 4, 5, 6, and 7. ZP1-TPP was added and adjusted to a final concentration of 1 μM. After a 30 min equilibration period, emission spectra were recorded to establish baseline levels. 5 μM $ZnCl_2$ was then added to solution and the emission spectra recorded again. Data for all pH levels were normalized to the zinc-free, or *apo,* state.

Mammalian Cell Culture, Labeling, and Imaging Procedures. Human cervical cancer cells (HeLa) were cultured at 37 °C under a 5% CO_2 humidified atmosphere in Dulbecco's Modified Eagle Medium (High Glucose DMEM, Invitrogen) supplemented with 10% fetal bovine serum (FBS, HyClone), penicillin (100 μg/mL), and streptomycin (100 μg/mL). For live cell imaging, cells were seeded in 35-mm poly- D-Lys coated glass-bottom culture dishes (MatTek).

Fluorescence Microscopy. The imaging experiments were performed using a Zeiss Axiovert 200M inverted epifluorescence microscope equipped with an EM-CCD digital camera (Hamamatsu) and a MS200 XY Piezo Z stage (Applied Scientific Instruments). The light source was an X-Cite 120 metal-halide lamp (EXFO) and the fluorescence images were obtained using an oil-immersion objective at 63× magnification. The microscope was operated using Volocity software (Perkin-Elmer).

Quantification of Zinc Turn-On. Images were processed using ImageJ. All settings (i.e. exposure time, sensitivity, brightness, contrast) were kept constant for each image series.

Pearson's correlation coefficients (*r*). To calculate *r*, images were first deconvoluted using a calculated point-spread function (PSF) map based on emission wavelength, refractive index of the media (n = 1.518), and the numerical aperture (1.4). Deconvoluted channels (i.e. sensor and organelle trackers) were merged and analyzed. For each image, a minimum of three regions-of-interest (ROI) were selected and the *r*-value calculated using an ImageJ plugin.[16] This process was repeated for at least three cell areas from several different plates.

Cell sensitivity assay (MTT assay). Hela cells were cultured as described above, and then seeded into a 96 well plate. C343-TPP was added to each well to achieve final concentrations ranging from 1 nM to 100 μM. After a 24h incubation with C343-TPP, the wells were aspirated, refilled with media, and allowed to recover for 24h. The media was replaced with a 1.5 μM MTT solution in DMEM and incubated for 4h, after which the MTT solution was replaced with a 1:25 solution of ammonia hydroxide in DMSO. The plates were then imaged on a plate reader observing at 570 nm with replicate plates (n=6).

2.3. Results and Discussion

Synthesis and Characterization of Mitochondria-targeted Fluorophores

Previously, long alkyl linkers were used to separate the TPP and fluorophore.[17] Extensive photophysical characterization of ZP1-TPP showed that the ethyl linker provides sufficient separation to preserve desired sensor attributes. The TPP-conjugated ZP1-TPP had largely unaltered photophysical properties compared to those of the parent sensor, ZP1 (Table 2.1).

---

[16] French, A. P.; Mills, S.; Swarup, R.; Bennett, M. J.; Pridmore, T. P. *Nat. Protoc.* **2008**, *3*, 619.
[17] Xue, L.; Li, G.; Yu, C.; Jiang, H. *Chem. Eur.* **2012,** 18, 1050-1054.

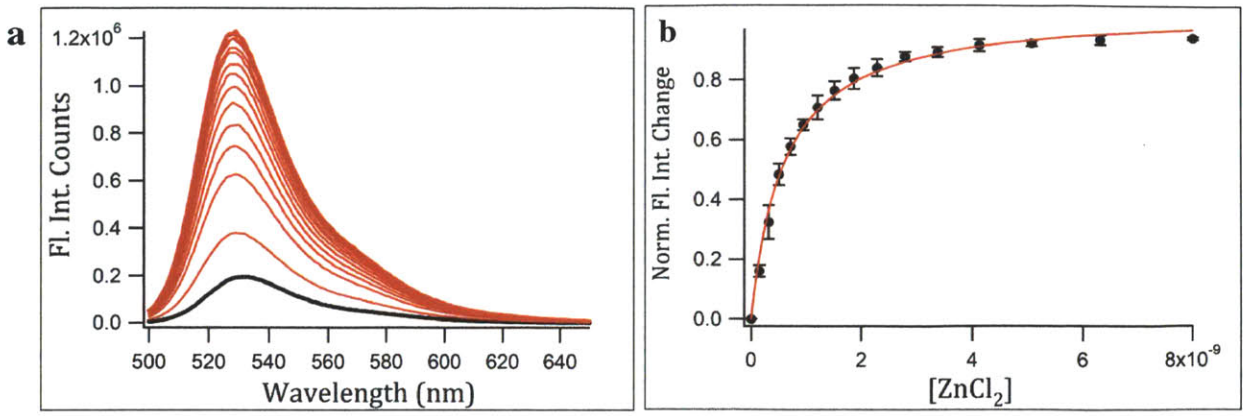

Figure 2.5. Measurement of the zinc-binding affinity, by fluorescence spectroscopy, of a 1 μM solution of ZP1-TPP in 50 mM PIPES buffer (pH 7) with 100 mM KCl. Observed changes in the emission spectra of ZP1-TPP (a) upon addition of increasing amounts of free zinc, with binding isotherm and fit (b). Apparent $K_{d\text{-}Zn}$ values are given in Table 2.1. Samples were excited at 470 nm with an emission window of 475-675 nm.

Sensor	λ_{abs} (nm), $\varepsilon \times 10^4$ ($M^{-1}cm^{-1}$)		Φ_{apo}	Φ_{Zn}	$K_{d\text{-}Zn}$ (M)[c]
	Apo	Zn(II)			
ZP1-TPP, [a]	519, 7.9	510, 8.6	0.15 ± 0.02	0.75 ± 0.03	$6.0(1) \times 10^{-10}$
ZP1[b]	515, 7.9	507, 8.4	0.38	0.87	7.0×10^{-10}

Table 2.1. Photophysical and zinc-binding properties of ZP1-TPP. [a] Spectroscopic data and apparent zinc dissociation constants ($K_{d\text{-}Zn}$) were determined in 50 mM PIPES buffer (pH 7) with 100 mM KCl. [b]Φ, absorption, ε, and $K_{d\text{-}Zn}$ values for ZP1 were taken from literature.[18]

In the absence of zinc, ZP1-TPP has a λ_{abs} = 519 nm and λ_{em} = 531 nm (Φ_{apo} = 0.15 ± 0.02) (Table 2.1). Upon addition of $ZnCl_2$, ZP1-TPP undergoes a characteristic blue shift in both absorbance and emission to λ_{abs} = 510 nm and λ_{em} = 528 nm, accompanied by a strong increase in fluorescence intensity (Φ_{apo} = 0.75 ± 0.03) (Table 2.1). The zinc-affinity of ZP1-TPP was measured in a CaEDTA buffered solution and found to be 0.6 ± 0.03 nM, a value that is within 15% of the free sensor zinc affinity (Figure 2.5). Conjugation of ZP1 to the TPP cation did not detract from ZP1 photophysics or zinc binding properties, and was also achieved with a simple,

[18] Nolan, E. M.; Lippard, S. J. *Acc. Chem. Res.* **2009**, *42*, 193

one-step coupling, in contrast to the lengthy syntheses required by some existing TPP-incorporating zinc sensors.[19]

Imaging of ZP1-TPP and Fl-TPP in Live HeLa Cells

To test the functionality of the TPP-conjugated sensors, HeLa cells were incubated with ZP1-TPP and Fl-TPP. Cells were also coincubated with MitoTracker Red FM, a commercially available mitochondrial dye, to quantify mitochondrial localization. Although ZP1-TPP was able to enter HeLa cells, ZP1-TPP stained the cells with bright punctate patterns distributed throughout the cytosol excluding the nucleus (Figure 2.6). Quantification of the overlay image of MitoTracker and ZP1-TPP signals shows poor colocalization between the two images ($r = -0.15 \pm 0.07$), indicating that ZP1-TPP does not localize to the mitochondria (Figure 2.6).

As a control, the 6-carboxyfluorescein version (Fl-TPP) was also synthesized and tested in HeLa cells under the same conditions. Fl-TPP consists of a TPP-conjugated fluorescein core without the two dipicolylamine (DPA) arms present in ZP1-TPP (Figure 2.1). Unlike the punctate staining patterns observed with ZP1-TPP, Fl-TPP was cell impermeable and did not stain the cells with any detectable patterns (Figure 2.7). Although carboxyfluorescein itself is membrane-impermeant and often used for extracellular applications, the conjugation of the TPP cation did not render the resulting construct membrane-permeable. At the physiological pH of 7.4, a significant proportion of fluorescein is in the dianionic state due to the acidity of the phenolic oxygen and carboxyl group, which has a pKa of ~6.8.[20] Because of the dianionic nature of fluorescein, Fl-TPP most likely exists as an anion, which detracts from its ability to passively diffuse across membranes and confines it to extracellular localization.

---

[19] Baek, N.Y.; Heo, C.H.; Lim, C.S.; Masanta, G.; Cho, B.R.; Kim, H.M. *Chem. Commun.* **2012**, 48, 4546-4548.
[20] Smith, S.A.; Pretorius, W.A. *Water SA.* **2002**, 28, 4, 395.

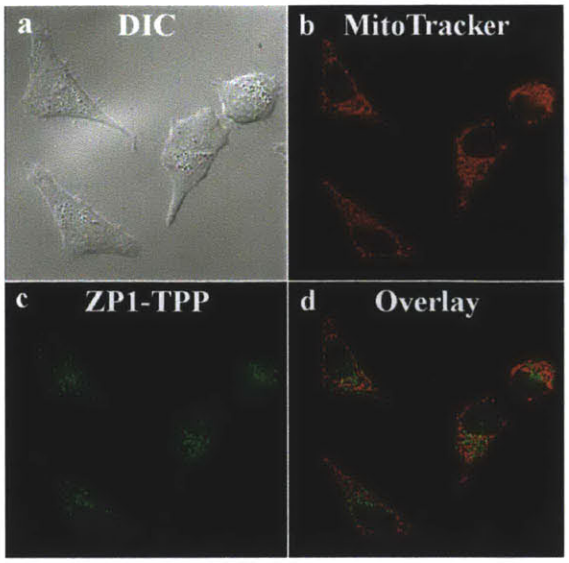

Figure 2.6. Fluorescence microscope images depicting uptake and localization of ZP1-TPP in live HeLa cells. (a) Differential interference contrast (DIC) image. (b) Signal from mitochondria dye MitoTracker Red FM. (c) Signal from ZP1-TPP (d) Overlay of (b) and (c). Pearson's correlation coefficient r = -0.15 ±0.07.

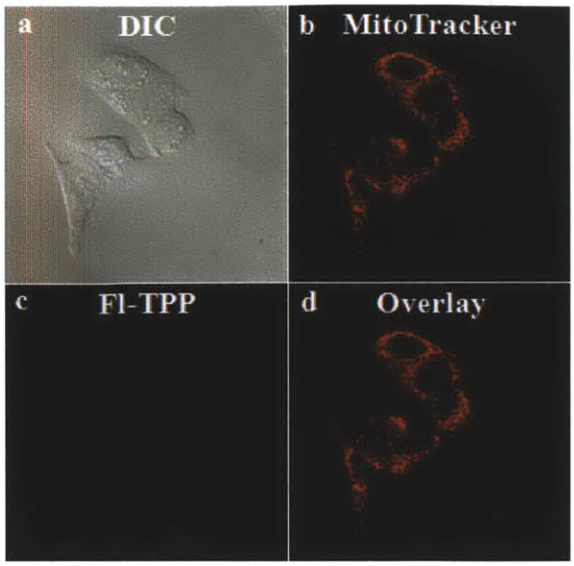

Figure 2.7. Fluorescence microscope images depicting uptake and localization of Fl-TPP in live HeLa cells. (a) Differential interference contrast (DIC) image. (b) Signal from mitochondria dye MitoTracker Red FM. (c) Signal from Fl-TPP (d) Overlay of (b) and (c).

However, this restriction is not observed with ZP1-TPP even though ZP1 also has anionic phenol and carboxyl groups. In ZP1, the two chlorine atoms on the 4'- and 5'-positions of the fluorescein ring lower the phenolic pK_a.[21] The two tertiary amines on the DPA arms are partially protonated at pH 7.4 due to protons binding the zinc-binding pockets formed by the DPA arms and phenolic oxygens. Speciation plots for pH titrations of ZP1 show that a mixture of neutral and singly anionic species is predominant at pH 7.[22] The 6-carboxyl group is not considered in discussion of the overall charge because it is used to conjugate the sensor and TPP via amide linkage. Because conjugation to TPP adds an additional positive charge, ZP1-TPP has an overall positive or neutral charge (Figure 2.8).

---

[21] Walkup, G.K.; Burdette, S.C.; Lippard, S.J.; Tsien, R.Y. *J. Am. Chem. Soc.* **2000**, 122, 5644-5645.
[22] Wong, B.A.; Friedle, S.; Lippard, S.J. *J. Am. Chem. Soc.* **2009**, 131, 7142-7152.

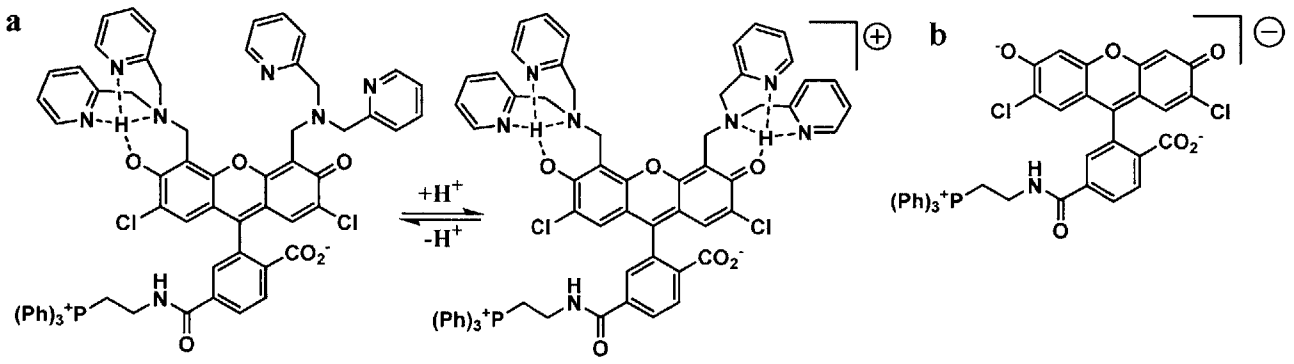

Figure 2.8. Protonation states of ZP1-TPP and Fl-TPP at physiological pH. (a) Predominant neutral and positively-charged states of ZP1-TPP at pH 7.4 due to partial or complete protonation of the zinc-binding pockets. (b) Fl-TPP predominately assumes a negatively-charged state due to the acidic 2-carboxyl and phenol groups.

Evidence for Endocytic Pathways of ZP1-TPP Uptake and Trapping

Although ZP1-TPP was able to enter and stain cells with a punctate pattern, ZP1-TPP was unresponsive to addition of $ZnCl_2$. The ionophore pyrithione was added to assist uptake of $ZnCl_2$. In contrast to the ~4-fold turn-on of the free ZP1 sensor in HeLa cells (Figure 2.9a), the turn-on of ZP1-TPP upon addition of $ZnCl_2$ was not statistically significant. The punctate pattern of ZP1-TPP and lack of zinc-responsiveness suggested that ZP1-TPP could be sequestered in late-stage endosomes or lysosomes. Late-stage endosomes are acidified by the continuous activity of proton pumps and eventually fuse with lysosomes. Because the interior of lysosomes and late-stage endosomes are moderately acidic around pH 5-5.5, [23] ZP1 fluorescence increases due to DPA protonation, which attenuates PeT quenching of the fluorescein.[22] This behavior results in a greatly reduced difference in fluorescence signal between the initial and zinc-bound states. Furthermore, *in vitro* ZP1-TPP titrations show that as the pH is lowered, the initial fluorescence increases due to protonation of the DPA arms (Figure 2.9b). At pH 5, the higher initial fluorescence of protonated ZP1-TPP significantly reduces the magnitude of zinc-responsive turn-on upon addition of zinc (Figure 2.9b).

---

[23] Geisow, M.J.; Evans, W.H. *Exp. Cell Res.* **1984**, 150, 36-46.

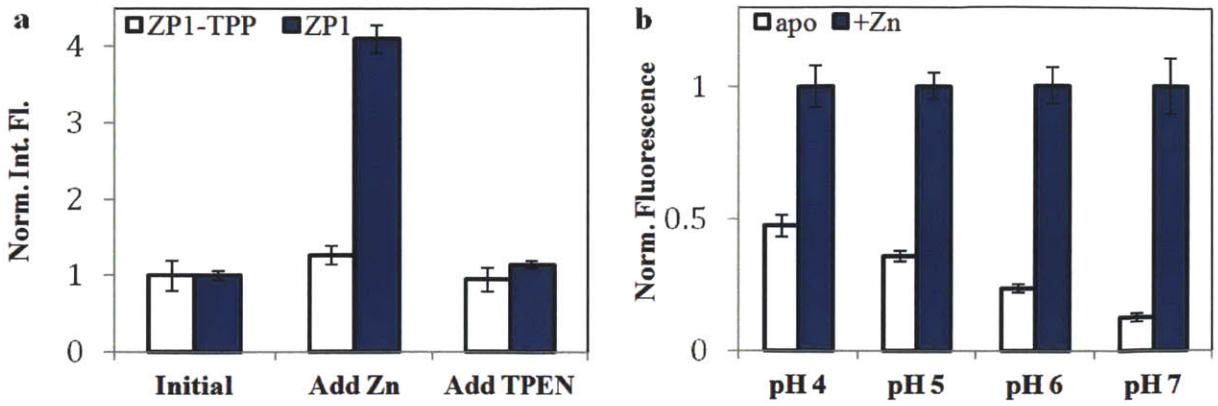

Figure 2.9. ZP1-TPP turn-on in live HeLa cells and ZP1-TPP pH dependency *in vitro*. (a) Comparison of zinc-responsive turn-on of ZP1-TPP and ZP1 in live HeLa cells showing significantly reduced zinc-response. (b) pH sensitivity of the ZP1-TPP *apo* state caused by protonation of the DPA tertiary amine.

To further investigate the localization of ZP1-TPP, HeLa cells were incubated with both ZP1-TPP and LysoTracker Red, a pH-sensitive dye that can readily diffuse across membranes but becomes trapped upon protonation in acidic compartments such as late-stage endosomes or lysosomes.[24] Quantification of the images reveals that ZP1-TPP and LysoTracker Red colocalize strongly with a Pearson's correlation coefficient of $r = 0.45 \pm 0.15$ (Figure 2.10). As seen in some of the green punctate patterns in the overlaid image (Figure 2.10d), the ZP1-TPP signal in early to mid-stage endosomes does not correlate well with that from LysoTracker Red because the latter fluoresces only under acidic conditions.[24]

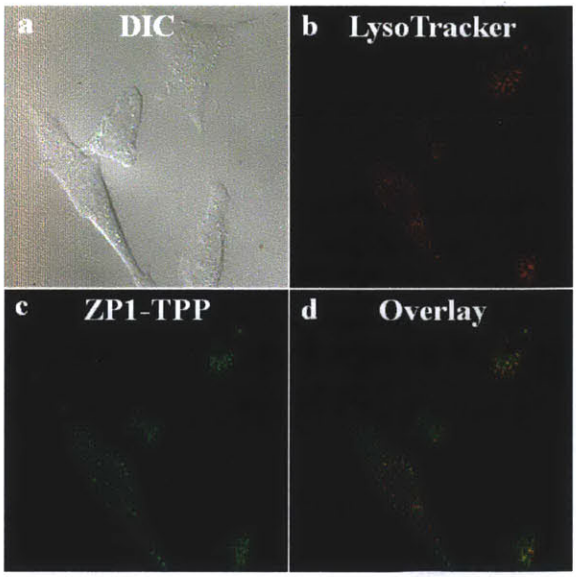

Figure 2.10. Lysosomal localization of ZP1-TPP in live HeLa Cells. (a) Differential interference contrast (DIC) image. (b) Signal from lysosome-specific dye LysoTracker. (c) Signal from ZP1-TPP. (d) Overlay of (b) and (c). Pearson's correlation coefficient r = 0.45 ± 0.15.

To further verify the endocytic pathway of ZP1-TPP uptake and subsequent

[24] Invitrogen, LysoTracker and LysoSensor Probes Manual. **2007**

localization to lysosomes and late-stage endosomes, HeLa cells were incubated with ZP1-TPP at 4°C. Cells incubated with ZP1-TPP and MitoTracker at 4°C did not show uptake of ZP1-TPP, but exhibited normal uptake and localization of MitoTracker. Because MitoTracker is transported by gradient-assisted diffusion,[25] MitoTracker uptake and localization are not affected by the lower incubation temperature. The lack of any ZP1-TPP signal in cells incubated at 4°C indicated no significant uptake of ZP1-TPP, suggesting that the mechanism of uptake was energy-dependent, which is consistent with an endocytic uptake pathway.

Imaging of C343-TPP in Live HeLa Cells

The inability of ZP1-TPP to escape endosomes and lysosomes suggests that ZP1-TPP may not be membrane-permeable due to size, charge, or hydrophobicity properties. To explore this possibility, the coumarin 343 (C343) analog of ZP1-TPP was created. Coumarin 343 is smaller than 6-CO_2H ZP1, more hydrophobic, and neutral at physiological pH, although it is also less bright than fluorescein-based fluorophores. Conjugation of C343 to TPP results in a targeted fluorophore with greater cationic nature than ZP1-TPP.

As seen in Figure 2.11, the free C343 fluorophore is not membrane-permeable due to the anionic carboxylate present in C343. In contrast, conjugation of TPP to C343 results in a mitochondria-targeted fluorophore construct. C343-TPP strongly localizes to the mitochondria, as evidenced by the correlation between C343-TPP and MitoTracker (Pearson's correlation coefficient $r = 0.72 \pm 0.02$) (Figure 2.11). The incubation concentrations were lowered to 0.25 μM for C343-TPP from previously used concentrations because of cytotoxicity at higher concentrations.

---

[25] Invitrogen, MitoTracker Mitochondrion-Selective Probes Manual. **2008**

The observed cytotoxicity also prompted further investigation into dose-dependent survivability of HeLa cells exposed to C343-TPP. As reported in literature, accumulation of excessively high concentrations of TPP cations in the matrix causes permeabilization of the inner mitochondrial membrane, resulting in mitochondrial swelling and loss of potential across that membrane via permeabilization.[26] In addition, TPP cations in the matrix cause the rapid generation of a large amount of reactive oxygen species (ROS) such as hydrogen peroxide.[25] Because of the concentrating effect of the large potential across the inner mitochondrial membrane, TPP cations can be concentrated in the mitochondria by up to four orders of magnitude.[26] In agreement with this proposed mechanism of toxicity, a diffuse cytosolic and nuclear staining pattern was observed at any C343-TPP incubation concentrations above 1 μM.

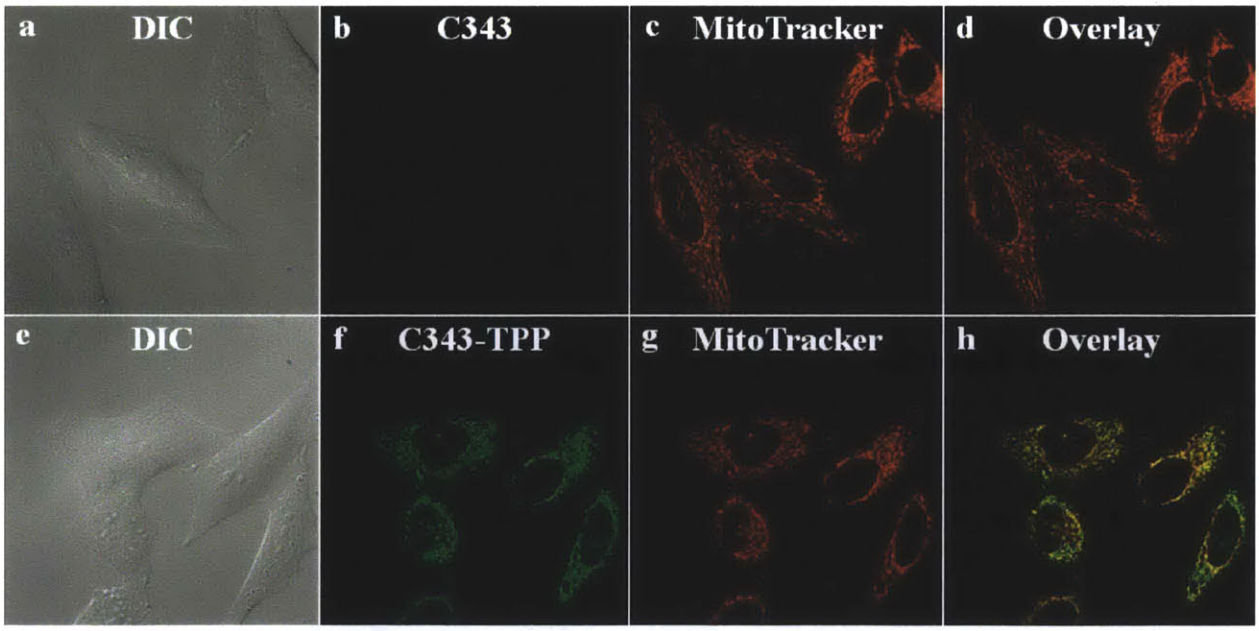

Figure 2.11. Effects of TPP conjugation on coumarin 343 localization. (a)-(d) 5 μM coumarin 343 without conjugation to the TPP moiety does not enter live HeLa cells. (e)-(h) Conjugation of TPP to coumarin 343 results in uptake of C343-TPP (0.25 μM) into live HeLa cells and subsequent mitochondrial localization. Pearson's correlation coefficient $r = 0.72 \pm 0.02$.

---

[26] Ojovan, S.M.; Knorre, D.A.; Markova, O.V.; Smirnova, E.A.; Bakeeva, L.E.; Severin, F.F. *J. Bioenerg. Biomembr.* **2011**, 43, 175-180.

At incubation concentrations of 1 μM, the concentration effect of mitochondrial membrane potential could generate C343-TPP concentrations of as high as 10 mM within the mitochondria, leading to swelling and permeabilization.[26] After C343-TPP escape from the mitochondria, C343-TPP is able to stain the cytsol and diffuse across the nuclear membrane into the nucleus because of its small size. A more quantitative measure of C343-TPP cytotoxicity was obtained by measuring the dose-dependent percent survivability of HeLa cells by an MTT assay (Figure 2.12). Survivability was measured via reduction of MTT by live cells, resulting in signal measurable by UV-vis absorbance. The IC_{50} of C343-TPP was found to be 386 ± 33 nM.

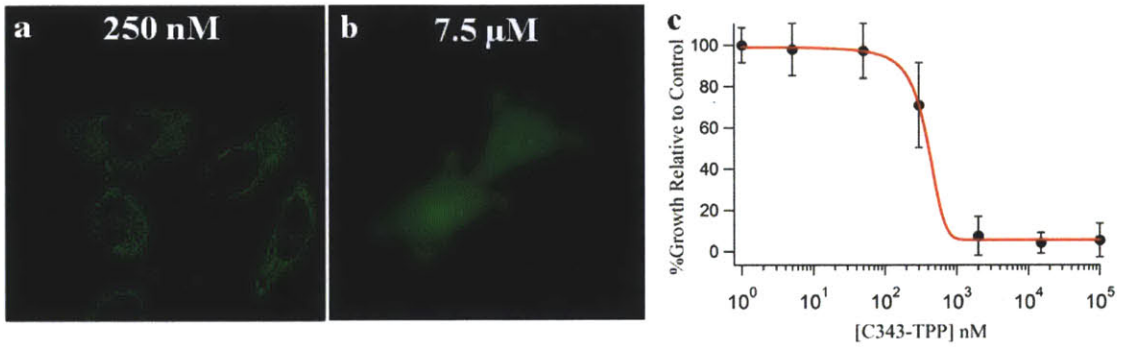

Figure 2.12. Cytotoxicity of C343-TPP in HeLa cells. Comparison of localization at (a) 250 nM and (b) 7.5 μM C343-TPP incubation concentrations. (c) Dose-response curve of HeLa cells incubated with varying concentrations of C343-TPP. C343-TPP IC_{50} = 386 ± 33 nM.

2.4 Conclusions

The lipophilic triphenylphosphonium cation (TPP) was conjugated to several different sensors and fluorophores. These constructs provided insight into the cellular transport and uptake processes of small-molecule targeted compounds. Fluorescein-TPP (Fl-TPP) did not stain the cells significantly, most likely as a consequence of the overall negative charge of the construct. On the other hand, ZP1-TPP, which is overall neutral or positively charged at physiological pH, was able to enter the cell, although it localized to lysosomes and late-stage endosomes instead of

mitochondria. In addition, ZP1-TPP sequestered in lysosomes and late-stage endosomes exhibited severely attenuated zinc-responsive turn-on due to the acidic environment constitutively turning on the fluorescein scaffold. ZP1-TPP is not readily membrane-permeable and instead relies mostly on endocytic transport to enter cells, as suggested by the energy-dependent nature of the uptake process and colocalization to lysosome trackers. Nevertheless, conjugation to TPP itself does not negatively affect sensor properties, and ZP1-TPP has similar photophysical and zinc-binding properties to free ZP1.

Coumarin 343 was then selected for further studies of the uptake and transport process due to its smaller size, greater lipophilicity, and neutral charge. The resulting C343-TPP construct stained mitochondria in HeLa cells at sub-micromolar incubation conditions. C343-TPP strongly correlated to MitoTracker Red FM as determined by Pearson's correlation coefficient of the signal overlay. Due to the concentrating effects of the potential across the mitochondrial inner membrane, incubations of C343-TPP in excess of 1 μM caused toxic accumulations of the cation due to mitochondrial swelling and rupture resulting in diffuse staining. The LC_{50} of C343-TPP was found to be 386 ± 33 nM by MTT survivability assay.

Proper uptake and localization of C343-TPP indicate that the inability of ZP1-TPP to reach mitochondria and escape the endosome could be due to larger size, decreased hydrophobicity, and decreased cationic nature of ZP1-TPP. Since conjugation of the targeting moiety to the 6-carboxy position of 6-CO_2H ZP1 does not detract from sensor photophysics and zinc-binding properties, a fully functional mitochondrial zinc sensor can be achieved by altering the construct or switching the sensor to achieve smaller size or greater lipophilicity. Application of a generalizable chemical modification to ZP1-TPP resulting in successful localization and dramatic improvements in photophysics is outlined in Chapter 4.

CHAPTER 3. Peptide-based Targeting of Fluorescent Zinc Sensors to the Plasma Membrane and Intracellular Targets in Live Cells

3.1. Introduction

Because of the biological importance of mobile zinc in various cellular locations including the synapse, cell vesicles, and mitochondria, it is highly desirable to develop a series of zinc sensors with different properties and targeted locations. As discussed in Chapter 1, a peptide-based approach offers great promise for easily customizable targeted sensor design and synthesis. In addition to the photophysical and zinc-binding tunability benefits retained from small molecule sensors, peptide-based sensors can be biocompatible and more specifically targeted relative to the individual small-molecule sensors. In comparison to the restrictions of small molecule targeting moieties to single location targeting such as the mitochondria-targeting TPP ion (Chapter 2), peptide-based zinc probes have no such restriction and can be easily adapted to specifically target a variety of locations. The ability to change the target of peptide-sensor constructs is described in this chapter by using peptides to target sensors to both extracellular and intracellular locations.

Peptides are easy to assemble reliably through solid phase peptide synthesis (SPPS), a technique pioneered by Merrifield in 1963.[1] SPPS employs a resin scaffold for sequential addition of amino acid residues with protected *N*-termini to ensure single addition. Stepwise addition and deprotection of amino acids allow the preparation of peptides with high yield, although yields begin to suffer at longer residue lengths because of the compounding effects of sequential addition errors.

Synthesis of peptide-based sensors provides multiple methods and attachment sites for sensors, fluorophores, or additional targeting moieties. Sensors can be incorporated through conjugation to the *N*-terminus of the completed peptide, addition to nucleophilic side chains, or

---

[1] Merrifield, R.B. *J.Am. Chem. Soc.* **1963**, 85, 2149-2154.

incorporation in the middle of the sequence through the use of unnatural amino acids. Orthogonal protecting groups on side chains allow site-selective attachment of probes or targeting moieties at any point along the peptide sequence. This orthogonal protection allows each peptide to have multiple points of attachment and readily accommodate a variety of conjugated sensors or other moieties.

Conjugation of payloads to peptides with specific physical properties offers improved uptake and localization. These sequences, often known as cell-penetrating peptides (CPP), enhance the uptake of the peptide and payload into the cell.[2] The majority of reported CPP constructs are thought to enter cells either through direct translocation across the membrane or through the endocytic pathway and subsequent escape from the endosomes.[3] Potential enhancement of sensor uptake and specific localization as a result of conjugation to CPPs would improve signal-to-noise ratio and spatial information obtained by the probe.

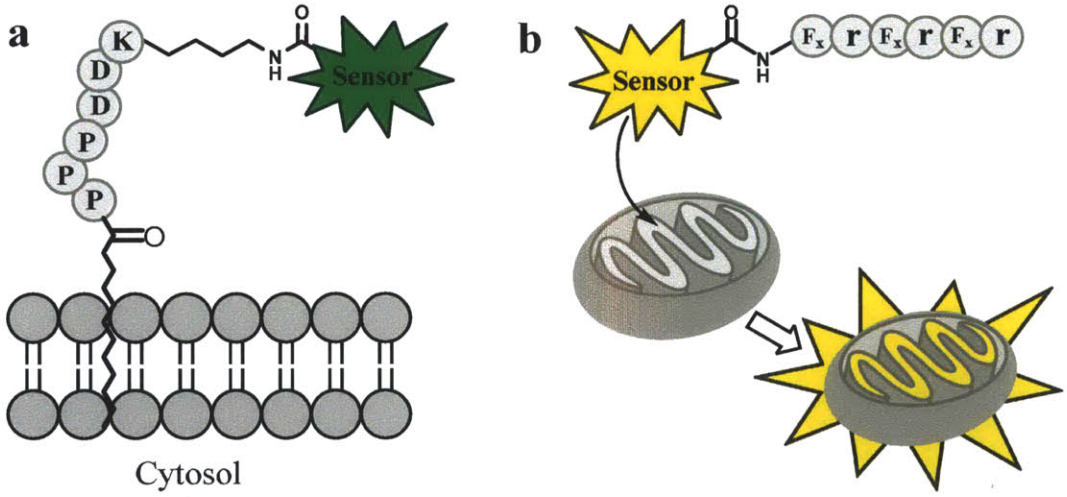

Figure 3.1. Targeting of zinc sensors to specific locations using peptides. (a) Extracellular plasma membrane zinc sensor consisting of anionic peptide with palmitoylated *N*-terminus and lysine-conjugated sensor. (b) Intracellular sensor targeted to the mitochondria by *N*-terminus conjugation to a mitochondria-penetrating peptide.

---

[2] Stewart, K.M.; Horton, K.L.; Kelley, S.O. *Org. Biomol. Chem.*. **2008**, 6, 2242-2255.

[3] (a)Trabulo, S.; Cardoso, A.L.; Mano, Miguel.; Pedroso de Lima, M.C. *Pharmaceuticals*, **2010**, 3, 961-993. (b) El-Sayed, A.; Khalil, I.A.; Kogure, K.; Futakl, S.; Harashima, H. *J. Biol. Chem.* **2008**, 283, 23450-23461.

To take advantage of the benefits and flexibility of SPPS for sensor synthesis, two different cell locations were targeted because of the biological importance of mobile zinc in those areas. The first location, the exterior surface of the cell plasma membrane, was selected to develop tools for investigation of mobile zinc in secretory tissues such as the release of zinc into the synapse.[4] A short, anionic peptide was designed to be a membrane-impermeant scaffold for attachment of a zinc sensor and a palmitoyl targeting moiety was attached to promote insertion into the plasma membrane (Figure 3.1a). In contrast, the second target was intracellular; peptide-sensor constructs were targeted to the mitochondria, where mobile zinc is thought to play a significant role in prostate cancer.[5] Several cationic CPPs conjugated to fluorophores and sensors were utilized to target uptake and delivery to the mitochondria (Figure 3.1b). In both cases, the modularity of SPPS and the spatial localization of the resulting constructs were harnessed to rapidly generate sensors targeted to different cell locations.

3.2 Materials and Methods

General Considerations

HPLC grade acetonitrile, anhydrous *N,N*-dimethylformamide (DMF), dichloromethane, 4-methylpiperidine, *N,N*-diisopropylethylamine (DIPEA), trifluoroacetic acid (TFA), triisopropylsilane, and palmitic acid were purchased from Sigma-Aldrich. FMOC-Pro-OH, FMOC-Asp(OtBu)-OH, and Rink amide AM resin (0.61 mmol/g, 100-200 mesh) were obtained from Novabiochem. FMOC-Lys(MTT)-OH, FMOC-F_x-OH (FMOC-Cha-OH), and the D-isomer of FMOC-Arg(Pbf)-OH were purchased from Aapptec. 2-(7-Aza-1H-benzotriazole-1-yl)-1,1,3,3-

---

[4] (a) Kay, A.R.; Toth, K. *Sci. Signal.* **2008**, 1:re3. (b) Sensi, S.L.; Paoletti, P.; Bush, A.I.; Sekler, I. *Nat. Rev. Neurosci.* **2009**, 10, 780-791.(c) Takeda, A.; Tamano, H. *Nat. Brain Res. Rev.* **2009**, 62, 33-44.

[5] (a) Costello, L. C.; Franklin, R. B.; Feng, P. *Mitochondrion* **2005**, *5*, 143 (b) Costello, L. C.; Franklin, R. B. *J. Biol. Inorg. Chem.* **2011**, *16*, 3.

tetramethyluronium hexafluorophosphate (HATU) was procured from Oakwood Chemicals. *N*-(6-Methoxy-8-quinolyl)-*p*-toluenesulfonamide (TSQ) was acquired from Enzo Life Sciences. Disposable 2.5-mL reaction vessels were ordered from Torviq. All solvents were reagent grade unless otherwise specified, and commercially available reagents were used as received. 6-CO_2H ZP1[6] and Zinquin acid[7] were prepared according to literature procedures. Buffers, purification, characterization, and spectroscopy techniques were similar to those outlined in chapter 2.

Peptide-Sensor Construct Synthesis Materials and Methods

Peptides were manually synthesized according to a modified literature protocol[8] as outlined below. Table 3.1 provides a list of peptide sequences, sensors and fluorophores, and other conjugations for selected intracellular peptide-sensor constructs.

Name	Peptide Sequence	Conjugation to *N*-Terminus	Conjugation to ε-NH_2
Palm-ZP1	PPPDDK*	Palmitic Acid	6-CO_2H ZP1
Palm-ZQ	PPPDDK*	Palmitic Acid	Zinquin Acid
ZQ-MPP	$F_xrF_xrF_xr$	Zinquin Acid	-
ZP1-MPP	$F_xrF_xrF_xr$	6-CO_2H ZP1	-
C343-MPP	$F_xrF_xrF_xr$	coumarin 343	-
DCF-MPP	F_xrF_xK	6-CO_2H DCF	-
ZP1-R_9	RRRRRRRRR	6-CO_2H ZP1	-
ZP1-Tat	GRGRKKRRQRRPPQ	6-CO_2H ZP1	-

Table 3.1. List of selected peptide-sensor constructs detailing name, peptide sequence, and conjugated sensors and targeting moieties. Amino acid residues marked with an asterisk (*) denotes residues with sensors coupled to their ε-amine groups. 6-carboxy-2,7,-dichlorofluorescein is abbreviated 6-CO_2H DCF.

---

[6] (a) Woodroofe, C. C.; Masalha, R.; Barnes, K. R.; Frederickson, C. J.; Lippard, S. J. *Chem. Biol.* **2004**, *11*, 1659. (b) Nolan, E. M.; Lippard, S. J. *Acc. Chem. Res.* **2009**, *42*, 193.

[7] Fahrni, C. J.; O'Halloran, T. V. *J. Am. Chem. Soc.* **1999**, *121*, 11448.

[8] Kirin, S. I.; Noor, F.; Metzler-Nolte, N.; Mier, W. *J. Chem. Educ.* **2007**, *84*, 108.

Palm-ZP1 (Palmitic acid-PPPDDK(ZP1)-CONH$_2$). Palm-ZP1 was synthesized on the 15-μmol scale using Rink amide AM resin in a fritted 2.5-mL syringe. The resin was swelled for 1 hour in 2 mL of anhydrous DMF. *N*-terminal FMOC groups were removed by shaking resin with 20% 4-methylpiperidine in DMF (v/v) for 10 min, followed by a 5 × 1.5 mL wash with DMF. For coupling reactions, 60 μmol (4 equiv) of FMOC-protected amino acids or fluorophore were combined as solids with 60 μmol (23 mg) of HATU, were dissolved in 1.5 mL of freshly prepared 10% DIPEA/DMF (v/v) solution, and shaken for 25 min. After coupling, the resin was washed with 5 × 1.5 mL of DMF. Following addition of all amino acids and the *N*-terminal palmitic acid moiety, the 4-methyltrityl group was removed from the *C*-terminal Lys as follows. The resin was first immersed in dichloromethane (DCM). A 3% TFA/DCM (v/v) solution was prepared, and the resin was mixed with the TFA/DCM mixture 2 × 1.5 mL for 10 min/ea. After MTT deprotection, the resin was washed with 5 × 1.5 mL DCM followed by 5 × 1.5 mL DMF. 6-CO_2H ZP1 was then coupled to the ε-amino group of the *C*-terminal Lys as described above. Following Palm-ZP1 synthesis, the resin was washed with 5 × 1.5 mL DCM and dried *in vacuo*. Palm-ZP1 was cleaved from the resin by treating with a TFA/water/triisopropylsilane 95/2.5/2.5% (v/v) solution for 90 min. The resulting crude peptide was purified by HPLC on the semi-preparative scale using a C18 reverse-phase column (VYDAC, 9.5 mm × 250 mm). Purification conditions are summarized in Table 3.2. Purity was assessed by analytical HPLC (Vydac, C18, 5 μm, 4.6 mm i.d. x 250 mm, Table 3.2). Palm-ZP1 (retention time = 31.2 min) was judged to be ≥ 95% pure based on the integrated chromatogram (Figure 3.2). Observed peaks (calculated) in ESI-MS (m/z, amu): 1755.8 (1755.9) $[M+H]^+$; 878.2 (878.5) $[M+2H]^{2+}$.

Palm-ZQ (Palmitic acid-PPPDDK(ZQ)-CONH$_2$). Palm-ZQ was synthesized on the 15-μmol scale in a procedure similar to that used for Palm-ZP1, with the exception that 60 μmol (23

mg) of Zinquin acid was coupled to the ε-amino group of the *C*-terminal Lys for 60 min. The resin was then washed, cleaved, and purified via HPLC (conditions listed in Table 3.2). The purity of the final product was assessed by analytical HPLC (Table 3.2). Palm-ZQ (retention time = 38.6 min) was judged to be ≥ 90% pure at all wavelengths based on the integrated chromatogram (Figure 3.2). Observed peaks (calculated) in ESI-MS (m/z; amu): 1295.7 (1296.2) $[M+Na]^+$, 1274.0 (1274.2) $[M+H]^+$.

ZQ-MPP (ZQ-F_xrF_xrF_xr-$CONH_2$). ZQ-MPP was synthesized on the 15-μmol scale in a procedure similar to that used for Palm-ZP1. 60 μmol (23 mg) of Zinquin acid was conjugated to the *N*-terminus as described for ZQ-MPP, after which the resin was washed, cleaved, and purified by HPLC (conditions in Table 3.2). The purity of the final product was assessed by analytical (Table 3.2). ZQ-MPP (retention time = 14.7 min) was judged to be ≥ 95% pure based on the integrated chromatogram (Figure 3.2). Observed peaks (calculated) in ESI-MS (m/z; amu): 1313.9 (1313.8) $[M+H]^+$; 657.7 (657.4) $[M+2H]^{2+}$, 438.8 (438.9) $[M+3H]^{3+}$.

ZP1-MPP (ZP1-F_xrF_xrF_xr-$CONH_2$). ZP1-MPP was synthesized on the 15-μmol scale in a procedure similar to that used for Palm-ZP1. 60 μmol (52 mg) of 6-CO_2H ZP1 were conjugated to the *N*-terminus as described for ZQ-MPP, after which the resin was washed, cleaved, and purified by HPLC (conditions in Table 3.2). The purity of the final product was assessed by analytical HPLC (Table 3.2). ZP1-MPP (retention time = 14.7 min) was judged to be ≥ 95% pure based on the integrated chromatogram (Figure 3.2). Observed peaks (calculated) in ESI-MS (m/z; amu): 1796.0 (1795.8) $[M+H]^+$; 898.5 (898.4) $[M+2H]^{2+}$.

DCF-MPP (DCF-F_xrF_xK-$CONH_2$. DCF-MPP was synthesized on the 15-μmol scale in a procedure similar to that used for Palm-ZP1. 60 μmol (27 mg) of 5(6)-carboxy-2,7-dichlorofluorescein were conjugated to the *N*-terminus as described for ZQ-MPP, after which the

resin was washed, cleaved, and purified via HPLC (conditions in Table 3.2). The purity of the final product was assessed by analytical HPLC (Table 3.2). DCF-MPP (retention time = 20.2 min) was judged to be ≥ 95% pure based on the integrated chromatogram (Figure 3.3). Observed peaks (calculated) in ESI-MS (m/z; amu): 1034.7 (1034.9) $[M+H]^+$; 517.9 (518.0) $[M+2H]^{2+}$.

C343-MPP (C343-$F_xrF_xrF_xr$-$CONH_2$). C343-MPP was synthesized on the 15-μmol scale in a procedure similar to that used for Palm-ZP1. 60 μmol (27 mg) of coumarin 343 were conjugated to the *N*-terminus as described for ZQ-MPP, after which the resin was washed, cleaved, and purified via HPLC (conditions in Table 3.2). The purity of the final product was assessed by analytical HPLC (Table 3.2). C343-MPP (retention time = 18 min) was judged to be ≥ 95% pure based on the integrated chromatogram (Figure 3.3). Observed peaks (calculated) in ESI-MS (m/z; amu): 1212.8 (1212.4) $[M+H]^+$; 607.1 (606.7) $[M+2H]^{2+}$, 405.3 (404.8) $[M+3H]^{3+}$.

ZP1-R_9 (ZP1-RRRRRRRRR-$CONH_2$). ZP1-R_9 was synthesized on the 15-μmol scale in a procedure similar to that used for Palm-ZP1. 60 μmol (52 mg) of 6-CO_2H ZP1 was conjugated to the *N*-terminus as described for ZQ-MPP, after which the resin was washed, cleaved, and purified via HPLC (conditions in Table 3.2). The purity of the final product was assessed by analytical HPLC (Table 3.2). ZP1-R_9 (retention time = 15.8 min) was judged to be ≥ 99% pure based on the integrated chromatogram (Figure 3.3). Observed peaks (calculated) in ESI-MS (m/z; amu): 1136.6 (1136.55) $[M+2H]^{2+}$; 758.5 (758.03) $[M+3H]^{3+}$, 569.1 (568.8) $[M+4H]^{4+}$.

ZP1-Tat (ZP1- GRGRKKRRQRRPPQ-*$CONH_2$).* ZP1-TAT was synthesized on the 15-μmol scale in a procedure similar to that used for Palm-ZP1. 60 μmol (52 mg) of 6-CO_2H ZP1 were conjugated to the *N*-terminus as described for ZQ-MPP, after which the resin was washed, cleaved, and purified via HPLC (conditions in Table 3.2). The purity of the final product

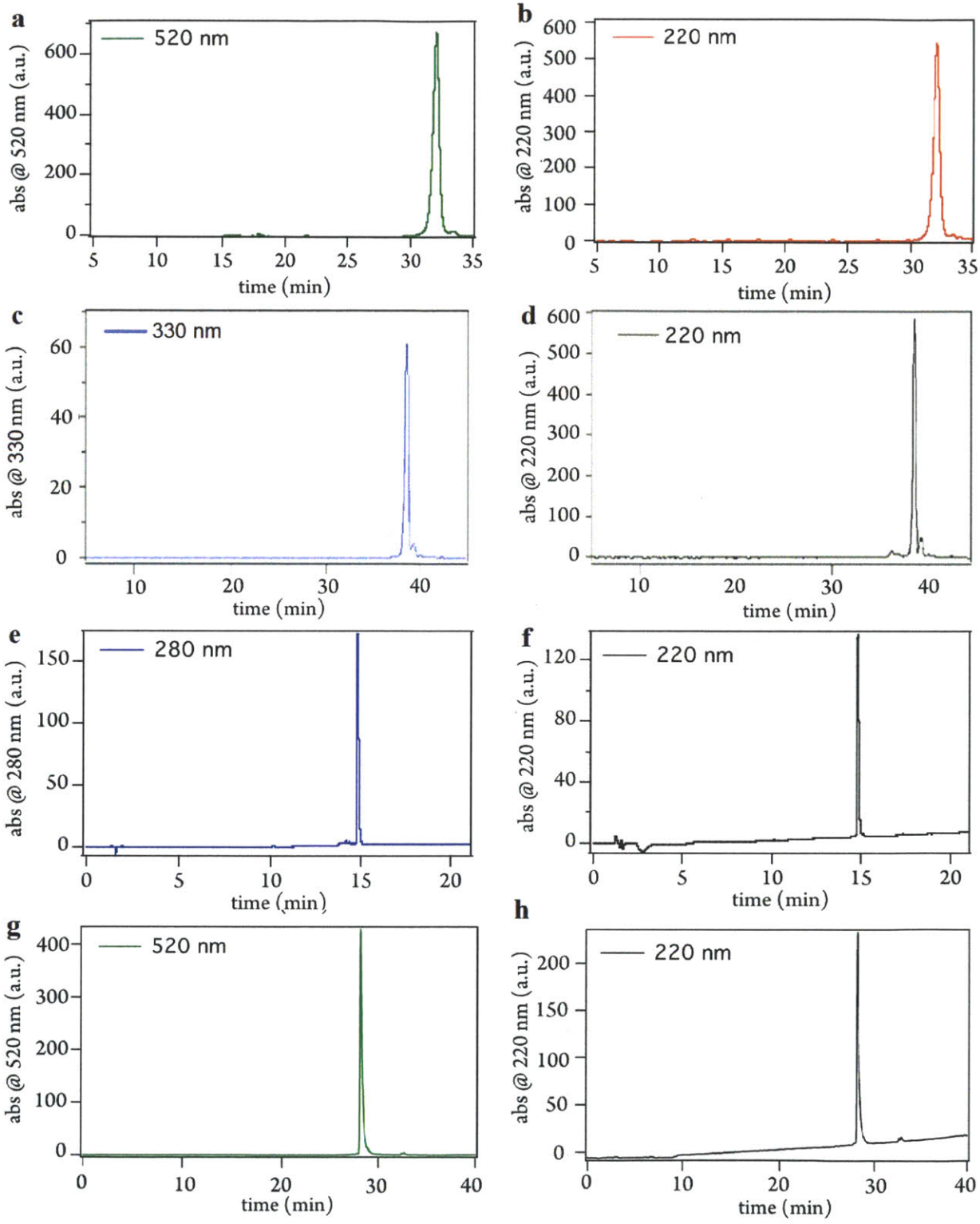

Figure 3.2. Analytical HPLC chromatograms of peptide-sensor constructs. Analytical HPLC chromatograms of (a-b) Palm-ZP1, (c-d) Palm-ZQ, (e-f) ZQ-MPP, (g-h) ZP1-MPP.

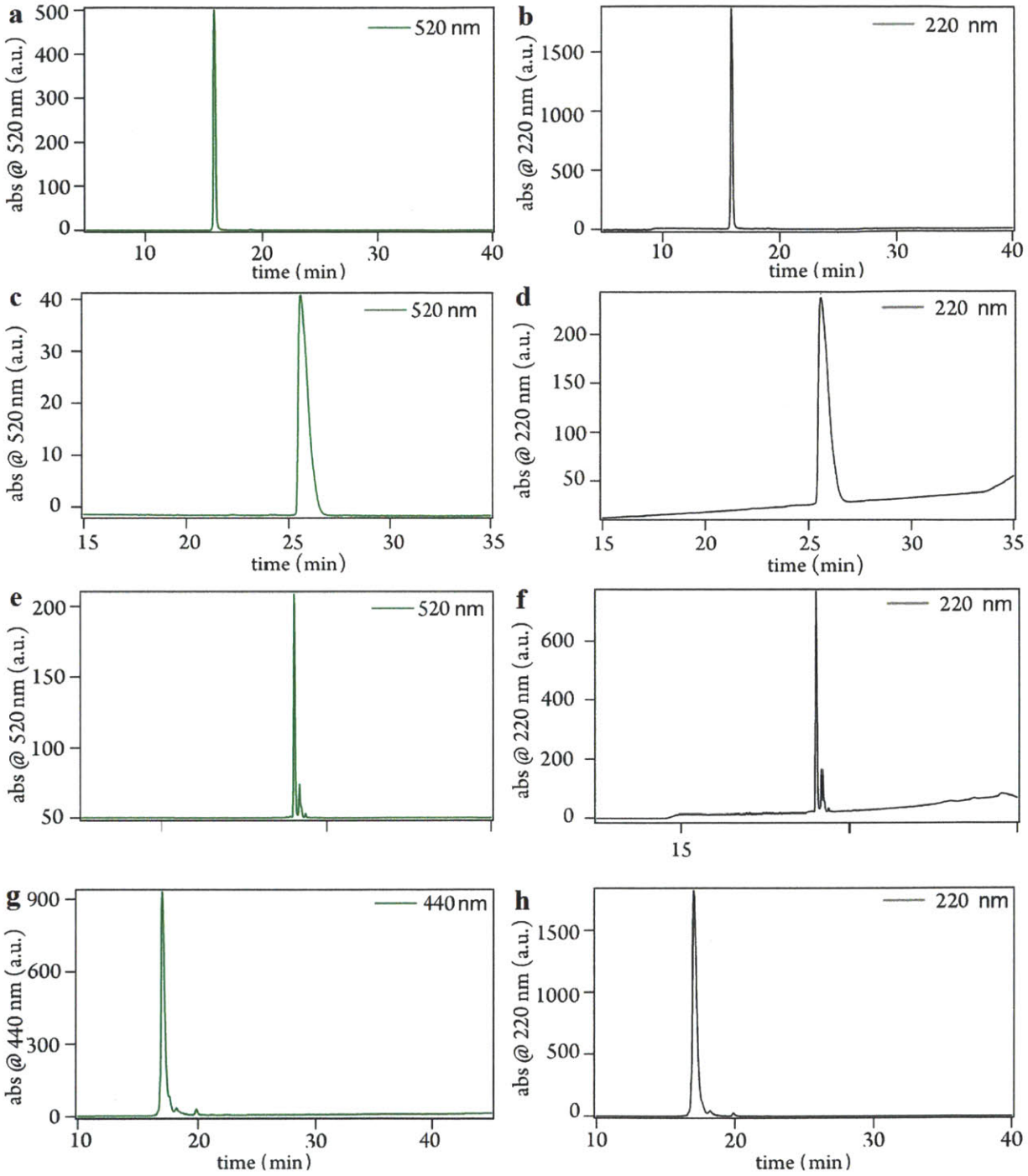

Figure 3.3. Analytical HPLC chromatograms of peptide-sensor constructs. Analytical HPLC chromatograms of (a-b) DCF-MPP, (c-d) ZP1-R_9, (e-f) ZP1-Tat), and (g-h) C343-MPP.

Construct	Purification		Analytical	
Palm-ZP1	0-5 mins	20 %B	0-5 mins	10 %B
	5-10 mins	20-50 %B	5-35 mins	10-75 %B
	10-35 mins	50-95 %B		
Palm-ZQ	0-2 mins	10 %B	0-5 mins	10 %B
	2-5 mins	10-50 %B	5-40 mins	10-90 %B
	5-25 mins	50-99 %B		
ZQ-MPP	0-5 mins	30 %B	0-5 mins	30 %B
	5-35 mins	30-75 %B	5-30 mins	30-60 %B
ZP1-MPP	0-5 mins	10 %B	0-5 mins	30 %B
	5-25 mins	10-60 %B	5-30 mins	30-60 %B
C343-MPP	0-5 mins	10 %B	0-5 mins	10 %B
	5-25 mins	10-60 %B	5-30 mins	10-95% B
DCF-MPP	0-5 mins	10 %B	0-5 mins	30 %B
	5-25 mins	10-60 %B	5-30 mins	30-60% B
ZP1-R_9	0-5 mins	10 %B	0-5 mins	10 %B
	5-35 mins	10-50 %B	5-35 mins	10-50 %B
ZP1-Tat	0-5 mins	10 %B	0-5 mins	10 %B
	5-25 mins	10-50 %B	5-45 mins	10-95 %B

Table 3.2. HPLC conditions of peptide-sensor constructs for both preparative purification and analytical testing. Purification was conducted by HPLC on the semi-preparative scale using a C18 reverse-phase column (VYDAC, 9.5 mm × 250 mm) with 3 mL min^{-1} flow rates. Purity was assessed by analytical HPLC (Vydac, C18, 5 μm, 4.6 mm i.d. x 250 mm) with 1 mL min^{-1} flow rates. A two-solvent system (A = 0.1% (v/v) TFA in H_2O; B = 0.1% TFA in acetonitrile (v/v)) was employed in both cases.

was assessed by analytical HPLC (Table 3.2). ZP1-TAT (retention time = 17.0 min) was judged to be ≥ 95% pure based on the integrated chromatogram (Figure 3.3). Observed peaks (calculated) in ESI-MS (m/z; amu): 1282.9 (1282.7) $[M+2H]^{2+}$; 858.7 (855.5) $[M+3H]^{3+}$, 645.3 (641.9) $[M+4H]^{4+}$.

Characterization of Photophysical and Zinc-Binding Properties

Photophyscial and Zinc-Binding Properties of Palm-ZP1. Spectroscopic measurements for Palm-ZP1 were conducted in a mixed solvent system consisting of 25 mM PIPES buffer (pH 7) with 50 mM KCl and 50% acetonitrile (v/v). Except where noted, all fluorescence data were obtained by exciting at 495 nm and observing 500-650 nm, with 0.1 sec integration time and 1.6 nm slit widths. Emission spectra represent the average of three scans. Palm-ZP1 quantum yield

of was referenced to fluorescein in 0.1 M $NaOH_{(aq)}$ (reported quantum yield of $\Phi = 0.95$).[9]

Apparent $K_{d\text{-}Zn}$ for Palm-ZP1. Apparent zinc-binding affinities ($K_{d\text{-}Zn}$) were determined by a modified literature procedure.[10] For each zinc-binding titration, 1 mM EDTA and 2 mM $CaCl_2$ were added to the MeCN/PIPES buffered solution. Palm-ZP1 or ZP1 was added, and the system was allowed to reach equilibrium (30 min). Aliquots of $ZnCl_2$ were successively added, and the emission spectra recorded once the emission spectrum stabilized (~30 min). The amount of free zinc for a given concentration of total zinc was calculated using the maxchelator program (http://maxchelator.stanford.edu/webmaxc/webmaxcS.htm) based on initial values of 1 mM EDTA, 2mM $CaCl_2$, an ionic strength of I = 0.05 mol dm^{-3} , and a pH of 7.0. Because of the addition of acetonitrile to the buffered solution, the apparent $K_{d\text{-}Zn}$ for Palm-ZP1 was compared to ZP1 under identical conditions (Figure 3.4 and Table 3.3).

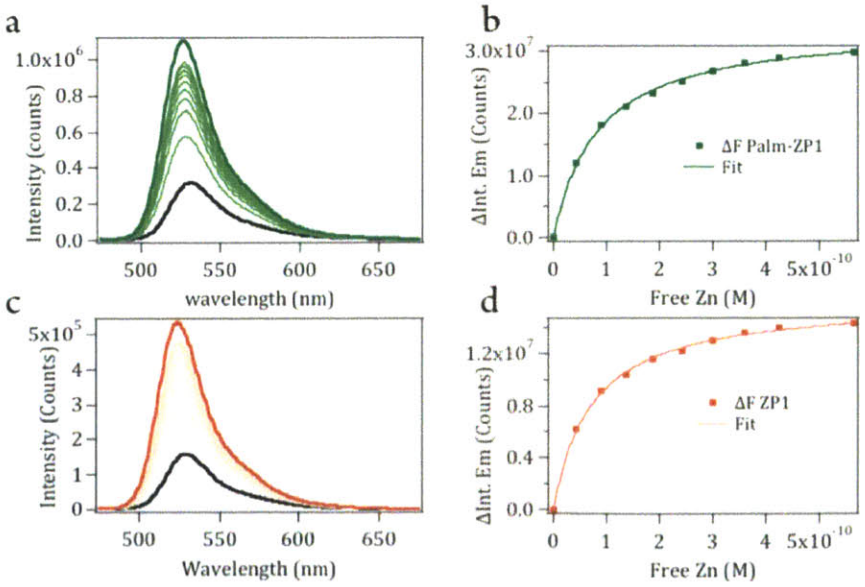

Figure 3.4. Measurement of the zinc-binding affinities, by fluorescence spectroscopy, for Palm-ZP1 (green) and ZP1 (red) in 25 mM PIPES buffer (pH 7) with 50 mM KCl, and 50% (v/v) acetonitrile. Changes in the emission spectra of Palm-ZP1 (a) and ZP1 (c) upon addition of increasing amounts of free zinc. Representative binding isotherms and fits for Palm-ZP1 (b) and ZP1 (d). Samples were excited at 470 nm and monitored over 475-675 nm.

---

[9] Lakowicz, J. R. *Principles of fluorescence spectroscopy*; 2nd ed.; Kluwer Academic/Plenum: New York, 1999.

[10] Walkup, G. K.; Burdette, S. C.; Lippard, S. J.; Tsien, R. Y. *J. Am. Chem. Soc.* **2000**, *122*, 5644.

Photophysical and Zinc-Binding Properties of Palm-ZQ. Characterization of Palm-ZQ and ZQ-MPP was performed in a similar mixed solvent system as described for Palm-ZP1. Quantum yields for Palm-ZQ, ZQ-MPP, and TSQ were referenced to quinine sulfate in 0.1 M H_2SO_4, which has a known quantum yield of $\Phi = 0.55$.[11]

Apparent $K_{d\text{-}Zn}$ for Palm-ZQ and ZQ-MPP. Apparent zinc-binding affinities ($K_{d\text{-}Zn}$) were determined using a modified literature procedure.[10] For each zinc-binding titration, 2 mM EGTA was added to the MeCN/PIPES buffered solution. Palm-ZQ or TSQ was added and the system was allowed to reach equilibrium before the titration (30 min). Free zinc was calculated as described for Palm-ZP1. Because of mixed solvent, the apparent $K_{d\text{-}Zn}$ for Palm-ZQ and ZQ-MPP was compared to TSQ under identical conditions (Figure 3.5, Figure 3.6, Table 3.3).

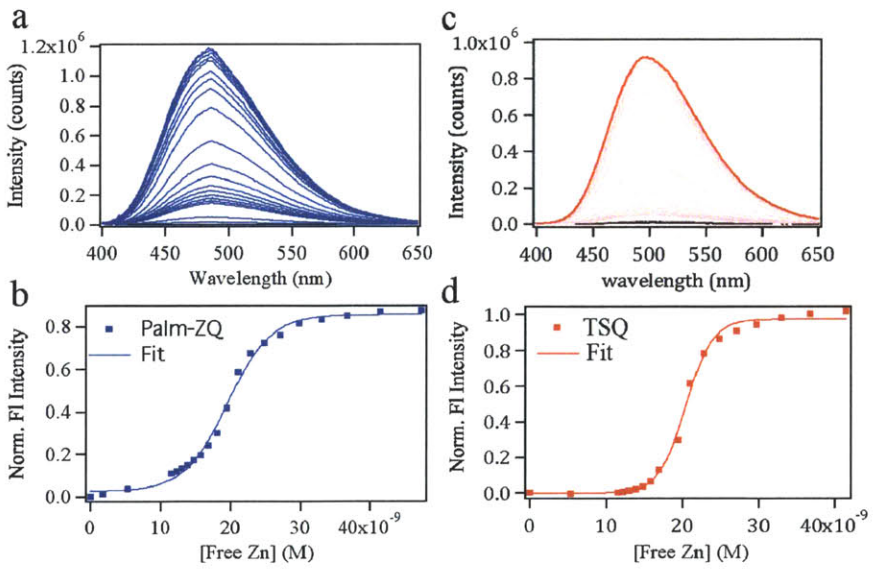

Figure 3.5. Measurement of the zinc-binding affinities, by fluorescence spectroscopy, of Palm-ZQ (blue) and TSQ (red) in 25 mM PIPES buffer (pH 7) with 50 mM KCl, and 50% (v/v) acetonitrile. Observed changes in the emission spectra of Palm-ZQ (a) and TSQ (c) upon addition of increasing amounts of free zinc. Representative normalized binding isotherm and fits for Palm-ZQ (b) and TSQ (d). Apparent $K_{d\text{-}Zn}$ values, which are the average of three trials, are given in Table S2.

---

[11] Eastman, J. W. *Photochem. Photobio.* **1967**, *6*, 55.

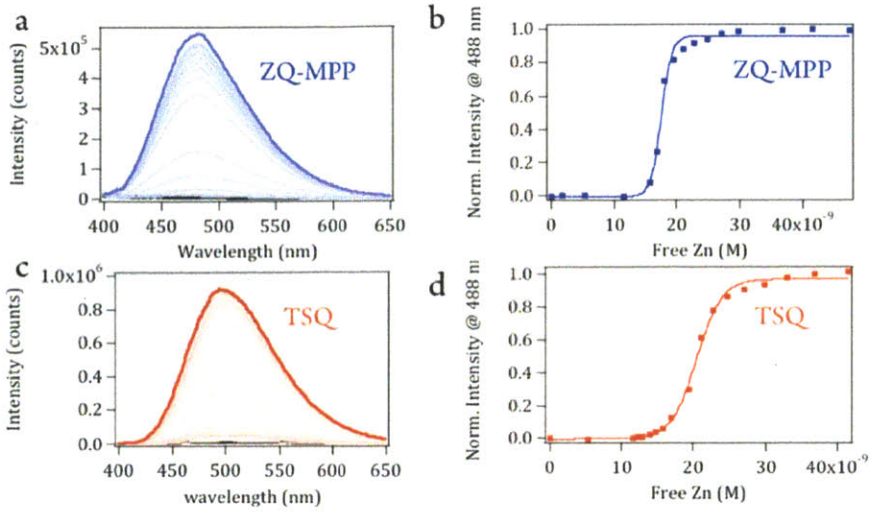

Figure 3.6. Measurement of the zinc-binding affinities of ZQ-MPP (blue) and TSQ (red) in mixed solvent. Zinc titration of ZQ-MPP (a) and TSQ (c). Normalized binding isotherms for ZQ-MPP (b) and TSQ (d).

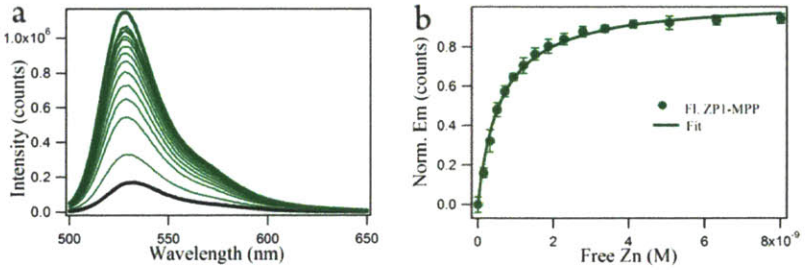

Figure 3.7. Measurement of the zinc-binding affinities of ZP1-MPP (green) in 50 mM PIPES buffer (pH 7) with 100 mM KCl. (a) Observed changes in the emission spectra of ZP1-MPP upon addition of increasing amounts of free zinc. (b) Normalized binding isotherms and corresponding fit for ZP1-MPP.

Sensor	λ_{abs} (nm), $\varepsilon \times 10^3$ ($M^{-1}cm^{-1}$)		Φ_{apo}	Φ_{Zn}	$K_{d\text{-}Zn}$ (M)	Normalized $K_{d\text{-}zn}$
	Apo	Zn(II)				
ZP1[a]	515, 79	507, 84	0.38	0.87	$7.1(3) \times 10^{-11}$	1[b]
Palm-ZP1[a]	519, 66	508, 74	0.16 ± 0.053	0.79 ± 0.049	$8.2(3) \times 10^{-11}$	1.15[b]
ZP1-MPP	521, 61	510, 48	0.13 ± 0.043	0.71 ± 0.062	$6.8(4) \times 10^{-9}$	0.98[c]
TSQ[a]	336, 3.5	360, 3.5	≤ 0.002	0.34 ± 0.01	$2.0(0) \times 10^{-8}$	1[d]
Palm-ZQ[a]	244, 39 336, 3.9	263, 34 360, 3.6	≤ 0.014	0.35 ± 0.01	$1.95(2) \times 10^{-8}$	0.975[d]
ZQ-MPP[a]	336, 5.3	360, 5.8	≤ 0.002	0.36 ± 0.03	$1.75(1) \times 10^{-8}$	0.875[d]

Table 3.3. Summary of photophysical and zinc-binding properties of peptide constructs and reference sensors. [a]Measured properties in 25 mM PIPES buffer (pH 7) with 50 mM KCl and 50% (v/v) acetonitrile mixed solvent. [b]Normalized to ZP1 measured in mixed solvent. [c]Normalized to ZP1 in buffer (50 mM PIPES (7) with 100 mM KCl). [d]Normalized to ZQ measured in mixed solvent.

Photophysical and Zinc-Binding Properties of ZP1-MPP. Characterization of ZP1-MPP was carried out in 50 mM PIPES buffer (pH 7) with 100 mM KCl. Fluorescence data and quantum yield were acquired under identical fluorimeter settings and standards as described for Palm-ZP1.

Apparent $K_{d\text{-}Zn}$ for ZP1-MPP. Apparent zinc-binding affinities ($K_{d\text{-}Zn}$) were determined by a modified literature procedure.[6] For each zinc-binding titration, 1 mM EDTA and 2 mM $CaCl_2$ were added to the PIPES buffered solution. ZP1-MPP was added, and the system was allowed to reach equilibrium (30 min). Free zinc at each subsequent titration point was calculated as described for Palm-ZP1. The apparent $K_{d\text{-}Zn}$ of ZP1-MPP was directly measured and was compared to the apparent $K_{d\text{-}Zn}$ of ZP1 (Figure 3.7 and Table 3.3).

Mammalian Cell Culture, Labeling, and Imaging Procedures.

HeLa cells were cultured as previously described in Chapter 2.2. RWPE-1 and RWPE-2 cells were cultured under the same conditions in keratinocyte serum-free media (Life Technologies) supplemented with prequalified human recombinant Epidermal Growth Factor 1-53 (EGF 1- 53) and Bovine Pituitary Extract (BPE). For live cell imaging, cells were seeded in coated dishes as previously described. Fluorescence microscopy setup and calculations of Pearson's correlation coefficients were the same as described in Chapter 2.2.

Palm-ZP1 and Palm-ZQ. Palm-ZP1 (2.5 μM) and Palm-ZQ (10 μM) were incubated for 30 min at 37° C and 5% CO_2 in dye- and serum-free DMEM. For multichannel imaging and colocalization studies, Cell Mask Orange (Life Technologies, final concentration 2.5 μg/mL) was added for 15-20 min to stain the plasma membrane and MitoTracker Red FM (0.25 μM) was added to stain mitochondria. Prior to imaging, cells were rinsed with warm dye- and serum-free

DMEM (2 × 2 mL) and bathed in warm dye- and serum-free DMEM (2 mL). To assess zinc responsiveness, stock solutions of $ZnCl_2$ (10 mM) were diluted in warm dye- and serum-free DMEM to a final concentration of 50 μM. The zinc-enriched media was exchanged in the cell culture dish directly on the microscope stage. Similarly, a stock solution of ethylenediaminetetraacetic acid (EDTA, 100 mM) in water (pH 7) was diluted in warm dye- and serum-free DMEM to a concentration of 100 μM. Media containing EDTA was exchanged in the culture dishes on the microscope stage.

Internalization and Surface Studies. To investigate the timescale of internalization, HeLa cells were incubated with 2.5 μM Palm-ZP1 and prepared for imaging as previously described. DMEM media was exchanged for zinc-enriched media to improve signal-background ratio and images acquired initially and at 1h, 2h, 4h, and 8h time points. For the surface studies, HeLa cells were incubated with Palm-ZP1 and prepared for imaging as previously described. On the stand, the media was exchanged for zinc-enriched media and an image acquired. A concentrated solution of sodium pyrithione was added to the media to achieve a final concentration of 100 μM sodium pyrithione. After equilibration (15 min), a third image was acquired. Finally, the media was replaced with EDTA solution as previously described and a final image acquired.

Imaging intracellular constructs. HeLa, RWPE1, and RWPE2 cell lines were used for intracellular imaging purposes. The intracellular probes include ZQ-MPP, ZP1-MPP, DCF-MPP, C343-MPP, and ZP1-R_9. For multichannel colocalization imaging and zinc-responsive turn-on imaging, the selected dish of cells was incubated with 0.25-50 μM of the appropriate construct in dye- and serum-free media for 30 min at 37°C under 5% CO_2. The cells were then washed twice with 2 mL dye- and serum-free media and bathed in the same media. After initial images were acquired, media in the dish was replaced with a solution of 50 μM $ZnCl_2$ and

100 μM sodium pyrithione on the stage. Images were acquired after equilibration (15 min), and the media was then exchanged again for a solution of 100 μM TPEN in dye-and serum-free media. For colocalization studies, MitoTracker Red FM, LysoTracker Red, and Dextran Tetramethylrhodamine 10 kDa were used to label the mitochondria, lysosomes, and endosomes respectively.

3.3 Results and Discussion

Design and Characterization of Palm Plasma Membrane Sensors

Zinc release is essential for the physiology of specialized secretory tissues.[12] Investigating zinc release from cells, however, is challenging owing to the difficulty of directing zinc sensors specifically to the plasma membrane. To date, there are only one protein-based[13] and two small-molecule[14] zinc sensors that localize here. To achieve such targeting, a short peptide was designed, consisting of an *N*-terminal palmitoyl group, a 3-residue (~9.8 Å) polyproline helix, two sequential Asp residues, and a *C*-terminal Lys to serve as the point of attachment for the zinc probe (Figure 3.8). As a defining member of the Zinpyr family of zinc sensors, ZP1[15] was a logical choice for the first plasma membrane-targeted construct. Based on a modified fluorescein core, the ZP family of zinc sensors has binding affinities that span five orders of magnitude, a well documented record of zinc-induced turn-on in cells, and members that have carboxylates at the 5- or 6-postion of the fluorescein, which make them amenable for peptide coupling.[16]

---

[12] (a) Frederickson, C.J.; Koh, J.Y.; Bush, A.I. *Nat. Rev. Neurosci.* **2005**, 6, 449-462. (b) Kelleher, S.L.; McCormick, N.H.; Velasquez, V.; and Lopez, V. *Adv. Nutr.* **2011**, 2, 101-111.

[13] Dittmer, P. J.; Miranda, J.G.; Gorski, J.A.; Palmer, A.E. *J. Biol. Chem.*, **2009**, 284, 16289-16297;

[14] Iyoshi, S.; Taki, M.; Yamamoto, Y. *Org. Lett.* **2011**, 13, 4558-4561. (b) Li, D.; Chen, S.; Bellomo, E.A.; Tarasov, A.I.; Kaut, C.; Rutter, G.A.; Li, W.H. *Proc. Natl. Acad. Sci. USA*, **2011**, 108, 21063-21068.

[15] Walkup, G.K.; Burdette, S. C.; Lippard, S. J.; Tsien, R. Y. *J. Am. Chem. Soc.*, **2000**, 122, 5644-5645.

[16] Domaille, D.W.; Que, E. L.; Chang, C. J. *Nat. Chem. Biol.*, **2008**, 4, 168-175.

The desired construct, designated Palm-ZP1 (Figure 3.8a), was designed to localize the zinc-sensing unit to the extracellular side of the plasma membrane. The palmitoyl moiety mimics palmitoylation, a post-translational modification that can direct proteins to the plasma membrane.[17] The polyproline helix provides a rigid spacer,[18] separating ZP1 from surface-bound proteins and biomolecules that might quench its fluoresence.[19] The two sequential Asp residues provide additional negative charge, which impedes diffusion across the lipid bilayer,[20] assuring localization to the cell exterior. Finally, the ε-amino group on Lys serves as a point of attachment for 6-CO_2H ZP1.

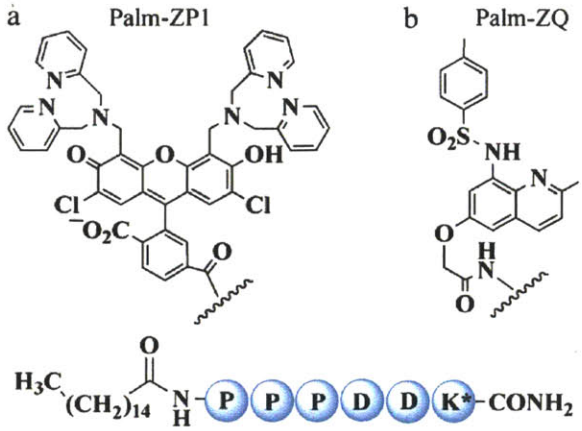

Figure 3.8. Illustrations of the two plasma membrane sensor constructs (a) Palm-ZP1 and (b) Palm-ZQ. Blue circles depict the peptide sequence, with K* indicating the zinc probe is attached to the ε-amino group of the Lys (K) side chain.

The modularity of the Palm sensor construct was explored by changing the zinc-sensing unit. One inherent advantage of a peptide targeting methodology is the modularity of SPPS. Being able to "mix and match" targeting motifs and zinc sensors enables the development of a sensor for a specific biological application without the investment involved in *de novo* sensor design. As a demonstration, the Zinquin version of Palm-ZP1 was prepared, featuring Zinquin appended to the ε-amino group on the Lys residue of the Palm peptide (Figure 3.8a). Based on a tosylated quinaldine scaffold, Zinquin has known zinc-binding and photophysical properties[21] and a large zinc-specific fluorescence response.[21] Although the inherent dimness of Zinquin and

---

[17] Smotrys, J. E.; Linder, M. E. *Annu. Rev. Biochem.* **2004**, 73, 559-587.
[18] Sahoo, H.; Roccatano, D.; Hennig, A.; Nau, W.M. *J. Am. Chem. Soc.* **2007**, 129, 9762-9772.
[19] Togashi, D.M.; Szczupak, B.; Ryder, A.G.; Calvet, A.; O'Loughlin, M. *J. Phys. Chem. A.* **2009**, 113, 2757-2767.
[20] Iyoshi, S.; Taki, M.; Yamamoto, Y. *Org. Lett.* **2011**, 13, 4558-4561. (b) Li, D.; Chen, S.; Bellomo, E.A.; Tarasov, A.I.; Kaut, C.; Rutter, G.A.; Li, W.H. *Proc. Natl. Acad. Sci. USA*, **2011**, 108, 21063-21068.
[21] Bozym, R.A.; Chimienti, F.; Giblin, L.J.; Gross, G.W.; Korichneva, I.; Li, Y.; Libert, S.; Maret, W.; Parviz, M.; Frederickson, C.J.; Thompson, R.B.; *Exp. Biol. Med.*, **2010**, 235, 741-750.

its tendency to compartmentalize within cells have dampened enthusiasm for the probe, the sensor is still widely used due to its commercial availability and compatibility with green and red probes in multichannel microscopy.

Palm-ZP1 was manually synthesized on Rink amide AM resin by using standard FMOC coupling chemistry. First, the peptide scaffold was constructed by sequential addition of amino acids using published procedures.[22] Next, palmitic acid was coupled to the *N*-terminus under analogous conditions. The acid-sensitive 4-methyltrityl (MTT) protecting group was then selectively removed from the ε-amino moiety on the *C*-terminal Lys,[23] providing a convenient route for "on-resin" incorporation of 6-CO_2H ZP1. Palm-ZP1 was subsequently cleaved from the resin and purified using standard procedures.

To investigate whether the zinc-sensing properties of the ZP1 moiety survived the conditions of solid-phase peptide synthesis (SPPS), the zinc-binding and photophysical properties of Palm-ZP1 were studied *in vitro*. Because of the hydrophobic palmitoyl moiety, Palm-ZP1 was dissolved for characterization in a mixed solvent system consisting of 25 mM PIPES buffer (pH 7) with 50 mM KCl and 50% acetonitrile (v/v). In the absence of zinc, Palm-ZP1 has spectral features that are similar to those of other ZP1 derivatives.[15] *Apo* Palm-ZP1 has a λ_{abs} = 517 nm and λ_{em} = 534 nm (Φ_{apo} = 0.16 ± 0.05) (Figure 3.9). Addition of $ZnCl_2$ to a solution of Palm-ZP1 produced a characteristic blue-shift in absorption and emission spectra[15] (λ_{abs} = 506 nm; λ_{em} = 529 nm) and an enhancement of fluorescence (Φ_{Zn} = 0.79 ± 0.05) (Figure 3.9). Measurement of the zinc affinity in a CaEDTA buffered solution indicated that the $K_{d\text{-}Zn}$ value of PalmZP1 closely approximates that of $K_{d\text{-}Zn}$ of ZP1.

---

[22] Kirin, S. I.; Noor, F.; Metzler-Nolte, N.; Mier, W. *J. Chem. Educ.* **2007**, *84*, 108.
[23] Bourel, L.; Carion, O.; Gras-Masse, H.; Melnyk, O. *J. Pept. Sci.*, **2000**, 6, 264-270.

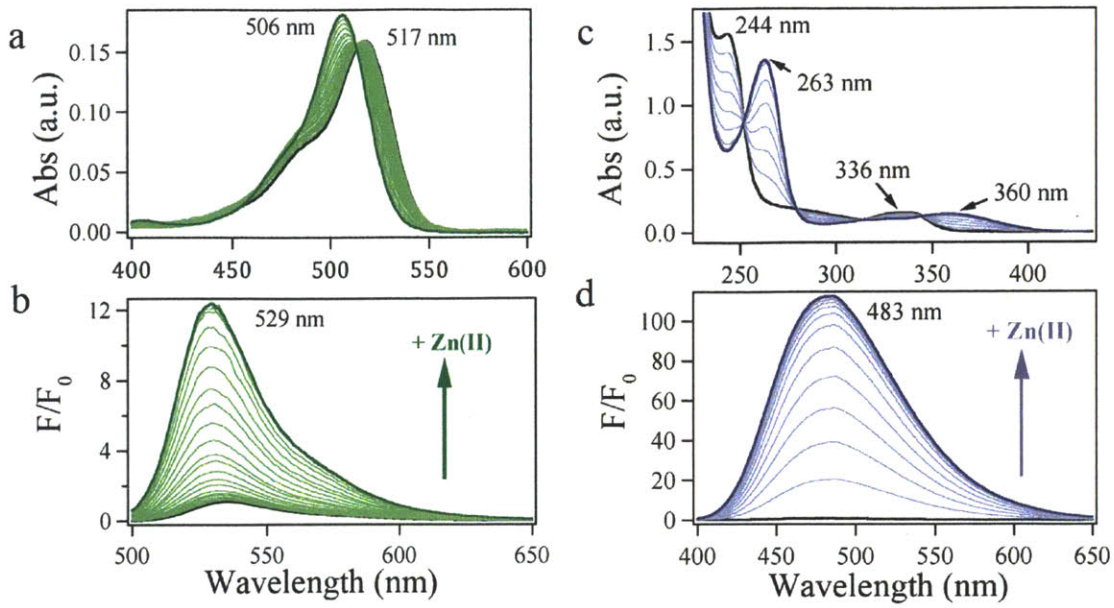

Figure 3.9. Observed changes in the absorption (a) and emission (b) spectra of an ~ 2.3 μM solution of Palm-ZP1 (black) upon addition of successive amounts of $ZnCl_2$ (green). Observed changes in the absorption (c) and emission (d) spectra of an ~39.5 μM solution of Palm-ZQ (black) upon addition of successive amounts of $ZnCl_2$ (blue). Spectra were acquired in a mixed buffered system consisting of 25 mM PIPES (pH 7) with 50 mM KCl and 50 % (v/v) MeCN.

Palm-ZQ was synthesized by methods analogous to SPPS preparation of Palm-ZP1. The zinc-binding and photophysical properties of Palm-ZQ were found to be similar to those of Zinquin and TSQ (6-methoxy-(8-ptoluenesulfonamido)quinoline) (Figure 3.5, Table 3.3).[21] In the absence of zinc, Palm-ZQ has two main absorption bands with maxima at λ_{abs} = 244 and 336 nm (Figure 3.8), and is essentially non-emissive ($\Phi_{apo} \leq 0.005$). Addition of $ZnCl_2$ gives rise to two new features in the absorption spectrum (λ_{abs} = 263 and 360 nm), and a large increase in fluorescence intensity (>100-fold, λ_{em} = 483 nm, $\Phi_{Zn} = 0.36 \pm 0.01$) (Figure 3.9).

Detecting Extracellular Zinc with Palm Sensors in HeLa and RWPE1 Cells

To assess whether Palm-ZP1 could function in the context of a cellular environment, HeLa cells were coincubated in dye- and serum-free Dulbecco's Modified Eagle Media (DMEM)

with 2.5 μM Palm-ZP1 and 2.5 μg/L Cell Mask Orange for 15 min (37° C, 5% CO_2) prior to imaging. Serum-free media was used to minimize zinc contamination originating from the serum.[24] After incubation, the cells were washed with PBS, fresh dye- and serum-free media was added, and the cells were mounted on the fluorescence microscope. $ZnCl_2$ (50 μM) was added, and images of both Palm-ZP1 and Cell Mask Orange were acquired using multichannel fluorescence microscopy. Qualitatively, both dyes preferentially localize to the plasma membrane (Figure 3.10) and appear to have good colocalization. Quantitative image analysis corroborated these findings; Palm-ZP1 and Cell Mask Orange strongly co-localize with Pearson's correlation coefficient $r = 0.70 \pm 0.05$.

Next, the ability of Palm-ZP1 to respond reversibly to an extracellular zinc source was evaluated. Initial cell images had minimal Palm-ZP1 emission, consistent with the low quantum yield for the *apo* form of the sensor. Upon addition of 50 μM $ZnCl_2$, an ~1.7-fold increase in Palm-ZP1 fluorescence intensity was observed at the peripheral membrane of the cell (Figure 3.11), in stark contrast to the Golgi apparatus localization of ZP1 without the peptide moiety.[15] Notably, no exogenous ionophore such as pyrithione was present, suggesting that Palm-ZP1 responds to changes in extracellular zinc concentrations. Subsequent addition of 100 μM EDTA, a cell-impermeable chelator, attenuated the fluorescent signal to initial levels within 5 min (Figure 3.11).

To verify the extracellular location of the ZP1 unit, sodium pyrithione, a known zinc ionophore, was added to live HeLa cells that had been pretreated with Palm-ZP1 and turned-on by addition of 50 μM $ZnCl_2$ to the media. There were no significant changes to the cellular distribution or fluorescent signal intensity (Figure 3.12). The ability of EDTA to quench the zinc-

---

[24] L. Technologies, *The Molecular Probes Handbook.* ed. 11, **2010**.

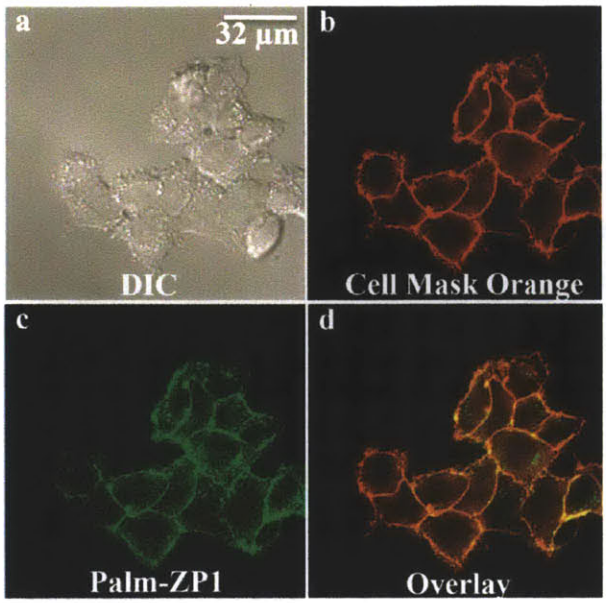

Figure 3.10. Localization study of Palm-ZP1 in live HeLa cells. (a) Differential interference contrast (DIC) image. (b) Signal from plasma membrane specific Cell Mask Orange. (c) Signal from zinc-bound Palm-ZP1. (d) Overlay of (b) and (c). Pearson's correlation coefficient r = 0.70 ± 0.05.

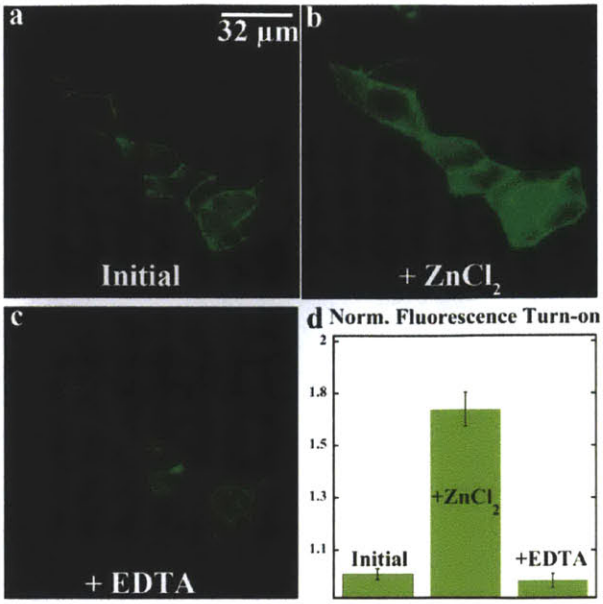

Figure 3.11. Zinc response of Palm-ZP1 in fluorescence imaging of live HeLa cells. (a) Initial signal intensity. (b) Emission after addition of 50 μM $ZnCl_2$. (c) Signal after addition of 100 μM EDTA. (d) Average normalized fluorescence signal of Palm-ZP1 during live cell imaging. (n = 18)

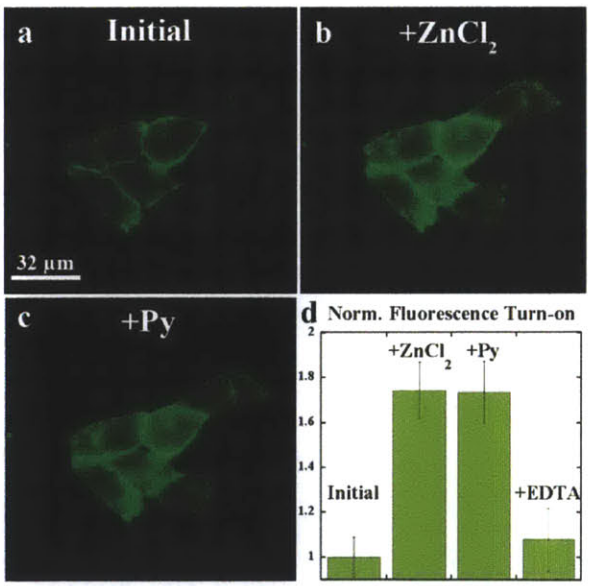

Figure 3.12. Fluorescent imaging of Palm-ZP1 in live HeLa cells. Fluorescent signal (a) initially, (b) after addition of 50 μM $ZnCl_2$, and (c) after addition of 100 μM sodium pyrithione. (d) Quantification of Palm-ZP1 fluorescence from individual cells in the presence of $ZnCl_2$, Zn/Py (+Py), or EDTA. (n = 12).

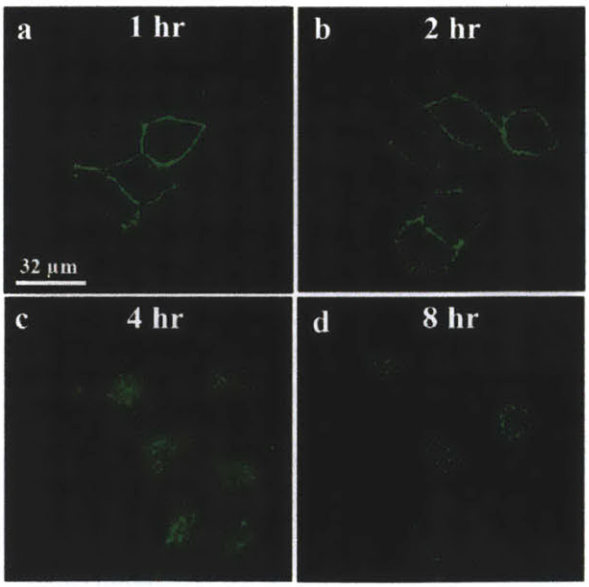

Figure 3.13. Location of Palm-ZP1 in live HeLa cells after 1 (a), 2 (b), 4 (c), or 8 hr (d) of incubation at 37 °C and 5 % CO_2. Prior to image acquisition, 50 μM $ZnCl_2$ was added to the cell media to improve signal intensity.

induced fluorescence signal combined with the inability of pyrithione to effect an additional fluorescence signal strongly suggest that the zinc sensing moiety of Palm-ZP1 is located extracellularly.

To verify the extracellular location of the ZP1 unit, sodium pyrithione, a known zinc ionophore, was added to live HeLa cells that had been pretreated with Palm-ZP1 and turned-on by addition of 50 μM $ZnCl_2$ to the media. There were no significant changes to the cellular distribution or fluorescence signal intensity (Figure 3.12). The ability of EDTA to quench the zinc-induced fluorescent signal combined with the inability of pyrithione to effect an additional fluorescent signal strongly suggest that the zinc sensing moiety of Palm-ZP1 is located extracellularly.

With the localization and zinc responsiveness of Palm-ZP1 established, the robustness by which the construct labeled the plasma membrane was evaluated. An inherent difficulty in working with some plasma membrane dyes is their narrow range of useful imaging lifetime due to rapid internalization.[25] To determine the practical imaging window of Palm-ZP1, HeLa cells were incubated with the sensor for different time periods (Figure 3.13). Palm-ZP1 is retained in the plasma membrane for prolonged periods of time, ~ 2 hr, before eventually being internalized.

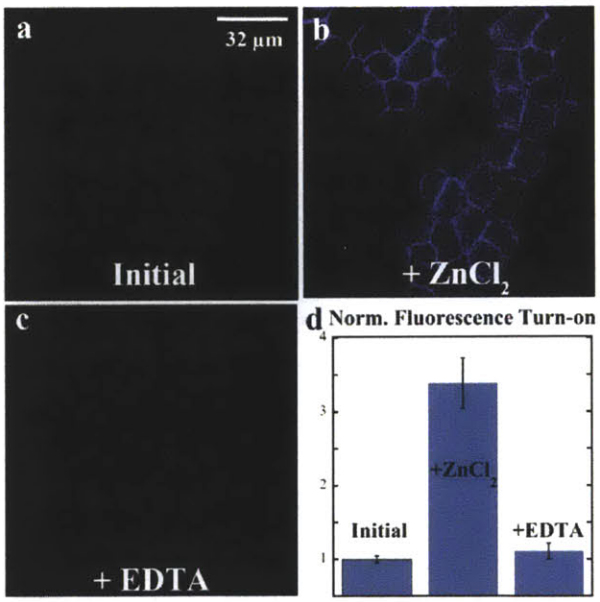

Figure 3.14. Zinc response of Palm-ZQ in live cell fluorescence imaging of HeLa cells. (a) Initial signal intensity. (b) Emission after addition of 50 μM $ZnCl_2$. (c) Signal after addition of 100 μM EDTA. (d) Average normalized fluorescence signal of Palm-ZQ during live cell imaging. (n = 20).

---

[25] Life Technologies, *The Molecular Probes Handbook.* ed. 11, **2010**.

To assess the ability of Palm-ZQ to report on changes in extracellular zinc concentration, live cell imaging in normal epithelial prostrate cells was conducted (RWPE-1 (Figure 3.14) as well as HeLa). Initial fluorescence images showed virtually no signal originating from the Palm-ZQ (Figure 3.14a). Addition of 50 μM $ZnCl_2$ resulted in an ~3.7-fold increase in Palm-ZQ intensity localized to the periphery of the cell (Figure 3.14b). Again, no ionophore was used, consistent with the Zinquin moiety responding to changes in extracellular zinc levels. The signal returned to near baseline levels upon addition of 100 μM EDTA (Figure 3.14c,d). As expected, during that same period there was negligible change in the fluorescence intensity of MitoTracker Red.

Palm-ZQ was much more challenging to image than Palm-ZP1 owing to two competing factors inherent to the probe, namely, the increased hydrophobicity of the construct and lower brightness of the zinc-bound form. Comparing the percentage of acetonitrile (MeCN) necessary to elute the peptides from an analytical C18 reverse-phase column allows one to conclude that the hydrophobicity of Palm-ZQ surpasses that of Palm-ZP1. PalmZP1 elutes with 66 % MeCN whereas Palm-ZQ requires 91 % MeCN. The increased hydrophobicity of Palm-ZQ decreases its solubility in DMEM, which further exacerbates its brightness compared to that of Palm-ZP1, zinc-bound Palm-ZP1 being ~ 46-times brighter than zinc-bound Palm-ZQ. The dimness of PalmZQ means that higher sensor loading (~ 10 μM) is required to obtain an adequate signal-to-noise ratio for fluorescent microscopic imaging. This combination of lower solubility and brightness translated into Palm-ZQ being a much more difficult probe to use for live cell imaging. Although Palm-ZQ is not as effective in imaging the plasma membrane as Palm-ZP1, the construct does effectively demonstrate the modularity of the Palm system.

Synthesis and Characterization of MPP Constructs

The two palm constructs, Palm-ZP1 and Palm-ZQ, demonstrate the modularity of changing the zinc-sensing unit in peptide constructs and also showed that conjugation of sensors to peptides does not negatively impact photophysics and zinc-binding properties. The flexibility of the peptide-based approach was further explored by attempting to target probes to an intracellular target. The mitochondrial matrix was selected as a representative intracellular target due to its biological importance in prostate mobile zinc biology. Mitochondria-penetrating peptides (MPP) were used as targeting sequences to direct mobile zinc reporters. In order to reach the matrix of the mitochondria, MPP-sensor constructs must penetrate two membranes—the cell membrane and the mitochondrial inner membrane. The outer membrane of the mitochondria does not pose a barrier to sensor constructs due to its semiporous nature, allowing small molecules such as MPP-sensor constructs to diffuse into the intermembrane space.[26]

MPPs are designed to improve the uptake and membrane permeability of conjugated payloads by enhancing membrane penetration and subsequent localization to the mitochondria. MPPs are a type of cell-penetrating peptide (CPP) that consists of a combination of cationic and lipophilic amino acids. In contrast to amphiphilic peptides that contain two distinct regions of cationic and lipophilic nature, MPPs have alternating cationic and lipophilic residues and can range from four to twelve residues in length.[27] Although there are two generally accepted mechanisms of cell uptake for CPPs, there is no conclusive evidence for either mechanism with respect to MPP uptake. In the direct translocation model, the peptide is able to insert into the membrane due to its lipophilic residues and translocates across the membrane to the other side.[27] In the endocytic transport model, the peptide is first brought into the cell by endocytosis, forming

---

[26] Murpy, M.P. *TIBTECH.* **1997**, 15, 326-331.
[27] Horton, K.L.; Pereira, M.P.; Stewart, K.M.; Fonseca, S.B.; Kelley, S.O. *Chem. Bio. Chem.* 2012, 13, 476-485.

endosomes with high concentrations of peptide. Subsequently, the peptide translocates out of the vesicles into the cytosol. Although the final destination of most CPPs is the cytosol, MPPs are cationic in nature and enter the mitochondrial matrix due to the membrane potential across the mitochondrial mesmbrane.

A hexamer version of MPP ($(F_xr)_3$) consisting of alternating cyclohexylalannine and D-arginine residues was selected due to its uptake and localization properties (Figure 3.15).[27] Both residues are unnatural amino acids, with cyclohexylalannine providing lipophilic character and each D-arginine residue adding one positive charge to the overall peptide. D-arginine was used instead of L-arginine to avoid possible cleavage by intracellular peptidases. To create the MPP-sensor constructs, the $(F_xr)_3$ MPP sequence was first prepared by SPPS and then the desired sensor was conjugated to the *N*-terminus of the MPP on resin. D-Arginine in the MPP sequence was protected by orthogonal groups such that the sensor specifically labeled the *N*-terminus. Both the ZP1 and Zinquin variants of MPP-sensor constructs (ZQ-MPP and ZP1-MPP, Figure 3.16) were synthesized and purified. Because the smaller and more hydrophobic coumarin 343 was more effective than ZP1 when used with TPP in Chapter 2, coumarin 343-MPP was also prepared to provide further information about uptake and localization (Figure 3.16). For additional study of the peptide-sensor construct uptake properties, ZP1 was also conjugated to Tat and R_9 peptides, two other commonly used cell-penetrating peptides.

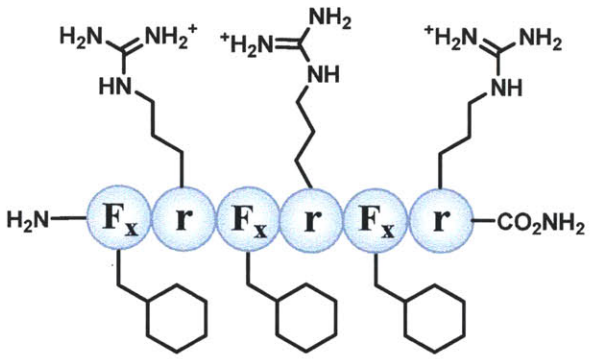

Figure 3.15. Structure of hexameric MPP $(F_xr)_3$ consisting of alternating cyclohexylalannine and D-arginine residues. Fluorophores and sensors are appended to the *N*-terminus amine.

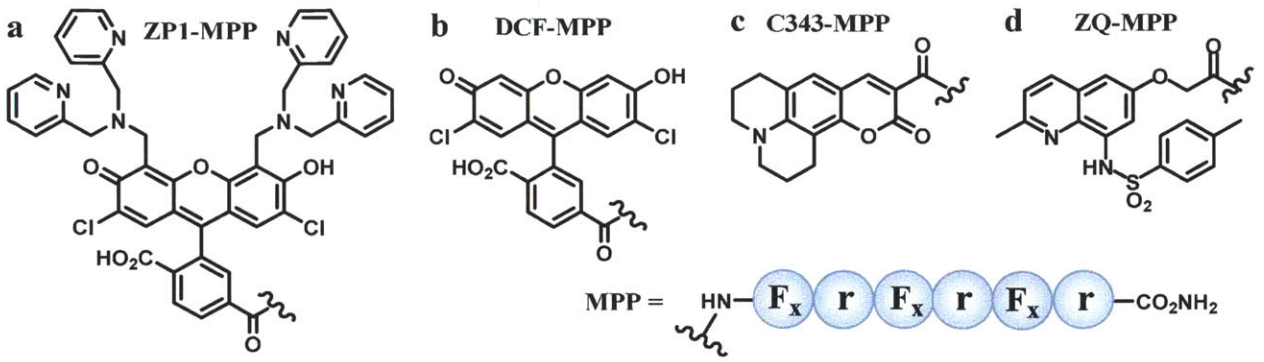

Figure 3.16. Structures of the MPP-sensor and MPP-fluorophore constructs (a) ZP1-MPP, (b) DCF-MPP, (c) C343-MPP, (d) ZQ-MPP.

As previously observed in Palm constructs, conjugation of peptides to the sensors did not significantly alter sensor photophysics or zinc binding properties. In the absence of zinc, ZQ-MPP resembles TSQ and has two main absorption bands with maxima at λ_{abs} = 243 and 336 nm (Figure 3.17), and is essentially nonemissive ($\phi \leq 0.002$). Addition of $ZnCl_2$ gives rise to two new features in the absorption spectrum (λ_{abs} = 264 and 358 nm), and a large increase (>100-fold; $\phi = 0.36 \pm 0.01$) in fluorescence intensity (λ_{em} = 484 nm).

Similarly, ZP1-MPP resembles the ZP1 sensor in its zinc-binding and photophysical properties. In the absence of zinc, ZP1-MPP has a λ_{abs} = 517 nm and λ_{em} = 534 nm ($\Phi_{apo} = 0.16 \pm 0.05$) (Table 3.3). Addition of $ZnCl_2$ to a solution of ZP1-MPP produced a characteristic blue-shift in absorption and emission spectra (λ_{abs} = 506 nm; λ_{em} = 529 nm) and an enhancement of fluorescence ($\Phi_{Zn} = 0.79 \pm 0.05$) (Figure 3.17). Measurement of the zinc affinity in a CaEDTA buffered solution indicated that the $K_{d\text{-}Zn}$ value of ZP1-MPP closely approximates that of $K_{d\text{-}Zn}$ of ZP1. A summary of sensor properties shows that ZP1-MPP and ZQ-MPP closely resemble their free sensor counterparts, ZP1 and TSQ (Table 3.3), indicating that conjugation of the MPP sequence to sensors leaves the sensors unaltered. ZP1-R_9 and ZP1-Tat, two constructs that share

the same sensor but have different conjugated peptides, were also similarly assayed and found to have high similarity to the parent sensor.

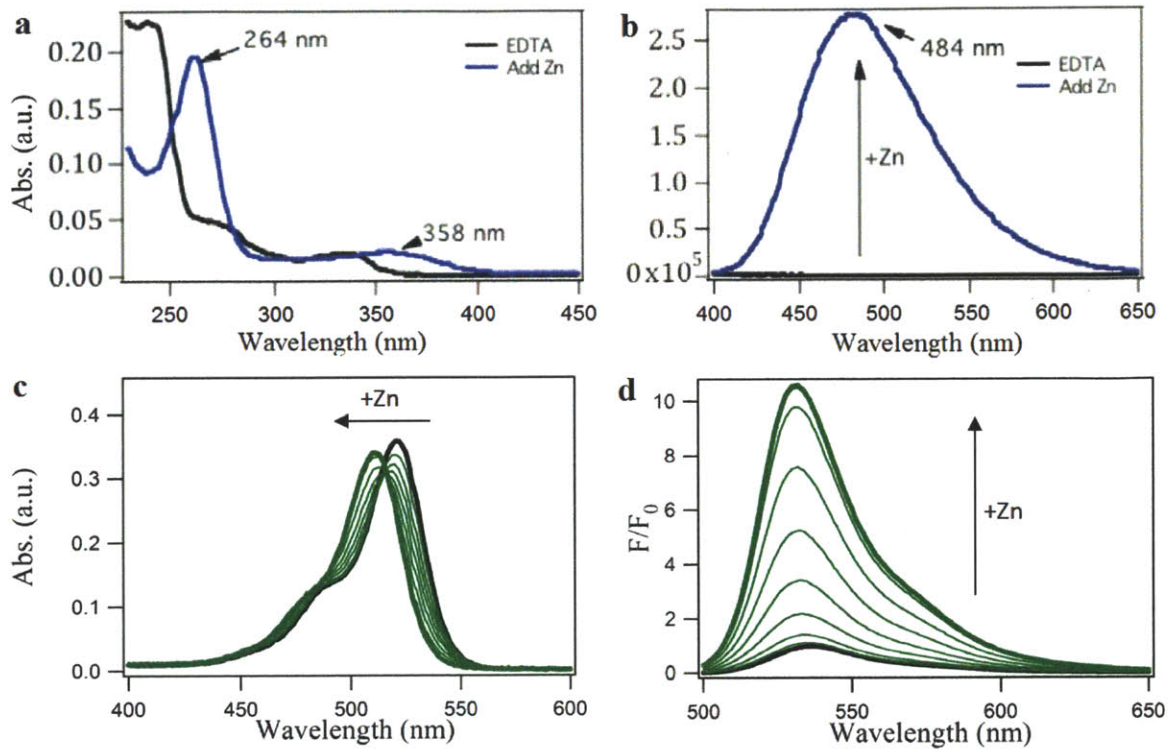

Figure 3.17. Observed changes in the absorption (a) and emission (b) spectra of an ~ 5 μM solution of ZQ-MPP (black) upon addition of excess $ZnCl_2$ (blue). Observed changes in the absorption (c) and emission (d) spectra of a 5 μM solution of ZP1-MPP (black) upon addition of successive amounts of $ZnCl_2$ (green).

Intracellular Application of MPP-ZP1 in Live Cell Imaging

To test the applicability of MPP-ZP1 for imaging intracellular zinc, HeLa cells were incubated with ZP1-MPP in concentrations ranging from 0.5 to 50 μM for 30 min. Under all conditions tested, plates incubated with ZP1-MPP showed a punctate staining pattern similar to the one observed in Chapter 2 with ZP1-TPP. Increase in concentration did cause an increase in brightness of the punctate staining pattern, but did not change the localization of the pattern. Addition of zinc and pyrithione did not significantly increase fluorescence from the punctate staining. Addition of TPEN, a membrane-permeable chelator, also failed to alter signal levels.

These observations of ZP1-MPP in live cell imaging suggest that the MPP-sensor construct was being sequestered to endosomes.

The endocytic uptake and subsequent trapping of ZP1-MPP was further investigated and characterized. HeLa cells were coincubated with ZP1-MPP and 10 kDa Alexa Fluor Dextran and imaged with multichannel microscopy to investigate the localization of ZP1-MPP. As expected, ZP1-MPP colocalized very strongly with dextran, which has been frequently used to label endosomes due to its large size and anionic nature.[28] The Pearsons' correlation coefficient for the ZP1-MPP and dextran image overlay, a quantitative measure of colocalization, was $r = 0.68 \pm 0.1$, indicating a strong spatial correlation between the two signals (Figure 3.17). The endosomal localization of ZP1-MPP suggests that it enters the cell through the endocytic pathway rather than through membrane translocation. The conjugation of MPP to ZP1 did not impart membrane permeability properties, and ZP1-MPP remains trapped in endosomes after uptake. As further verification of the endocytic mechanism of uptake, HeLa cells were incubated with 5 μM of ZP1-MPP at 4°C for 30 min, then imaged by fluorescence microscopy. The resulting images indicate that ZP1-MPP does not stain the cells significantly when incubated at 4°C, although MitoTracker is able to diffuse through the membrane and stain the mitochondria at the lower temperature. The lack of ZP1-MPP signal

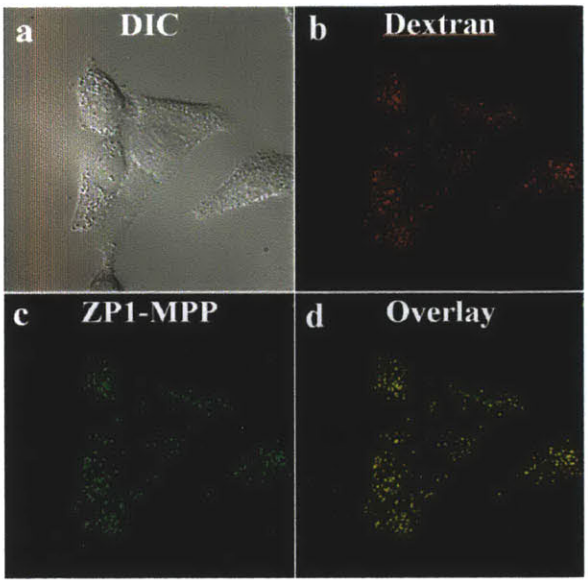

Figure 3.18. Localization study of ZP1-MPP in live HeLa cells. (a) Differential interference contrast image. Signal from (b) endosome dye AlexaFluor Dextran and (c) ZP1-MPP. (d) Overlay of (b) and (c). Pearson's correlation coefficient $r = 0.71 \pm 0.07$.

[28] Masedunskas, A. and Weigert, R. *Traffic* **2008**, 9, 1801.

coupled with the ability of endocytosis-independent MitoTracker to stain the mitochondria further corroborates the endocytic model of uptake for ZP1-MPP.

In order to rule out the contribution of the targeting peptide towards endosomal sequestration, two other peptides were conjugated to ZP1 and tested. ZP1-R_9 and ZP1-Tat were created and used to stain live cells, with identical punctate patterns observed in cells incubated with either ZP1-R_9 or ZP1-Tat (Figure 3.19). Because polyarginine and Tat are sequences that have been extensively used to deliver payloads to the cytosol,[29] the inability of all three ZP1 peptides to escape the endosomes most likely stemmed from specific characteristics of the ZP1 sensor itself rather than any peculiarities with the MPP peptide sequence.

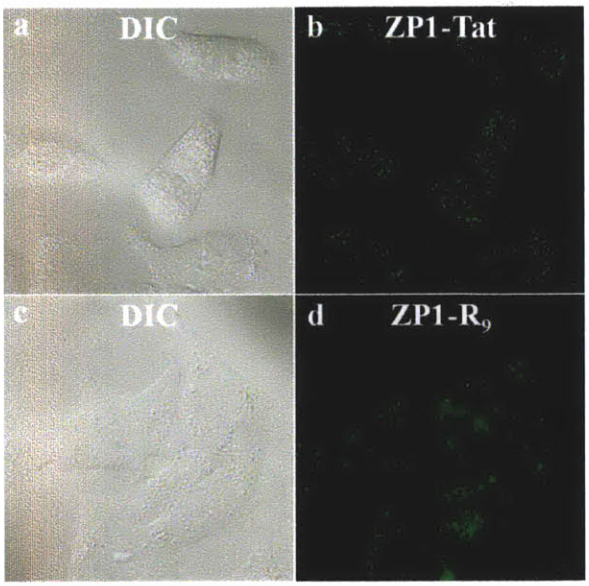

Figure 3.19. Endosomal sequestration of (a-b) ZP1-Tat and (c-d) ZP1-R_9 in live HeLa cells. (a,c) Differential interference contrast (DIC) images. (b,d) ZP1 channel images.

Investigation of Fluorophore Effect on Uptake and Localization

To obtain a more precise understanding of fluorophore requirements for membrane permeability, MPP-constructs incorporating 6-carboxy-2,7-dichlorofluorescein (DCF) and coumarin 343 (C343) were prepared. DCF is a fluorophore that closely resembles ZP1, but does not contain the two zinc-binding dipicolylamine (DPA) arms present in ZP1 (Figure 3.15) and is thus smaller in size. DCF is dianionic under physiological conditions, whereas ZP1 has an overall negative charge. Coumarin 343, on the other hand, is much smaller, neutral at

---

[29] (a) Patel, N.L.; Wang, J.; Kim, K.J.; Borok, Z.; Crandall, E.D.; Shen, W.C. *Mol. Pharm.* **2009**, 6, 492-503. (b) Silhol, M.; Tyagi, M.; Giacca, M.; Lebleu, B.; Vives, E. *Eur. J. Biochem.* **2002**, 269, 494-501.

physiological pH, and is more hydrophobic than either ZP1 or DCF (Figure 3.16). C343 and DCF were chosen to better define the limiting factors and requirements for endosomal escape. Possible contributing factors of ZP1-MPP and ZP1-TPP endosomal sequestration include size, hydrophobicity, and charge.

Subsequently, DCF-MPP and C343-MPP were used in live cell imaging. Live HeLa cells were coincubated with 5 μM DCF-MPP and 250 nM MitoTracker for 30 mins at 37°C under a 5% CO_2 environment. Imaging of the plate showed that DCF-MPP did not enter or stain the cell, whereas MitoTracker was able to enter and stain the mitochondria. These results mirrored the observed impermeability of Fl-TPP in Chapter 2 (Figure 2.7). In contrast to the impermeability of DCF-MPP, C343-MPP was able to enter the cell and localize to the mitochondria (Figure 3.19). The ability of both C343-MPP and C343-TPP to reach the mitochondria is in stark contrast to ZP1 and fluorescein constructs. C343-MPP strongly localizes to the mitochondria, as quantified by the high Pearson's correlation coefficient between C343-MPP and MitoTracker ($r = 0.60 \pm 0.1$).

As a further investigation of C343-MPP uptake, HeLa cells were incubated with several different C343-MPP concentrations ranging from 1 to 15 μM (Figure 3.21). At 1 μM and 5 μM concentrations, C343-MPP formed punctate staining patterns reminiscent of ZP1-MPP and ZP1-TPP staining patterns. At 10 μM, C343-MPP was able to escape the endosome and reach the mitochondria. At 15 μM and higher concentrations, C343-MPP had less specific staining as well as marked cytotoxicity. These results, along with MPP-ZP1 sequestration in endosomes, provide evidence towards the endocytic model of MPP-fluorophore uptake and concentration-dependent escape from the endosome. Below a threshold concentration (5 μM for C343-MPP), the MPP construct is unable to escape the endosome and remains trapped as the endosome is acidified and

matures. Above the threshold concentration, the MPP construct is able to escape the endosome and localize to the mitochondria. The threshold concentration is variable and depends on the ability of the construct to translocate across the endosomal membrane, as influenced by size and hydrophobicity. As seen with C343-TPP, excessively high concentrations result in cytotoxicity caused by swelling and leakage of the mitochondria.

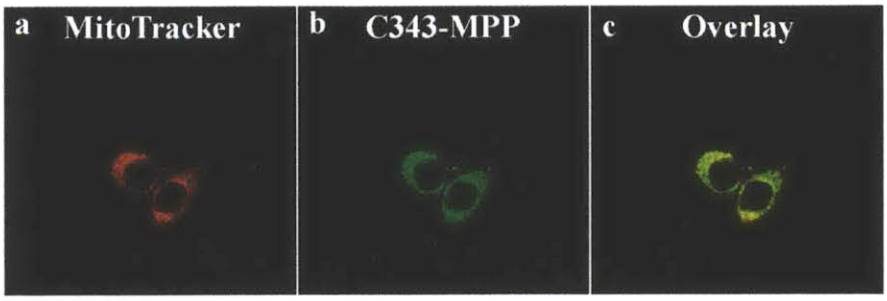

Figure 3.20. Localization study of C343-MPP (10 μM) in live HeLa cells. Signal from (a) MitoTracker and (b) ZP1-MPP. (c) Overlay of (a) and (b). Pearson's correlation coefficient $r = 0.60 \pm 0.1$.

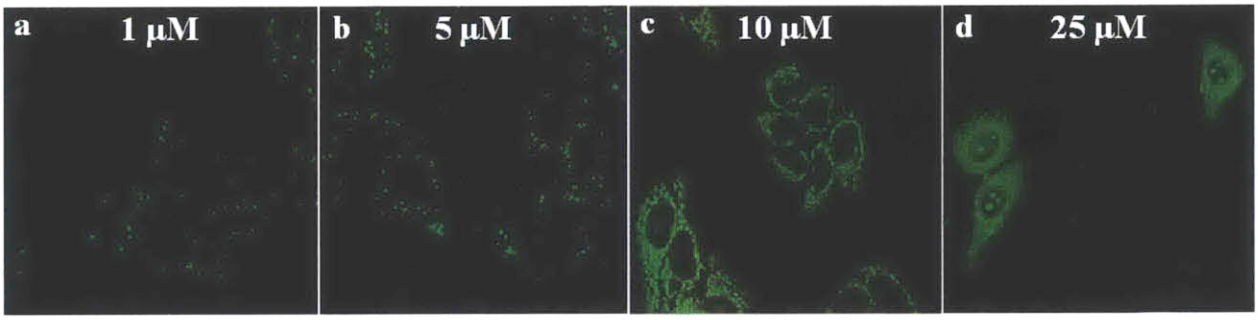

Figure 3.21. Concentration-dependent changes in C343-MPP localization. (a)-(b) At lower incubation concentrations, C343-MPP creates punctate stains resembling the endosomal distribution of ZP1-MPP and ZP1-TPP. (c) Intermediate concentrations allow endosomal escape and appropriate mitochondrial localization. (d) High concentrations cause cytotoxicity.

Based on the results of imaging with C343-MPP and other MPP constructs, the ability to translocate across the endosomal membrane is highly dependent on the nature of the fluorophore attached to the peptide. In the case of ZP1, it is most likely unable to penetrate the endosomal membrane due to a combination of size or lack of hydrophobicity. Charge does not seem to play

as significant of a role in membrane permeability, although it does reduce endocytosis in the case of DCF-MPP, which is more anionic than ZP1-MPP. Considering the proper uptake and localization of C343-MPP, careful selection or design of the fluorophore or sensor attached to the peptide would enable the construct to properly reach the mitochondria.

Imaging and Live Cell Studies with ZQ-MPP

In light of the fluorophore importance as seen in C343-MPP, ZP1-MPP, and DCF-MPP, the Zinquin version of the MPP-construct, ZQ-MPP, was an excellent candidate for proper endosomal escape and localization to the mitochondria because Zinquin is both smaller and more hydrophobic than ZP1. Live cell imaging with HeLa cells showed that ZQ-MPP was indeed able to escape endosomes and reach the cytosol, although ZQ-MPP was fairly toxic to cells. HeLa cells were treated with a 25 μM solution of ZQ-MPP, which also contained 1 μM MitoTracker Red. A zinc-responsive ~15-fold increase in ZQ-MPP signal was observed, and the reversibility of the turn-on was confirmed (Figure 3.22). ZQ-MPP also strongly colocalized with MitoTracker Red, with a Pearson's correlation coefficient yields an $r = 0.71 \pm 0.01$ (Figure 3.23).

Although ZQ-MPP was able to escape the endosomes and reach the mitochondria, there are two important drawbacks hindering the use of ZQ-MPP as a mitochondrial zinc sensor. Zinquin by nature is much less bright than ZP1 or even coumarin 343. Zinquin is more than 50 times less bright than ZP1, meaning that to acquire the same signal levels, concentrations of ZQ-MPP 50 times higher than ZP1-MPP incubation concentrations are required. The second shortfall of the ZQ-MPP system was its high cell toxicity. As measured by the MTT assay, the IC_{50} for ZQ-MPP was 5.1 μM. The dimness of the Zinquin sensor requires high concentrations of ZQ-MPP to produce appreciable signal, but the high toxicity of ZQ-MPP placed an upper limit

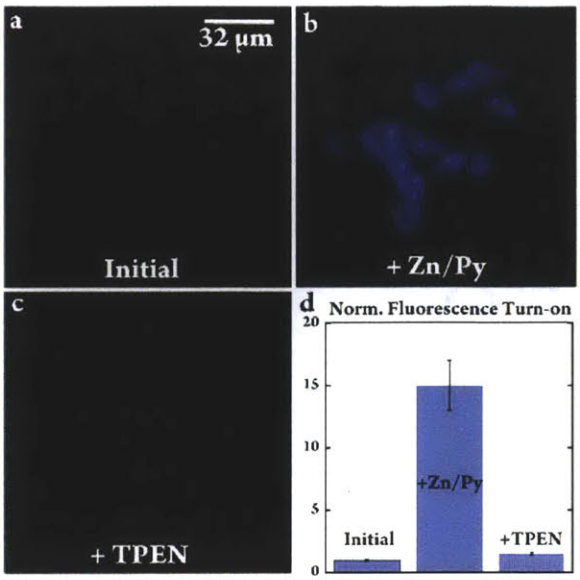

Figure 3.22. Fluorescence imaging of ZQ-MPP in live HeLa cells. Fluorescent signal (a) initially, (b) +50 μM $ZnCl_2$/100 μM pyrithione, (c) +100 μM TPEN. (d) Quantification of fluorescence (n = 12).

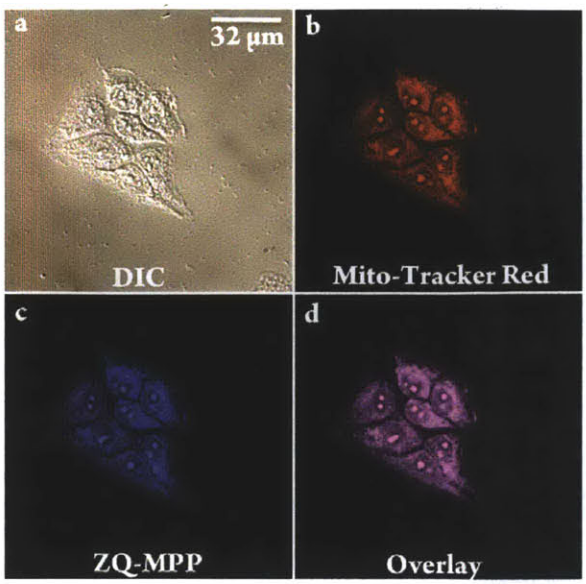

Figure 3.23. Localization study of ZQ-MPP in live HeLa cells. Signal from (a) MitoTracker and (b) ZQ-MPP. (c) Overlay of (a) and (b). Pearson's correlation coefficient r = 0.71 ± 0.01.

on the usable incubation concentrations. As a result, the window of useful incubation concentrations was precipitously narrow and straying to either side resulted in poor signal localized to endosomes or cell death. Even within useful incubation concentrations of 20-25 μM, ZQ-MPP was suboptimal due to its significant toxicity to cells. At these concentrations, ZQ-MPP caused mild swelling to the mitochondria and minor leakages resulting in some staining of nucleoli and the cytosol (Figure 3.23). The nucleolar and cytosolic signal can be identified as leakage from the mitochondria due to the concomitant presence of MitoTracker in those areas. Although ZQ-MPP successfully escaped endosomes and localized to mitochondria, ZQ-MPP exhibits the unfavorable characteristics of dimness, toxicity, and leakage that leave much to be desired.

3.4 Conclusions

In this chapter, the modularity and effectiveness of peptide-based probes were employed to create functional mobile zinc sensors. SPPS provided a simple and reliable paradigm for attaching sensors, targeting moieties, and fine tuning characteristics such as charge, structure, and hydrophobicity. Analysis of photophysical and zinc-binding properties showed that conjugation of sensors to various peptides preserved the original sensor properties.

Using this modular approach, two plasma-membrane targeted zinc sensors were prepared with ZP1 and Zinquin. The resulting Palm-ZP1 and Palm-ZQ sensors selectively labeled the exterior surface of the plasma membrane, resisted internalization for up to 2 hours, and responded exclusively to the presence and absence of extracellular zinc. Next, the flexibility of the SPPS process was used to create a series of constructs incorporating four different sensors and three peptides. Imaging studies of the ZP1-, DCF-, and C343-MPP constructs demonstrated the importance of fluorophore hydrophobicity and size for membrane permeability. In addition, energy dependent uptake and endosomal sequestration provided strong evidence for the endocytic mechanism of MPP construct uptake. Since these results suggested that smaller and more lipophilic sensors would have better uptake properties, ZQ-MPP was created and tested in live cells. As expected, ZQ-MPP localized to the mitochondria and possessed excellent zinc-responsiveness, but cytotoxicity and dimness limited its effectiveness as a sensor.

Palm and MPP sensors demonstrated that the synthetic ease and flexibility of SPPS can be used to target sensors to specific cellular locations. Although the MPP constructs showed that there are limitations to this methodology, with careful consideration of fluorophore properties, the peptide-based methodology can harness extensive libraries of analyte-specific sensors to create targeted probes that avoid the unpredictability and difficulty of *de novo* sensor design.

CHAPTER 4. Improvement of Sensor Uptake, Localization, and Photophysics Through Acetylation of Fluorescein-based Sensors

4.1 Introduction

In Chapter 2, fluorophores and zinc probes were directed to the mitochondria using the small molecule triphenylphosphonium (TPP) targeting moiety. Conjugation of targeting peptides to sensors was employed to generate intra- and extracellular-targeted probes, as presented in Chapter 3. The uptake of both the TPP and peptide constructs was highly dependent on the identity of the attached probe. TPP and peptide constructs incorporating the ZP1 sensor entered the cell through endocytosis and were subsequently sequestered in the endosomes, unable to reach their intended location. A prerequisite for proper localization of the zinc probe to its final location is escape from endosomes, which depends on the ability of the construct to translocate across the endosomal membrane.

Previously synthesized peptide constructs, TPP-based probes, and commercially-obtained MitoTracker dyes were evaluated and compared to develop guidelines for proper localization. Correlation between construct lipophilicity and endosomal escape was investigated by measuring the octanol water partition coefficients (Log *P*) of each peptide and small molecule probe, and a clear trend was observed. Commercial mitochondria dyes (MitoTracker Red and MitoTracker Green) have large Log *P* values relative to the ZP1- and fluorescein-incorporating TPP and peptide constructs, indicating greater lipophilicity. ZP1 and fluorescein constructs with low log *P* values were susceptible to endosomal sequestration or lack of uptake. On the other hand, coumarin 343 constructs that properly localized to the mitochondria (C343-TPP and C343-MPP) had log P values within the same range as MitoTracker dyes. These results suggested that zinc probe constructs required a minimum lipophilicity to translocate across the endosomal membrane en route to the cytosol or other intracellular location.

Compound	Log *P*	Charge	Localization
MitoTracker Red	1.15 ± 0.04	+1	Mitochondria
C343-MPP[a]	1.03 ± 0.21	+3	Mitochondria
C343-TPP[b]	0.72 ± 0.05	+1	Mitochondria
MitoTracker Green	0.56 ± 0.02	+1	Mitochondria
ZP1-MPP[a]	0.14 ± 0.04	+2	Endo/Lysosome
ZP1-Tat[a]	-0.10 ± 0.07	+7	Endo/Lysosome
ZP1-TPP[b]	-0.11 ± 0.01	Zwitterion	Endo/Lysosome
Fl-TPP[b]	-0.39 ± 0.03	-1	-

Table 4.1. Lipophilicites of peptide and small molecule zinc sensor constructs as measured by octanol water partition coefficient (Log *P*) [b]Peptide-sensor constructs (Chapter 3). [b]TPP-sensor constructs (Chapter 2).

Instead of designing and creating a new series of lipophilic zinc sensors, a one-step, generalizable modification was investigated to increase sensor lipophilicity. One common feature in fluorescein-based sensors and fluorophores is the presence of phenolic oxygen atoms on the xanthene ring portion.[1] Altering the phenolic oxygen atoms on fluorescein has been utilized to convert various fluorescein constructs into the lactone conformation, thereby mitigating two negative charges and increasing lipophilicity (Figure 4.1).[2] This modification has been used to convert 6-carboxyfluorescein, an anionic and membrane impermeable dye, into the more lipophilic 6-carboxyfluorescein diacetate, which is membrane permeable.[3] Acetylation converts the cell-impermeable 6-carboxyfluorescein into a permeable form by increasing lipophilicity and decreasing fluorophore anionic nature. Diacetylated fluorescein is frequently used as a dye for cell viability because of its ability to permeate the cell and accumulate in live cells by esterase hydrolysis of the acetyl groups.[3-4]

---

[1] Pluth, M.D.; Tomat, E.; Lippard, S.J. *Annu. Rev. Biochem.* **2011**, 80, 333-355.

[2] (a) Lavis, L.D.; Chao, T.; Raines, R.T. *Chem. Sci.* **2011**, 2, 521-530. (b) Yang, Y., Babiak, P.; Reymond, J.L. *Helv. Chim. Acta.* **2006**, 89, 404.

[3] Goodall, H.; Johnson, M.H. Nature. **1982**, 295, 524-526.

[4] (a) Breeuwer, P.; Drocourt, J.L.; Bunschoten, N.; Zwietering, M.H.; Rombouts, F.M.; Abee, T. *Appl. Environ. Microbiol.* **1995**, 61, 1614-1619. (b) Chen, J.C.; Chang, M.L.; Muench, M.O. *J. Immunol. Methods.* **2003**, 279, 123-133.

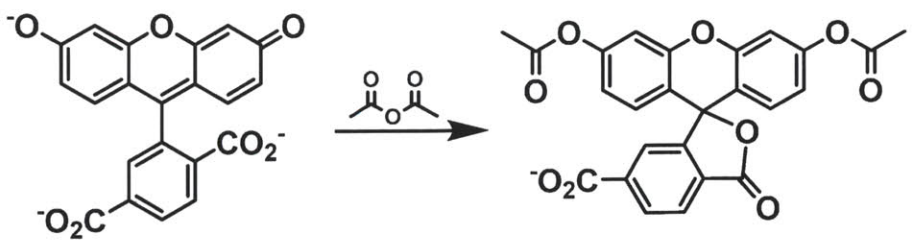

Figure 4.1. Acetylation of 6-carboxyfluorescein to generate the lactone form, 6-carboxyfluorescein diacetate. At physiological pH, acetylation mitigates two negative charges, increases hydrophobicity, and disrupts π conjugation.

Because ZP1 is based on a fluorescein scaffold[1], it is also amenable to acetylation as was applied to 6-carboxyfluorescein. Formation of the lactone form of ZP1 also interrupts the conjugated π system, sharply decreasing the visible absorbance and fluorescence of the sensor. Acetylation would allow convenient modification of construct lipophilicity and has the potential to improve probe photophysics. To investigate the utility of sensor construct acetylation, ZP1-TPP was selected as a representative case study for acetylation. As seen in Chapter 2, ZP1-TPP enters the cell through endocytosis and is trapped in endosomes due to its inability to cross the endosomal membrane. Acetylation of ZP1-TPP was pursued to improve the membrane permeability of the construct, allowing it to penetrate the endosomal membrane and localize to the matrix of the mitochondria (Figure 4.2).

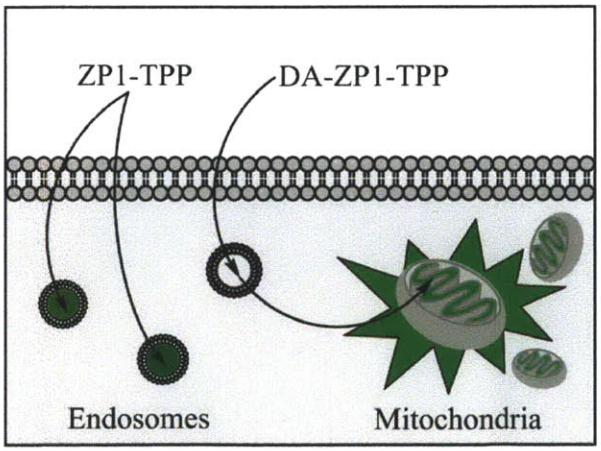

Figure 4.2. Differences in localization between diacetylated (DA) and non-acetylated ZP1-TPP. ZP1-TPP remains trapped in endosomes (Chapter 2.3). Increased DA-ZP1-TPP lipophilicity enhances escape from endosomes and subsequent localization to the mitochondria.

4.2 Materials and Methods

General Considerations. HPLC grade solvents, fluorophores, reagents, and porcine liver esterase were purchased from Sigma-Aldrich and used as received, unless otherwise noted. 2-(7-

Aza-1H-benzotriazole-1-yl)-1,1,3,3-tetramethyluronium hexafluorophosphate (HATU) was procured from Oakwood Chemicals. Octanol was purchased from Alfa Aesar. MitoTracker Red FM, Hoechst 34580 stain, and Lysotracker Red DND-99 were purchased from Life Technologies. 6-CO_2H Zinpyr1[5] and (2-aminoethyl)triphenylphosphonium bromide[6] were prepared according to literature procedures. Buffers, purification, characterization, and spectroscopy techniques were similar to those outlined in Chapter 2.2 (p.21). A 50 mM zinc(II) stock solution was prepared using 99.999% $ZnCl_2$ (Aldrich). Stock solutions for metal ion selectivity tests were prepared using 99.0% NaCl (Mallinckrodt), 99.9% $MgCl_2$ (Aldrich), 99.99% $MnCl_2$ (Alfa Aesar), 98% $NiCl_2$ (Aldrich), 98% $CuCl_2$ (Alfa Aesar), 99.9% $CaCl_2$ (Aldrich), and 99.999% $CdCl_2$ (Aldrich).

Synthesis and Purification of DA-ZP1-TPP. 2-(Aminoethyl)triphenylphosphonium bromide (25 mg, 82.1 μmol), 6-CO_2H Zinpyr1 (25 mg, 28.75 μmol), and HATU (10.95 mg, 28.75 μmol) were used to prepare ZP1-TPP as outlined in Chapter 2 (p. 24). Crude ZP1-TPP was dissolved in acetic anhydride and stirred at room temperature overnight. The initially coral-colored solution gradually became transparent and colorless over the course of the reaction. The reaction mixture was then lyophilized to yield crude product as a white powder, which was purified by HPLC (see p. 24 for column and solvent conditions) according to the following protocol: isocratic flow, 10% B, 0-5 min; gradient, 10-50% B, 5-20 min, with a constant flow-rate of 3 mL min^{-1}. Similar fractions were pooled and lyophilized, yielding DA-ZP1-TPP as a white solid (45.5% yield, as determined by integration of HPLC purification traces). The purity of the final product was

---

[5] (a) Woodroofe, C. C.; Masalha, R.; Barnes, K. R.; Frederickson, C. J.; Lippard, S. J. *Chem. Biol.* **2004**, *11*, 1659; (b) Nolan, E. M.; Lippard, S. J. *Acc. Chem. Res.* **2009**, *42*, 193.

[6] Maryanoff, B.E.; Reitz, A.B.; Duhl-Emswiler, A.D. *J. Am. Chem. Soc* **1985**, *107*, 218.

assessed via analytical HPLC (Vydac, C18, 5 μm, 4.6 mm i.d. x 250 mm). After a 5 min isocratic wash, a linear gradient of 5-50% B was run over 30 min (35 min total) at a flow rate of 1 mL min^{-1}. DA-ZP1-TPP (retention time = 31.1 min) was judged to be ≥ 99% pure based on the integrated chromatogram (Figure 4.3). ^{1}H NMR (DMSO-d_6, 300 MHz): δ 9.10 (1H, t), 8.53 (4H, d), 8.11 (1H, d), 8.04 (1H,d) 7.80 (15H, m), 7.64 (5H, m), 7.46 (4H, d), 7.34 (4H, ψt), 6.94 (2H, s), 5.76 (4H,s), 4.17 (2H, s), 4.12 (2H, s), 4.00 (8H, m), 3.79 (2H, m), 3.57 (2H, m). ^{31}P NMR (DMSO-d_6, 300 MHz): δ 22.19. ESI-MS: observed (expected) M/Z for $[M+H]^+$ = 1238.4 (1238.3), $[M+2H]^{2+}$ = 620.6 (620.2), $[M+3H]^{3+}$ = 413.5 (413.7).

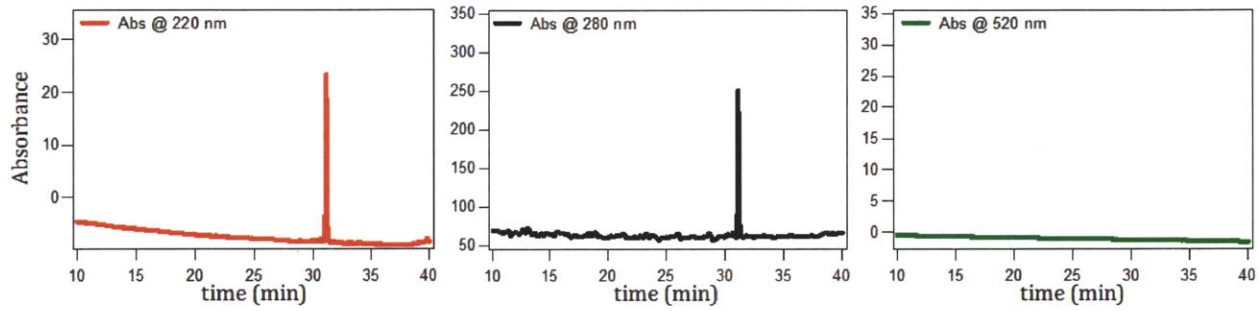

Figure 4.3. The analytical HPLC chromatogram of DA-ZP1-TPP, monitoring at 220, 280, and 520 nm. DA-ZP1-TPP has no absorbance at 520 nm in the acetylated form. DA-ZP1-TPP was judged to be ≥ 95% pure based on the integrated absorbance signal.

Determination of Octanol-water Partition Coefficients

Octanol-water partition coefficients (Log *P*) were measured using a modified literature protocol (Table 4.1).[7] 750 μL of water and 750 μL of n-octanol were added to a 1.5 mL microcentrifuge tube and mixed on a shaker for 6 hours to ensure saturation of the water and octanol phases. Subsequently, the sample was added to the tube and vortexed for 2 min. Sample concentrations were selected to ensure that saturation and precipitation did not occur in either

---

[7] OECD Guideline for the Testing of Chemicals. Partition Coefficient (n-octanol/water): Shake Flask Method. ©OECD **1995**, 107.

phase. After vortexing, the tube was centrifuged on a desktop centrifuge for 5 min, the lower aqueous layer was removed, and the amount of sample present was quantified by UV-visible spectroscopy. The Log *P* value for each sample was then calculated from the partitioning between the aqueous and octanol layers. Measurements were repeated in triplicate and were verified to be independent of the water:octanol ratios or sample concentrations.

Photophysical and Zinc-Binding Properties of DA-ZP1-TPP

Buffer conditions and reference fluorophores were identical to those for ZP1-TPP outlined in Chapter 2.2 (p. 25).

Zinc Sensitivity Measurements of DA-ZP1-TPP. A solution of 1 mM EDTA and 2 mM $CaCl_2$ was prepared in 30 mL PIPES buffer and allowed to equilibrate. For each point, DA-ZP1-TPP was added, and the system was allowed to reach equilibrium (30 min). For each data point (n), (64-2n) μL of a 50 mM $ZnCl_2$ stock were added to the stock CaEDTA solution and a 2 mL aliquot removed. DA-ZP1-TPP was added to each 2 mL aliquot to achieve a final sensor concentration of 1 μM. The emission spectrum for each data point was recorded once the emission spectrum stabilized (~30 min). For each data point, the amount of free zinc for that given concentration of total zinc was calculated as described for ZP1-TPP. Integrated DA-ZP1-TPP fluorescence was then plotted against the concentration of free zinc present (Table 4.2).

pH-Dependent Fluorescence Titrations. The pH-sensitivity of DA-ZP1-TPP was investigated. 1.1 μM DA-ZP1-TPP was dissolved in 17.5 mM sodium acetate buffer (pH 3.5) with 100 mM KCl and either 250 μM EDTA or $ZnCl_2$ at 25 °C. The pH of the solution was increased over a range from 3.5 to 8.5 with successive additions of KOH. After reaching equilibrium, fluorescence was measured as an average of 3 scans for each pH value.

Specificity and kinetics studies of DA-ZP1-TPP deacetylation

Metal Ion Selectivity. A previously reported procedure was used to measure the metal ion selectivity of DA-ZP1-TPP.[5a] The fluorescence spectrum of a 1.1 μM solution of DA-ZP1-TPP was acquired initially and after addition of a 4 μL ($CaCl_2$, $MgCl_2$, 1.00M) or 10 μL (NaCl 2.00 M, $MnSO_4$, $CoCl_2$, $NiCl_2$, $CuCl_2$, $CdCl_2$, $FeCl_3$, 10 mM) aliquot of metal stock solution. Next, a 10 μL aliquot of $ZnCl_2$ (10 mM) was added and the fluorescence spectrum was measured. Finally, a 10 μL aliquot of EDTA (0.1 M) was added and a final fluorescence spectrum was acquired. For each series of measurements, the fluorescence signal was integrated and normalized to the integrated metal-free fluorescence signal.

Relative half-lives of deacetylation. The half-life of a 2.75 μM solution of DA-ZP1-TPP in 50 mM PIPES buffer (pH 7) with 100 mM KCl was measured in the presence of excess $ZnCl_2$, (125 μM), EDTA (250 μM), or esterase (1.25 units) at 37 °C. Hydrolysis of the acetyl groups was monitored by UV-vis spectroscopy by measuring the absorbance at 519 nm (EDTA and esterase) or at 510 nm ($ZnCl_2$). The resulting data were fit to a single exponential using Igor Pro software and corresponding half-lives calculated (Figure 4.4 and Table 4.3).

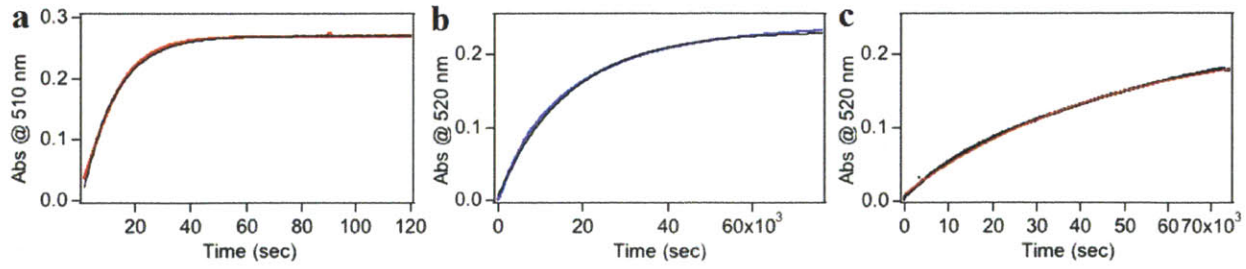

Figure 4.4. Kinetic traces of acetyl group hydrolysis in DA-ZP1-TPP. Trace and fit of (a) DA-ZP1-TPP in buffer supplemented with 125μM $ZnCl_2$, (b) DA-ZP1-TPP in buffer supplemented with esterase, (c) and DA-ZP1-TPP in buffer.

HPLC study of DA-ZP1-TPP. A 110 μM DA-ZP1-TPP in 50 μL of 5 mM PIPES buffer (pH 7) with 10 mM KCl was prepared and allowed to equilibrate for 5 min. A 10 μL aliquot was

removed, quenched with 50 μL 0.1% TFA in Millipore H_2O and flash frozen in liquid nitrogen. 0.5 equivalents of $ZnCl_2$ were then added and the mixture was allowed to equilibrate for 5 min. A 10 μL aliquot was then removed and flash frozen. This process was repeated to achieve data points at 1 eq., 1.5 eq., and excess $ZnCl_2$ conditions. The resulting samples were analyzed by reversed-phase analytical HPLC (Zorbax C18, 5 μm, 4.6 mm i.d. x 250 mm). The resulting peaks from HPLC analyses were collected and identified by ESI-MS.

Mammalian Cell Culture, Labeling, and Imaging Procedures

General procedures pertaining to cell cultures, fluorescence microscopy, turn-on quantification, and Pearson's correlation calculations are as outlined in Chapter 3.2 (p. 26) except where otherwise noted. PC3 prostate cells were cultured at 37°C with a 5% CO_2 atmosphere in RPMI 1640 media supplemented with 10% FBS and 1% penicillin/streptomycin.

Imaging of DA-ZP1-TPP in Live Cells. The stability of the acetyl groups on DA-ZP1-TPP in live cell environments was investigated. Live HeLa cells were incubated with 1 μM DA-ZP1-TPP for 30 min, and then washed with 2 x 1 mL dye- and serum-free DMEM. The plate was then bathed in 2 mL dye- and serum-free DMEM and imaged by multichannel fluorescence microscopy over a span of 2 hours with 15 min time points. Fluorescence signal in the resulting images was quantified by ImageJ.

To assess the zinc responsiveness of DA-ZP1-TPP, stock solutions of $ZnCl_2$ (10 mM) and sodium pyrithione (20 mM) were diluted in 37°C dye- and serum-free DMEM to a final $Zn(pyrithione)_2$ concentration of 50 μM. The zinc-enriched media was exchanged in the cell culture dish directly on the microscope stage. Similarly, a stock solution of tetrakis-(2-Pyridylmethyl) ethylenediamine (TPEN, 20 mM) in DMSO was diluted in warm dye- and

serum-free DMEM to a concentration of 100 μM. Media containing TPEN was exchanged in the culture dishes on the microscope stage. Localization of DA-ZP1-TPP in HeLa cells was investigated by coincubation of HeLa cells with 1 μM DA-ZP1-TPP and 250 nM MitoTracker Red FM for 30 mins. The plate was washed with 2 x 1 mL dye- and serum-free DMEM, then bathed in 2 mL dye- and serum-free DMEM. The zinc-bound form of the sensor was obtained as described above and imaged by multichannel fluorescence microscopy.

Mitochondrial colocalization studies were repeated in RPWE-1 and RPWE-2 prostate cell types using similar methodologies. Zinc uptake properties of these cells were investigated by using DA-ZP1-TPP to image zinc in cells incubated in zinc-free or zinc-enriched media. Three plates each of RWPE-1 and RWPE-2 were incubated in either zinc-free keratinocyte serum-free media (K-SFM) or K-SFM supplemented with 50 μM $ZnCl_2$ for 24 hours. The plates were then washed with 2 x 1 mL of zinc-free K-SFM and incubated with 1 μM DA-ZP1-TPP in 2 mL zinc-free K-SFM for 30 min. Subsequently, the cells were washed with 2 x 1 mL dye-free and serum-free DMEM and bathed in 2 mL of the same. The cell plates were imaged by fluorescence microscopy, and three regions of interest for each plate were quantified in ImageJ (n=9). The zinc uptake properties of PC3 prostate cells were also probed using the same methodologies, with the exception that PC3 cells were incubated in DMEM instead of K-SFM.

4.3 Results and Discussion

Assessing Effects of Acetylation on Sensor Function and Properties

Acetylation of ZP1-TPP was achieved by one-step reaction with acetic anhydride at room temperature overnight (Figure 4.6). Acetylation causes conversion into the non-fluorescent lactone conformation, effectively breaking up fluorescein ring conjugation (Figure 4.6).

Acetylation of ZP1-TPP was intended to achieve two purposes—augmentation of the construct lipophilicity to improve membrane permeability and improvement of sensor photophysics. The lipophilicity of acetylated ZP1-TPP (DA-ZP1-TPP) was assayed by measuring the octanol-water partition coefficient (Log *P*) which was found to have increased from -0.11 ± 0.01 to 0.77 ± 0.18 for non-acetylated ZP1-TPP. This increase in Log *P* value indicated that the lipophilicity of DA-ZP1-TPP was comparable to other dyes that successfully localize to the mitochondria (Table 4.1).

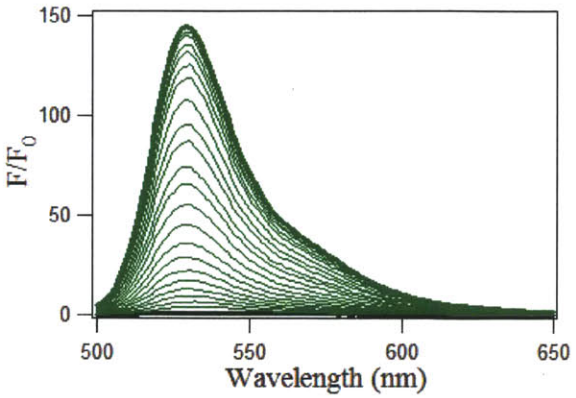

Figure 4.5. Fluorescence titration of DA-ZP1-TPP with $ZnCl_2$ in 50 mM PIPES (7) with 100 mM KCl.

In addition, titration of DA-ZP1-TPP with $ZnCl_2$ showed improved fluorescence response to zinc, in comparison to ZP1-TPP. Acetylation of the targeted probe improved zinc-responsive turn-on from ~7-fold to > 140-fold increase (Figure 4.5, Table 4.2). This improvement was due to the large attenuation of *apo* form absorbance in DA-ZP1-TPP, resulting in a decrease of the quantum yield, $\Phi = \leq 0.01$ (Table 4.2). Addition of zinc during the titration caused hydrolysis of the DA-ZP1-TPP acetyl groups, resulting in restoration of fluorescence. Complete zinc-mediated hydrolysis of DA-ZP1-TPP regenerates zinc-bound ZP1-TPP, such that DA-ZP1-TPP only differs from ZP1-TPP in the zinc-free state (Table 4.2). As seen in Figure 4.5, the acetylated DA-ZP1-TPP reacts with zinc through zinc-mediated acetyl hydrolysis, generating fluorescence signal as a result of the acetyl hydrolysis. Because zinc-induced DA-ZP1-TPP fluorescence signal is caused by the acetyl hydrolysis reaction, DA-ZP1-TPP is a reaction-based probe, a class of sensors that respond to specific analytes through often irreversible chemical reactions.

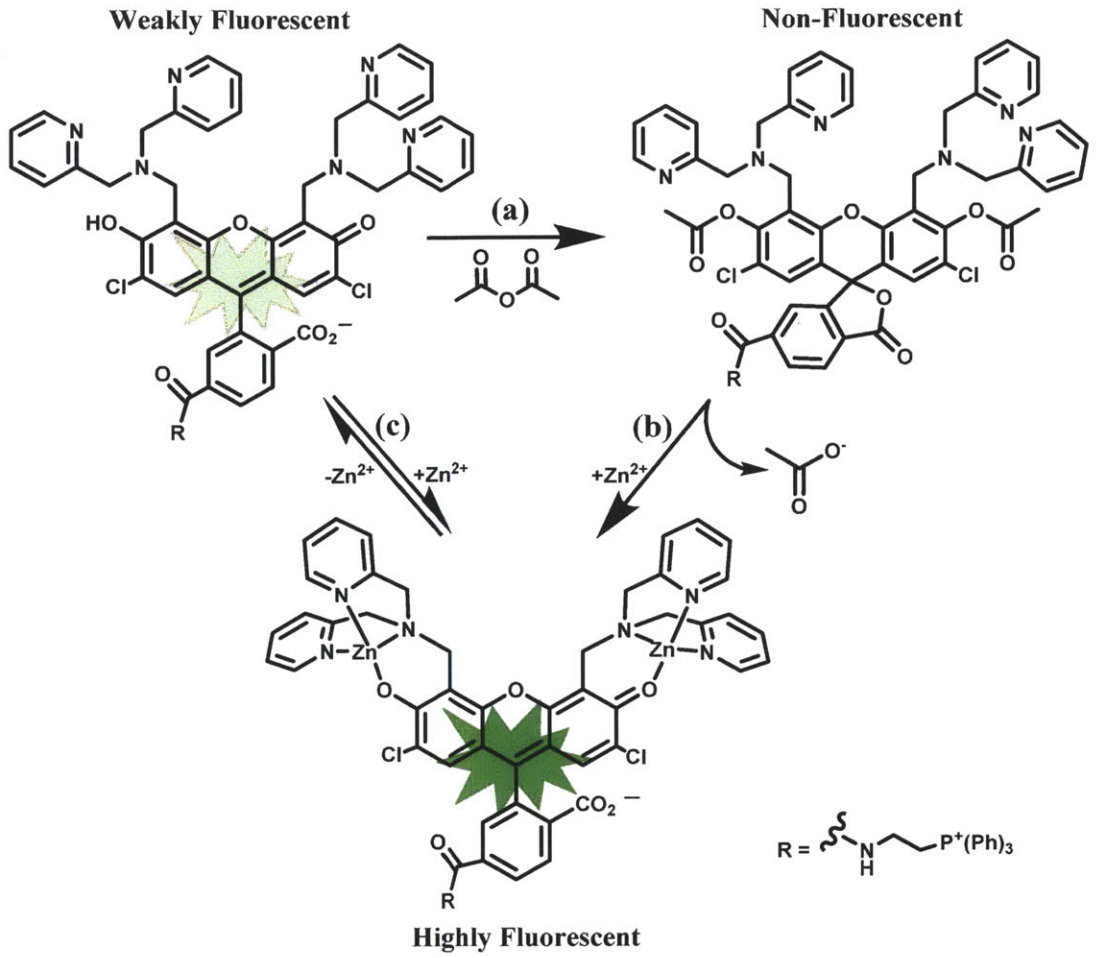

Figure 4.6. Preparation and utilization of DA-ZP1-TPP reaction-based probe. (a) Acetylation of ZP1-TPP to produce DA-ZP1-TPP. (b) Zinc-mediated acetyl hydrolysis and zinc-induced sensor turn-on. (c) Reverse of zinc response by removal of bound zinc, returning probe back to weakly-fluorescent state.

Sensor	Turn-on	Log *P*	λ_{abs} (nm)		Φ_{apo}	Φ_{Zn}	$K_{d\text{-}Zn}$ (M)
			Apo	Zn(II)			
ZP1[a]	6	1.98 ± 0.02	515	507	0.38	0.87	7.0×10^{-10}
ZP1-TPP[b]	7	-0.11 ± 0.01	519	510	0.15	0.75	6.01×10^{-10}
DA-ZP1-TPP	>140	0.77 ± 0.18	-	510	<0.01	0.75	3.47×10^{-9}

Table 4.2. Comparison of ZP1, ZP1-TPP, and DA-ZP1-TPP photophysical and zinc-binding properties. Spectroscopic properties were measured in 50 mM PIPES (7) with 100 mM KCl, and log P values were determined by octanol-water shake flask method. [a]Spectroscopic properties of ZP1 reported from literature values.[8] [b]ZP1-TPP properties from Chapter 2.

[8] Nolan, E. M.; Lippard, S. J. *Acc. Chem. Res.* **2009**, *42*, 193

Characterization of DA-ZP1-TPP Acetyl Hydrolysis

Detailed investigation of acetyl hydrolysis was undertaken to study the kinetics, selectivity, and conditions for the reaction-based zinc probe DA-ZP1-TPP. First, the selectivity of DA-ZP1-TPP hydrolysis for zinc was characterized by mixing DA-ZP1-TPP with metal ions in the same row of the periodic table as zinc. Even in the presence of these metals, DA-ZP1-TPP was able to selectively respond to zinc addition in most cases (Figure 4.7). Cadmium, the only metal other than zinc found to hydrolyze the acetyl groups and turn on the sensor, is not a biologically significant metal. Copper, nickel, and cobalt quenched fluorescence, a feature native to the parent ZP1 sensor.[9] DA-ZP1-TPP was insensitive to biologically relevant metal cations and remained sensitive to zinc. Most importantly, addition of the chelator EDTA attenuated probe fluorescence, demonstrating partial reversibility of zinc response (Figure 4.7). Most reaction-based probes are irreversible due to the nature of the deprotection reaction, but DA-ZP1-TPP provides a measure of reversibility due to reversible zinc-binding of ZP1-TPP and weak fluorescence of the zinc-free state (Figure 4.6). Even partial reversibility provides an additional method to verify that observed fluorescent signal actually originates from detecting the target analyte, rather than artificial turn-on in the absence of analyte.

Next, the pH sensitivity of the zinc-selective reaction-based probe was studied by measuring zinc responsive fluorescence in solutions buffered to pH 3.5-8.5. One of the limitations of the parent ZP1 sensor is sensitivity to low pH, caused by protonation of the DPA arms. As seen in the pH profile of ZP1, fluorescence increases significantly at pH below 7, restricting the functional range of the ZP1 probe to pH at or above 7 and also presents possibilities of artificial fluorescence signal due to protonation rather than detection of zinc. In

---

[9] Woodroofe, C.C.; Masalha, R.; Barnes, K.R.; Frederickson, C.J.; Lippard, S.J. *Chem. Biol.* **2004**, 11, 1659-1666.

comparison, DA-ZP1-TPP has minimal pH sensitivity in the zinc-free state resulting in a wider functional range for zinc detection at pH $\geq$ 5 (Figure 4.8). In addition, DA-ZP1-TPP remains quenched at low pH (< 5), ensuring that observed fluorescence signal will not include artificial contributions from DPA protonation.

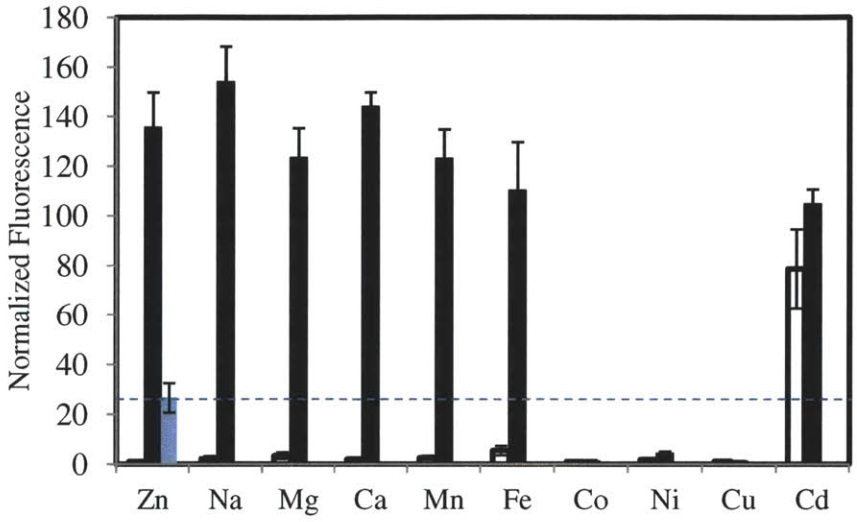

Figure 4.7. Metal ion selectivity of DA-ZP1-TPP. Emission spectra of 1 μM solutions of acetylated probe were acquired initially, after addition of metal ions, and after addition of $ZnCl_2$. The blue column represents sensor emission after addition of 100 μM EDTA, a chelator. Data was normalized to initial measured emission.

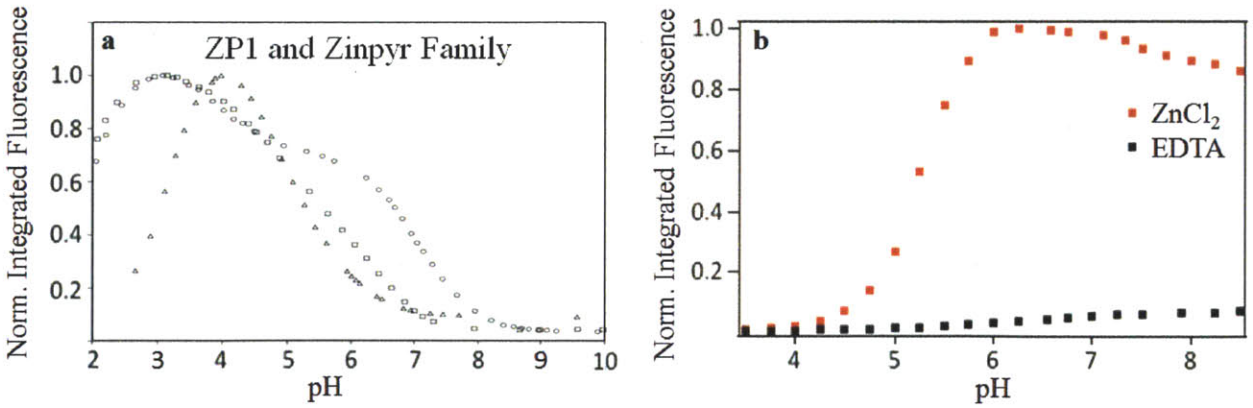

Figure 4.8. pH dependency of ZP1 and DA-ZP1-TPP fluorescence signal. (a) Zinc-free *apo* state integrated fluorescence of ZP1 and Zinpyr family sensors showing sensitivity under acidic conditions.[10] (b) Zinc-free (black) versus zinc-bound (red) fluorescence of DA-ZP1-TPP showing improved functional range and insensitivity to acidic conditions.

---

[10] Wong, B.A.; Friedle, S.; Lippard, S.J. *J. Am. Chem. Soc.* **2009**, 131, 7142-7152.

Characterization of DA-ZP1-TPP established that significant sensor improvements arose from the reaction-based functionality imbued by the acetyl groups. Subsequently, the kinetics and characteristics of the acetyl hydrolysis process were studied. To investigate the order of hydrolysis, DA-ZP1-TPP was mixed with sub-stoichiometric amounts of $ZnCl_2$ and then quenched and frozen. Each aliquot was characterized by analytical HPLC, with each resultant peak identified by MS. As seen in the HPLC trace monitoring at 220 nm, successive addition of zinc causes the conversion of DA-ZP1-TPP into the ZP1-TPP probe. At initial time points without any added zinc, DA-ZP1-TPP had no absorbance at 520 nm and existed entirely in the DA-ZP1-TPP form. At low sub-stoichiometric amounts of zinc, however, an intermediate peak was observed (Figure 4.9). The mass of this peak corresponded to singly-acetylated Ac-ZP1-TPP, indicating that hydrolysis of a single acetyl group occurred. The observation of this single-acetylated intermediate suggests that DA-ZP1-TPP deacetylation occurs in a stepwise manner, rather than concerted hydrolysis of both acetyl groups (Figure 4.10).

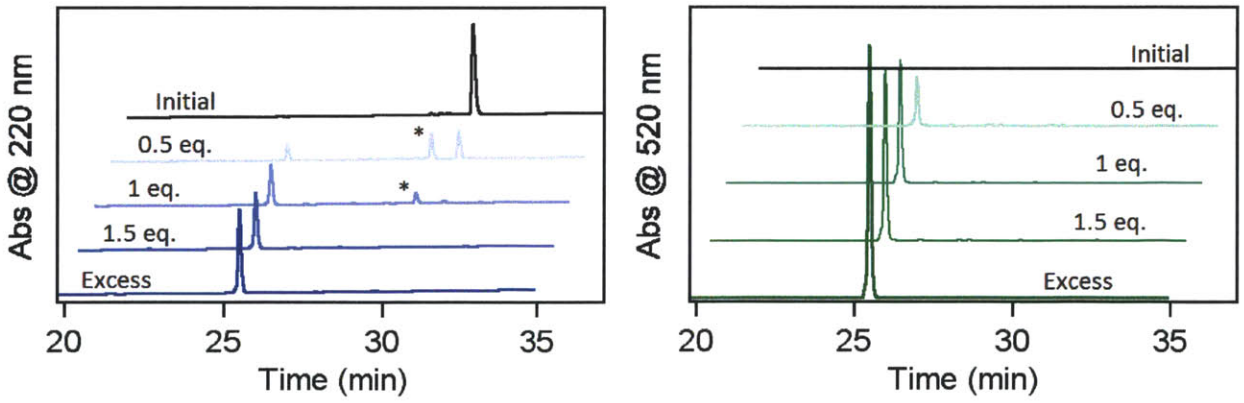

Figure 4.9. HPLC study of DA-ZP1-TPP deacetylation order. 100 μM DA-ZP1-TPP was incubated with varying amounts of zinc and analyzed by analytical HPLC. Peaks from HPLC were identified by MS with the rightmost peak found to be DA-ZP1-TPP and the leftmost peak found to be ZP1-TPP. The peak marked with an asterisk (*) corresponds to singly acetylated sensor, Ac-ZP1-TPP (ESI MS observed (expected): 598.8 (599.1)).

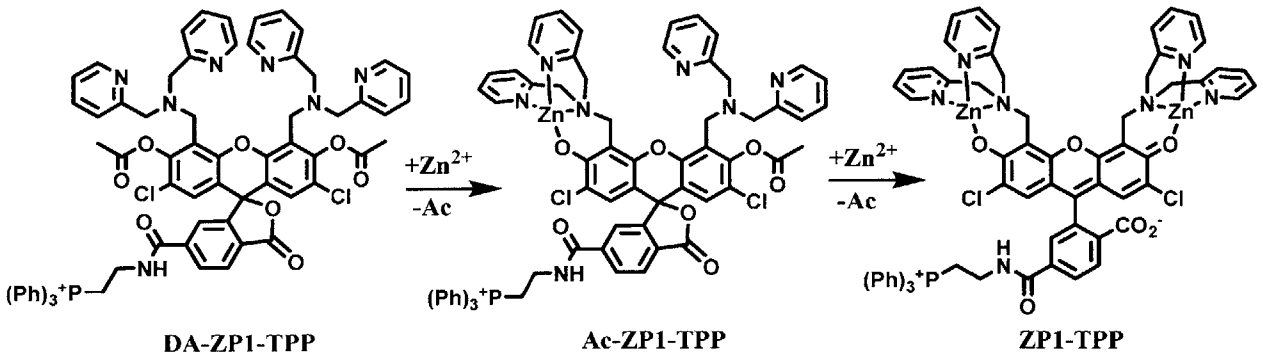

Figure 4.10. Stepwise hydrolysis of acetyl groups proceeding through a singly-acetylated Ac-ZP1-TPP intermediate.

In the context of these HPLC studies, one possible explanation for site-independent zinc-mediated hydrolysis is the nature of ZP1 sensor zinc binding. In the parent ZP1 sensor, each DPA arm binds zinc in a five coordinate configuration with one water molecule coordinated to zinc.[11] Since it is likely that DA-ZP1-TPP binds zinc with similar coordination as the parent sensor, the binding of zinc to the DPA arms and phenolic oxygen atoms could position and activate a water molecule near the acetyl ester moiety. Zinc bound to DA-ZP1-TPP would then serve two roles—to increase the nucleophilicity of the water molecule and to spatially position the activated water for backside ester attack. Previously, hydrolytic activity was observed in a computationally designed protein containing zinc with an open coordination site that activated water.[12] Each bound atom of zinc in DA-ZP1-TPP could also serve a similar water-activating role (Figure 4.11). The positioning and activating effects of bound zinc would serve to preferentially facilitate acetyl hydrolysis in the presence of zinc.

Qualitatively, acceleration of acetyl hydrolysis was observed in DA-ZP1-TPP whenever the probe was exposed to zinc. To quantify this acceleration, the rates of acetyl hydrolysis in DA-ZP1-TPP were measured by absorbance over time. In pure buffer, the hydrolysis proceeded

---

[11] Burdette, S.C.; Walkup, G.K.; Springler, B.; Tsien, R.Y.; Lippard, S.J. *J. Am. Chem. Soc.* **2001**, 123, 7831-7841.
[12] Der, B.S.; Edwards, D.R.; Kuhlman, B. *Biochemistry.* **2012**, 51, 3933-3940.

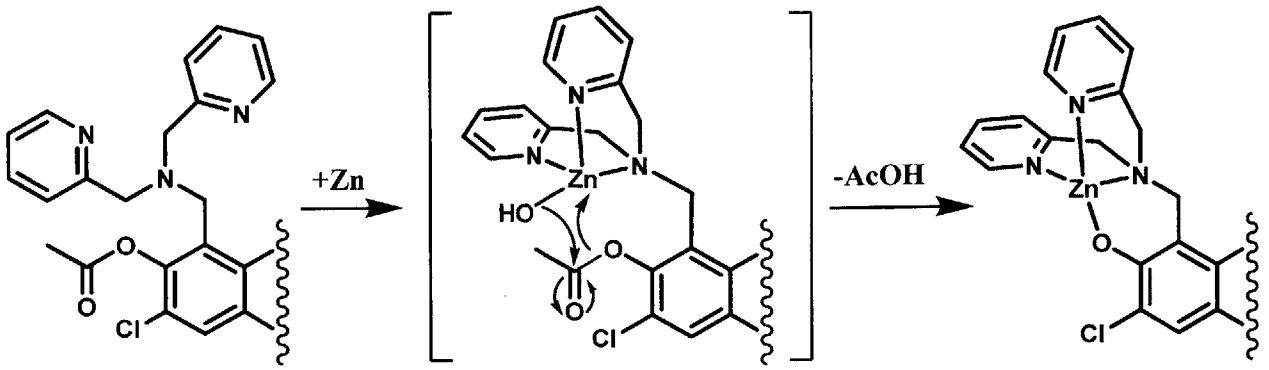

Figure 4.11. Possible mechanism of zinc-mediated acetyl hydrolysis depicting positioning and activation of water by bound zinc.

quite slowly with $t_{1/2}$ = 31,000 s (Figure 4.5c, Table 4.3). Addition of zinc increased the rate of hydrolysis by three orders of magnitude, lowering the half-life to $t_{1/2}$ = 8.2 s (Figure 4.5a, Table 4.3). The accelerating effect of zinc on DA-ZP1-TPP acetyl hydrolysis cannot be described as catalysis beecause zinc that is bound to the sensor is not subsequently released from the probe. Zinc in this case could be more accurately described as mediating the hydrolytic reaction, resulting in a net rate increase. Previous selectivity studies (Figure 4.7) showed that biologically relevant metals are poor mediators of acetyl hydrolysis in DA-ZP1-TPP relative to the accelerating effect of zinc, indicating that the large rate increase observed is specific to zinc.

On the other hand, biological environments are more complicated than solutions of metal ions in buffer. Cells typically have a variety of different esterases capable of hydrolyzing a wide variety of esters.[13] Some reaction-based probes, such as 6-carboxyfluorescein diacetate, utilize the activity of esterases to trap and activate the staining fluorophore within the cell.[3-4] With DA-ZP1-TPP, however, sensitivity to esterases was undesirable since esterase catalyzed hydrolysis could potentially increase sensor fluorescence in the absence of zinc. To test the sensitivity of DA-ZP1-TPP to esterases, the rate of hydrolysis was also measured in buffer with added

[13] Satoh, T.; Hosokawa, M. *Annu. Rev. Pharmacol. Toxicol.* **1998**, 38, 257-288.

esterase. DA-ZP1-TPP was be relatively resilient and impervious to esterase, as seen by the large half life value of $t_{1/2}$ = 11,000 s, which is comparable to that of DA-ZP1-TPP in buffer alone (Table 4.3). In addition to the photophysical and zinc-sensing advantages offered by acetylation, DA-ZP1-TPP is resilient to hydrolysis by esterase and is highly selective for zinc (Figure 4.12).

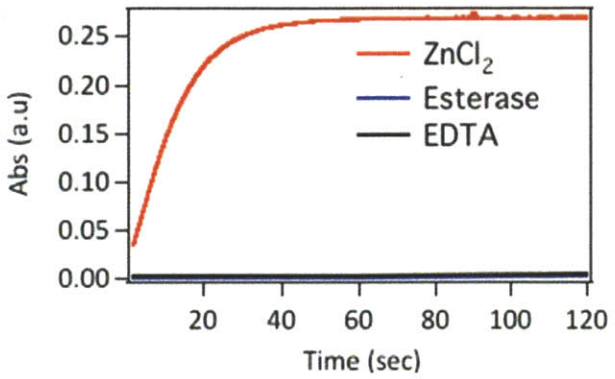

Figure 4.12. Kinetics traces of acetyl hydrolysis in the presence of buffer, esterase, or zinc. Addition of 125 μM zinc accelerates acetyl hydrolysis by three orders of magnitude over buffer or esterase conditions.

	Buffer	Esterase	Zn^{2+}
k_{obs}	2.23×10^{-5}	6.62×10^{-5}	8.55×10^{-2}
$t_{1/2}$ (s)	13,000	11,000	8.2

Table 4.3. Kinetics and half-lives for DA-ZP1-TPP acetyl hydrolysis (a) in 50 mM PIPES (7) with 100 mM KCl, (b) in buffer supplemented with porcine liver esterase, (c) in buffer with 125 μM $ZnCl_2$.

Utilization of DA-ZP1-TPP to Image Zinc in Mitochondria of Live HeLa Cells

Testing of the acetylated ZP1-TPP sensor, DA-ZP1-TPP, showed improvements in various photophysical and zinc-binding properties but also indicated a substantial increase in lipophilicity over the non-acetylated form. Acetylation of ZP1-TPP increased its Log *P* from -0.11 ± 0.01 to 0.77 ± 0.18. To examine whether this increase in lipophilicity was sufficient to allow DA-ZP1-TPP to escape the endosomes and localize to the mitochondria, HeLa cells were incubated with 1 μM DA-ZP1-TPP for 30 min and imaged by fluorescence microscopy. Zinc-enriched media was then added on stand to turn on the sensor, converting it back to Zn_2-ZP1-TPP, for easier visualization. As can be seen in the cell images, zinc-bound ZP1-TPP strongly localizes to the mitochondria, in comparison with the endosomal localization of ZP1-TPP (Figure 4.13).

Calculation of the Pearson's correlation between DA-ZP1-TPP and MitoTracker Red indicated strong colocalization with a coefficient of $r = 0.58 \pm 0.10$. The strong correlation of DA-ZP1-TPP to MitoTracker suggests that acetylation caused sufficient increase in lipophilicity to render the acetylated probe more membrane permeable. The new Log *P* value of DA-ZP1-TPP places it well within the range of constructs that properly localize to the mitochondria, further emphasizing the importance of sufficient lipophilicity for escape and localization.

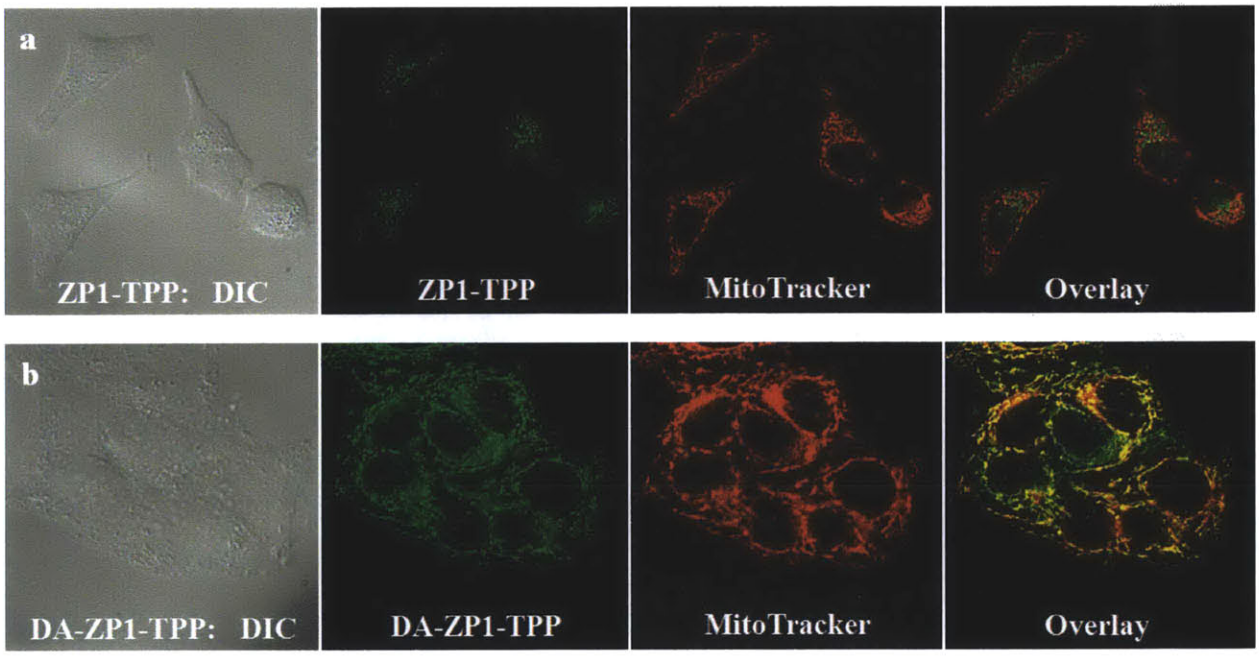

Figure 4.13. Comparison of ZP1-TPP and DA-ZP1-TPP localization in HeLa cells. (a) Image series of HeLa cells incubated with 5 μM ZP1-TPP. Pearson's correlation coefficient between ZP1-TPP and MitoTracker was found to be $r = -0.14 \pm 0.07$. (b) Image series of HeLa cells incubated with 1 μM DA-ZP1-TPP. Pearson's correlation coefficient $r = 0.58 \pm 0.10$.

Although acetylation of the sensor was effective at tuning lipophilicity and enabling proper mitochondrial targeting, the stability of the acetyl groups in live cell environments is important for proper function of the sensor within the cell. *In vitro* testing of DA-ZP1-TPP with isolated esterases showed high resistance to acetyl hydrolysis by esterase. To confirm this

observation within the more complex cell environment, HeLa cells were incubated with 5 μM DA-ZP1-TPP for 30 min and then imaged for 2 hours. Over this time span, there was no significant increase in fluorescence, indicating that the acetyl groups of the probe were stable in cells and not cleaved by esterases (Figure 4.14). Any acetyl hydrolysis would cause an increase in signal due to the weakly fluorescent nature of the zinc-free state. No such increase was observed over 2 hours, showing that DA-ZP1-TPP was resistant to hydrolysis in cells in the absence of zinc.

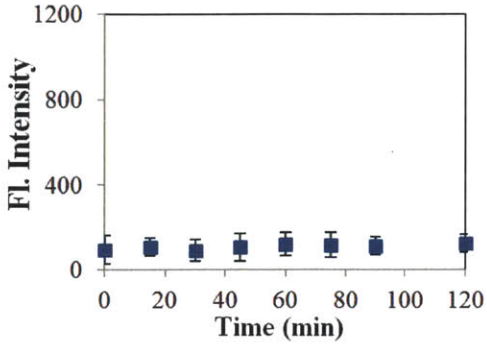

Figure 4.14. Stability of DA-ZP1-TPP in HeLa cells over 2 hours at 37°C.

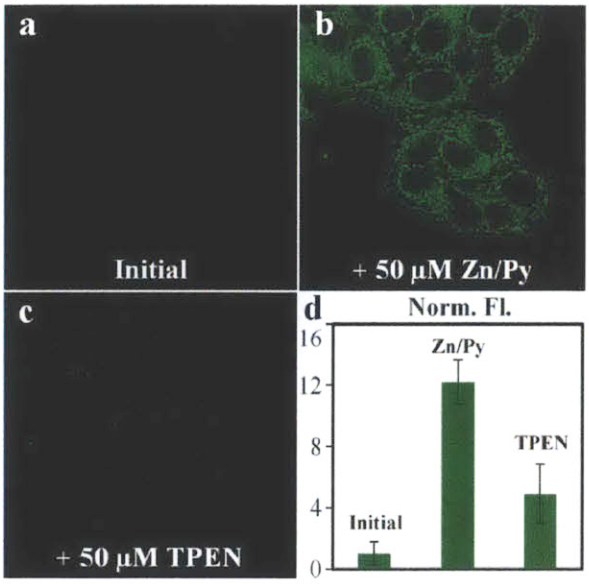

Figure 4.15. Zinc response of DA-ZP1-TPP in fluorescence imaging of live HeLa cells. (a) Initial signal intensity. (b) Emission after addition of 50 μM $ZnCl_2$/sodium pyrithione. (c) Signal after addition of 100 μM TPEN. (d) Average normalized fluorescence signal of DA-ZP1-TPP in live cells (n = 21).

The DA-ZP1-TPP probe was then tested for ability to reversibly detect zinc. HeLa cells were incubated as mentioned previously and imaged on a fluorescence microscope. Initial cell images had minimal DA-ZP1-TPP emission, consistent with the low quantum yield of the diacetylated form of the sensor. Upon addition of 50 μM $ZnCl_2$/pyrithione, a greater-than 12-fold increase in fluorescence intensity was observed in the mitochondria of the cell (Figure 4.15), in stark contrast to the zinc insensitivity with non-acetylated ZP1-TPP (Chapter 2.3, p. 32). Subsequent addition of 100 μM TPEN, an intracellular chelator, attenuated the fluorescence signal (Figure 4.15). The partial reversibility of

zinc-responsive fluorescence increase is an important indicator that the observed mitochondria staining pattern was due to sensor binding zinc, rather than hydrolysis of acetyl groups. DA-ZP1-TPP was found to localize properly to mitochondria in HeLa cells and exhibit large, reversible fluorescence zinc response.

Investigating Mitochondrial Zinc in the Prostrate using DA-ZP1-TPP

HeLa cells served as an excellent live cell environment to test the newly developed DA-ZP1-TPP sensor. HeLa cells, however, are not prostate cancer cells and served the primary purpose of vetting sensors prior to biological applications. Since the benefits and improvements of DA-ZP1-TPP have been explored in the previous section, the next area of focus was the prostate and the role of mitochondrial zinc in prostate cancer. The uptake and transport of mobile zinc into the cytosol and within certain organelles is fairly well understood, but relatively little is known about mitochondrial zinc transport in cancerous or non-cancerous cell lines.

The prostate cell lines RWPE-1 and RWPE-2 were selected for study with the newly characterized DA-ZP1-MPP. Cancerous prostate cell lines such as RWPE-2 have been reported to have lowered cytosolic zinc uptake.[14] Techniques previously used to monitor mobile zinc, however, were unable to provide site-specific information about mitochondrial zinc, where zinc plays the important role of inhibiting aconitase and the conversion of citrate into isocitrate.[15] Non-cancerous prostate cell lines such as RWPE-1, on the other hand, are thought to have normal uptake and proper localization of mobile zinc into the mitochondria in order to inhibit aconitase and promote the secretion of excess citrate, an essential buffering agent in seminal fluid.[16] The DA-ZP1-MPP zinc sensor developed in this chapter was then used to investigate the

---

[14] Huang, L.; Kirschke, C.P.; Zhang, Y. *Cancer Cell International.* **2006**, 6, 10.
[15] Costello, L.C.; Liu, Y.; Franklin, R.B.; Kennedy, M.C. *J. Biol. Chem.* **1997**, 272, 28875-28881.
[16] Kavanagh, J.P. *J. Reprod. Fer.* **1985**, 75, 35-41.

subcellular distributions of mobile zinc and probe whether or not mitochondrial zinc uptake differed between cancerous and non-cancerous prostate cell lines.

Before proceeding with application of the DA-ZP1-MPP probe, both RWPE-1 and RWPE-2 cell lines were tested with the acetylated sensor to ensure proper functionality and localization. Plates of each cell type were incubated with DA-ZP1-MPP using similar conditions as used for HeLa cells, and imaged via fluorescence microscopy. DA-ZP1-MPP in RWPE-1 and RWPE-2 possessed sensitive, reversible zinc-responsive fluorescence increases mirroring the results observed in HeLa cell lines and also localized strongly to the mitochondria (Figure 4.16).

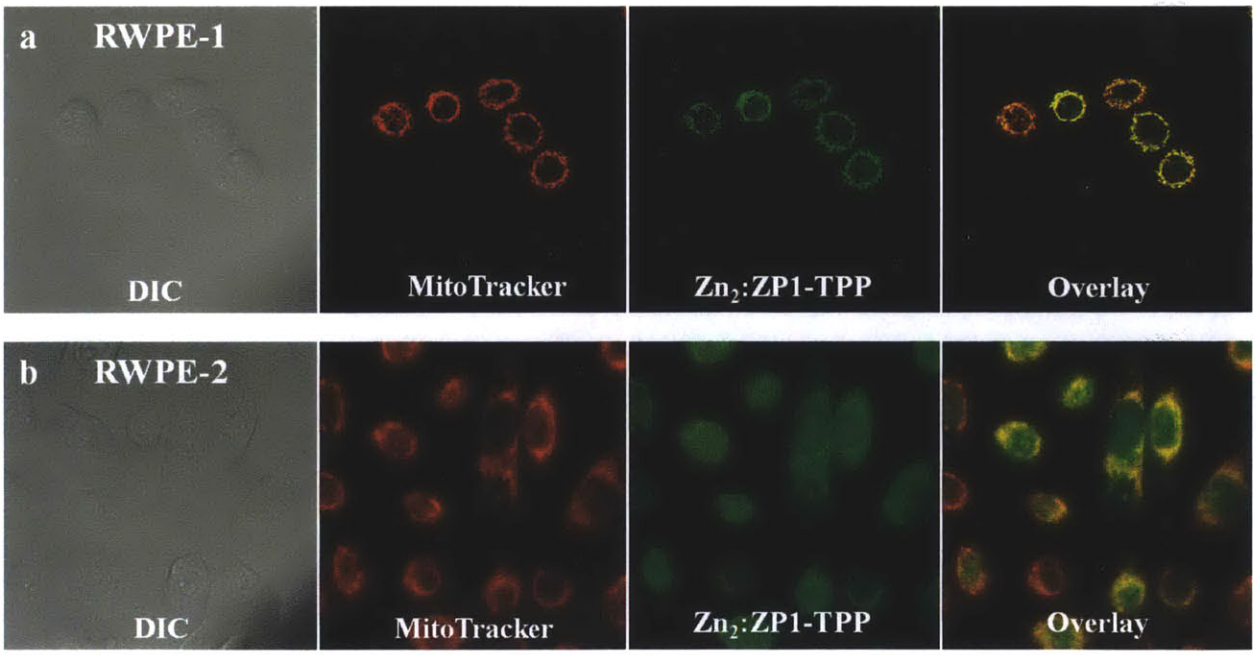

Figure 4.16. Mitochondrial localization of DA-ZP1-TPP in RWPE-1 and RWPE-2 Prostate cell lines. MitoTracker Red and DA-ZP1-TPP were coincubated in cell plates for 30 min prior to imaging. (a) Colocalization images for RWPE-1, Pearson's correlation coefficient $r = 0.68 \pm 0.09$. (b) Colocalization images for RWPE-2, Pearson's correlation coefficient $r = 0.59 \pm 0.1$.

After ensuring the proper localization and functionality of the DA-ZP1-MPP probe in prostate cell lines, RWPE-1 and RWPE-2 cells were grown in zinc-free media. 24 hours before imaging, half of the plates were switched into media enriched with $ZnCl_2$. DA-ZP1-MPP was

then used to visualize mitochondrial zinc in those cells. The initial fluorescence represented relative amounts of endogenous zinc contained in the prostate cell. To serve as a fixed reference point after measuring initial fluorescence, the cells were subsequently saturated with $ZnCl_2$/Pyrithione media and imaged again.

These imaging experiments showed that the non-cancerous RWPE-1 cell line has a statistically significant increase in mitochondrial zinc when incubated in elevated zinc conditions versus incubation in zinc-free media (Figure 4.17). In contrast, the cancerous prostate cell line RWPE-2 does not have a statistically significant difference in mitochondrial zinc when grown in either zinc-free or zinc-rich media. These results suggest that non-cancerous RWPE-1 cells have fully functioning zinc transport systems, causing an increase in zinc uptake and localization to the mitochondria when exposed to higher zinc conditions. On the other hand, RPWE-2 cells could have deficient cytosolic zinc uptake, inhibited mitochondrial zinc transport, or a combination of both factors. The effect of these physiological differences in the cancerous RWPE-2 cells was attenuated mitochondrial zinc uptake.

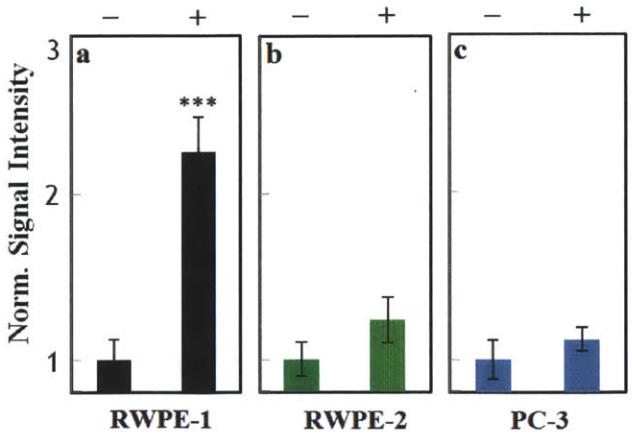

Figure 4.17. Decreased mitochondrial zinc uptake in cancerous cell lines. Cells from RWPE-1 (non-cancerous), RWPE-2 (cancerous), and PC-3 (cancerous) prostate cell lines were incubated for 24h in media with (+) and without (-) zinc. (a) Non-cancerous RWPE-1 have statistically significant ($p < 0.001$) increase in mitochondrial zinc uptake when incubated in zinc-enriched media. (b-c) RWPE-2 and PC-3 cells do not have statistically significant changes with or without zinc enriched media.

As further comparison, zinc uptake into the PC-3 cancerous prostate cell line was also investigated. Some researchers have previously presented evidence for a functional plasma-membrane zinc transporter in PC-3 cells, enabling accumulation of cytosolic zinc.[17] Due to the targeted nature of the DA-ZP1-TPP fluorophore, it is possible to measure the relative uptake of mobile zinc to the interior of the mitochondria. An analogous experiment using zinc or zinc-free 24h incubations was conducted, and the data showed no statistically significant increase in mitochondrial zinc when PC-3 cells were incubated with zinc-rich media, essentially mimicking the results observed with RWPE-2 cancerous prostate cells (Figure 4.17). Although the experiments with DA-ZP1-TPP do not rule out cytosolic uptake, they establish that PC-3 cells, without artificial stimuli, have markedly reduced mitochondrial zinc uptake compared to healthy prostate cells. Previous zinc quantification work has largely relied on tracing radiolabeled zinc in cell extracts, a method that does not provide any spatial information.[17] Assuming that PC-3 cells do have a transport protein for zinc import into the cytosol, imaging results using DA-ZP1-TPP suggest that the mechanism of mitochondrial zinc uptake is largely independent of the transporters and cellular machinery used to import zinc across the plasma membrane.

There are several reasons why inhibition of zinc uptake into the mitochondria might be advantageous for cancerous prostate cells. Zinc promotes secretion of citrate by inhibiting mitochondrial aconitase;[15] a scarcity of zinc in the mitochondria would allow the cancerous cell to generate more energy through the TCA cycle and avoid siphoning off citrate for secretion in seminal fluid. Zinc is also thought to be involved in mitochondria-initiated apoptosis, [18] thus

---

[17] Costello, L.C.; Liu, Y.; Zou, H.; Franklin, R.B. *J. Biol. Chem.* **1999**, 274, 17499-17504.
[18] (a) Untergasser, G.; Rumpold, H.; Plas, E.; Witkowski, M.; Pfister, G.; Berger, P. *Biochem. Biophys. Res. Commun.* **2000**, 279, 607-614. (b) Feng, P.; Li, T.; Guan, Z.; Franklin, R.B.; Costello, L.C. *Mol. Cancer.* **2008**, 7, 25.

cancerous cells could reduce potential tumoricidal effects by maintaining low levels of mitochondrial zinc.

4.4 Conclusions and Future Work

Two complementary targeting methods were introduced in Chapter 2 and 3—the small molecule triphenylphosphonium (TPP) cation and peptide-based targeting moieties. The synthetic flexibility and modularity of conjugating sensors and targeting moieties to peptide scaffolds allowed the generation of two extracellular, membrane-targeted sensors, which specifically label the exterior surface of the plasma membrane, resist internalization, and have reversible zinc-responsive fluorescence.

Intracellular targets using both small molecule TPP targeting and peptide targeting with mitochondria-penetrating peptides (MPP) proved to be challenging. A variety of peptides, targeting moieties, and fluorophores were explored, leading to the discovery that fluorophore lipophilicity and charge play very significant roles in endosomal escape. Both small molecule- and peptide-sensor constructs entered cells through endocytosis and all constructs with insufficient lipophilicity were found to be sequestered in late stage endosomes. In response, the neutral and lipophilic sensor Zinquin was conjugated to MPP, and the resulting ZQ-MPP construct was able to escape endosomes and reach the mitochondria. ZQ-MPP was severely handicapped by its high toxicity and poor photophysics, which combined to render ZQ-MPP either cytotoxic or too dim to observe.

Instead of creating new sensors, a one-step modification was developed to simultaneously increase the lipophilicity of fluorescein-based sensors and improve the sensor response and photophysics. Acetylation of phenolic oxygen atoms generated DA-ZP1-TPP, a zinc-selective

and reversible reaction-based probe easily obtained by mixing the sensor with acetic anhydride. DA-ZP1-TPP has vastly improved zinc-responsive turn-on (140-fold versus 7-fold in ZP1-TPP), non-absorbent *apo* state for decreased background fluorescence, elimination of pH-dependent artificial turn-on, and broadened range of functional pH conditions.

The kinetics of the DA-ZP1-TPP acetyl hydrolysis process was studied by a combination of methods. Hydrolysis of the acetyl groups on DA-ZP1-TPP was found to be a stepwise, independent process with hydrolysis of both acetyl groups required for restoration of absorbance and fluorescence. The reaction-based functionality of DA-ZP1-TPP arises from the zinc-mediated acceleration of hydrolysis—the addition of zinc increased the rate of hydrolysis by three orders of magnitude. This rate acceleration only occurs in the presence of zinc; the rate of hydrolysis is mostly unchanged in the presence of other biologically relevant cations or with esterases as tested *in vitro* and in live cells. DA-ZP1-TPP can be used for selective detection of zinc under a wide variety of conditions.

More importantly, DA-ZP1-TPP was capable of entering the cell and selectively staining the mitochondria in four different cell lines. Acetylation of ZP1-TPP attenuated anionic charge and simultaneously increased the lipophilicity. DA-ZP1-TPP was able to translocate across the endosomal membrane and stain the mitochondrial matrix. Mitochondria-specific localization and reversible zinc-responsive fluorescence increase were verified in both HeLa and prostate cell lines. The utility of targeted zinc probes was then demonstrated by using the newly developed DA-ZP1-TPP probe to investigate zinc biology in prostate mitochondria. Imaging with the acetylated sensor showed that non-cancerous RWPE-1 cells have functioning zinc import machinery that significantly increased mitochondrial zinc levels when exposed to extracellular

zinc in the media. In comparison, PC-3 and RWPE-2 cancerous cell lines exhibited severely decreased mitochondrial zinc uptake compared to non-cancerous RWPE-1 cells.

Characterization of mitochondrial zinc in prostate cancer is but one of the potential applications for sensor acetylation in conjunction with small molecule and peptide targeting. Each method and strategy developed was intentionally designed to be as straightforward as possible to enable facile adaptation to different fluorophores and sensors, intra- or extracellular targets, and structural scaffolds. As such, the acetylation strategy has been recently utilized to rapidly develop new targeted zinc sensors (Figure 4.18). Sensor acetylation represents an easily accessible chemical modification to enhance uptake and photophysics of the sensor to complement the varied targeting abilities of peptides sequences and small molecules.

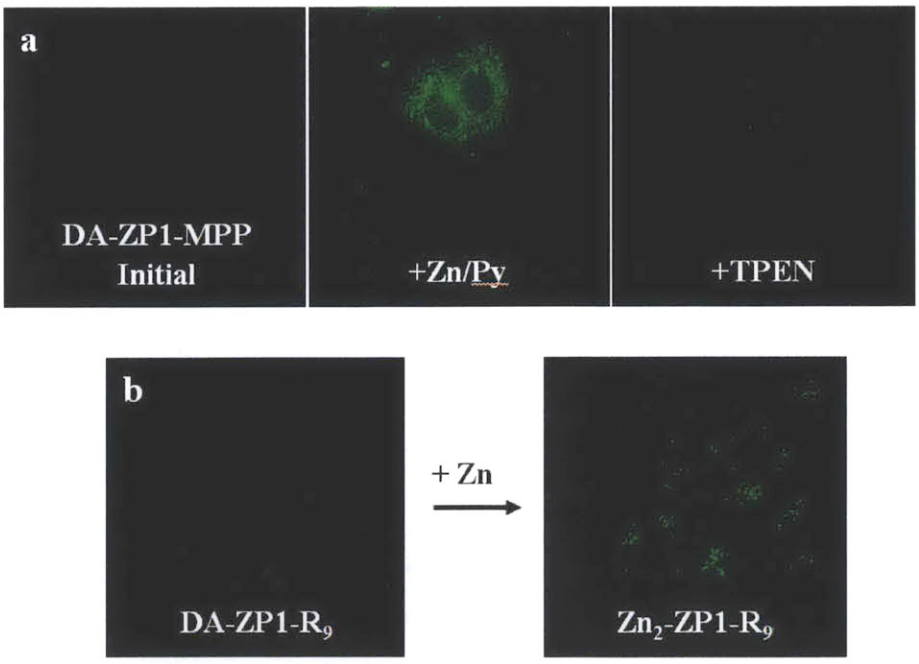

Figure 4.18. Two examples of new targeted sensors employing peptide targeting and sensor acetylation. (a) Mitochondria-targeted peptide sensor ZP1-MPP has improved photophysics and uptake after acetylation (ZP1-MPP, Chapter 3.3). (b) Acetylated peptide-sensor construct that localizes to endosomes but retains zinc responsiveness.

BIOGRAPHICAL NOTE

The author grew up in north Texas and developed an early passion for science during his homeschooling years. He then attended the Texas Academy of Mathematics and Science his junior and senior years in high school, during which he worked on antimicrobial hydrogel coatings under Professor Richard B. Timmons at the University of Texas at Arlington. After graduating, the author pursued his bachelor of science in chemistry at the Massachusetts Institute of Technology. The author studied new ligands for niobium complexes in Professor Christopher C. Cummins' group his first two years. Subsequently, the author developed research interests in chemical biology and bioinorganic chemistry, and spent the final two years at MIT researching targeted zinc sensors in Professor Stephen J. Lippard's laboratory. After receiving his B.S. in Chemistry, the author will pursue graduate studies in chemical biology at the University of Wisconsin at Madison.

CURRICULUM VITAE

Education

Massachusetts Institute of Technology, Cambridge, MA
Candidate for Bachelor of Science in Chemistry (2009-2013)

Texas Academy of Mathematics and Science, Denton, TX
(2007-2009)

Research

Massachusetts Institute of Technology, Cambridge, MA
Lippard Laboratory, Undergraduate Researcher (2012-2013)

Massachusetts Institute of Technology, Cambridge, MA
Cummins Laboratory, Undergraduate Researcher (2009-2011)

University of Texas at Arlington, Arlington, TX
Timmons Laboratory, Undergraduate Researcher (2007-2009)

Publications and Patents

Chyan, W.; Lippard, S.J.; Radford, R.J. Reaction-based Probes for Targeted Sensing of Mobile Zinc. *In Preparation,* **2013**.

Radford, R.J.; **Chyan, W.**; Lippard, S.J. Peptide-based Targeting of Fluorescent Zinc Sensors to the Plasma Membrane of Live Cells. *Chemical Science.* Accepted, **2013**.

Lippard, S.J.; Radford, R.J.; **Chyan, W.** Reaction-Based Fluorescent Probes for Detection of Zinc. Provisional Patent Application: Filed **2013**.

Timmons, R.B.; **Chyan, W.**; Bhattacharyya, D. Controlled Release Hydrogel Films Produced by Gas Phase Plasma Enhanced Chemical Vapor Deposition for Bioactive Agents and Medical Goods. *U.S. Patent Appl.* **2010.** *US 20100303877.*

Awards

MIT Department of Chemistry Inorganic Chemistry Award (2013)
Ruth M. Bacow Memorial Research Scholarship (2012)
Barry M. Goldwater Scholarship (2009)
Intel Science Talent Search National Finalist (2009)
Siemens Westinghouse Competition – National Grand Prize (2008)